©2019

Bhavna S. Paratala

ALL RIGHTS RESERVED

TRANSLATIONAL RELEVANCE OF RET GENE ALTERATIONS IN BREAST CANCER

by

BHAVNA S. PARATALA

A dissertation submitted to the

School of Graduate Studies

Rutgers, The State University of New Jersey

In partial fulfillment of the requirements

For the degree of

Doctor of Philosophy

Graduate Program in Cellular and Molecular Pharmacology

Written under the direction of

Kim M. Hirshfield, M.D., Ph.D.

And approved by

_____

_____

_____

_____

New Brunswick, New Jersey

January 2019

ABSTRACT OF THE DISSERTATION

Translational Relevance of RET Gene Alterations in Breast Cancer

By BHAVNA S. PARATALA

Dissertation Director:

Kim M. Hirshfield, M.D., Ph.D.

RET is a receptor tyrosine kinase that is crucial for normal tissue development and maintenance, but deregulation of its activity is a known contributor to oncogenesis in several cancers. Gain-of-function alterations in thyroid and lung cancers, causally-associated mutations in hereditary forms of endocrine disorders combined with the observed tumor responses to tyrosine kinase inhibitors with anti-RET activity underscore the potential use of RET as a therapeutic target in breast cancer. In breast cancer, correlations of RET overexpression with endocrine resistance and reduced expression with improved overall survival in estrogen receptor positive cases are driving clinical investigations of using RET-targeting kinase inhibitors for treatment of this disease. In efforts to identify clinically relevant biomarkers that may help direct individualized patient treatment, our initial finding of *RET* gene rearrangements in two independent breast cancers initiated our inquiry into the frequency and therapeutic relevance of *RET* gene alterations in breast cancer. Upon analyzing ~9,700 breast cancers that were deep-

sequenced using a targeted, hybrid capture assay, which includes relevant intronic details of *RET*, we discovered a spectrum of *RET* structural alterations in 121 cases (1.25%), of which, a majority were triple negative breast cancers that are known to have poorer prognosis and limited targeted treatment options. *RET* alterations were also identified in a subset of HER2-amplified breast cancers, primarily as *RET* amplification. We further characterized the functional consequence of *RET* amplification, the most frequent alteration, and the two initially identified *RET* rearrangements, *NCOA4-RET* and *RASGEF1A-RET*, by generating cell line and xenograft models. Comparison with an inactive RET kinase mutant and a known active RET kinase mutant by ectopic expression revealed constitutive kinase activation and downstream signaling of oncogenic pathways by both *RET* amplification and rearrangements. Results revealed that *RET* rearrangements induce transformation of non-tumorigenic cells, support xenograft tumor formation, and render cells carrying these alterations sensitive to RET inhibition *in vitro* and *in vivo*. Moreover, detection of the *NCOA4-RET* fusion in an index case of metastatic breast cancer that progressed on HER2-targeted therapy led to subsequent patient treatment with the RET inhibitor, cabozantinib, resulting in a rapid clinical and radiographic response. In another index case of advanced breast cancer, a *RET* amplification was detected and noted to be acquired in the setting of resistance to HER2-targeted therapy. RET expression was confirmed in a patient-derived cell line and xenograft model generated from this resistant tumor. Our xenograft model revealed tumor growth inhibition with cabozantinib and tested the applicability of its combination with HER2-targeting agents. Overall, this work presents a comprehensive, mutational analysis of *RET* in breast cancer and by using cell line models, patient-derived models, and index

case reports, signifies the functional role of RET alterations as well as the therapeutic relevance of targeting RET in this selected subset of breast cancers.

ACKNOWLEDGEMENT

Firstly, I would like to express my utmost gratitude to my advisor, Dr. Kim M. Hirshfield, for the constant support, encouragement and guidance throughout my time in her lab. Her dedication as a mentor, who is always available for feedback, motivation and constructive criticism, has inspired me to stay focused and enabled me to thoroughly enjoy the research experience as her student and as a scientist.

Throughout the course of my work, I was fortunate to receive guidance, collaborative insights and direction from my committee members and would like to sincerely thank Dr. Shridar Ganesan, Dr. Suzie Chen, Dr. Justin Drake and Dr. Zhaohui Feng for making this possible.

Additionally, I would like to thank my lab mates for their camaraderie and for enabling an enriching work environment. I would especially like to thank Sonia Dolfi for training and mentoring me, and for always being there to celebrate the successes and to overcome the setbacks. My special thanks to Aparna Kareddula, Whitney Petrosky and Kien Pham for sharing their expertise, their friendship and for making work fun. I would also like to acknowledge Stephanie Lin and Sopuru Ezeonu, who gave me an opportunity to impart my skills as their research mentor.

My sincere thanks to other graduate fellows and senior scientists at the Rutgers Cancer Institute of New Jersey (CINJ), especially to Atul Kulkarni, Dan Medina, and, Crissy Dudgeon for thought-provoking discussions, constant guidance and advice. I would also like to thank Jacqueline Harris and Ming Yao for always ensuring smooth progress on administrative matters and providing support.

My special acknowledgement to Dr. Shridar Ganesan and Dr. Lorna Rodriguez-Rodriguez from Precision Medicine Oncology at CINJ; Dr. Siraj M. Ali and Dr. Jon H. Chung from Foundation Medicine, MA; Dr. Brian Leyland-Jones and Dr. Casey B. Williams from Avera Cancer Institute, SD; and, Dr. Chen Liu for enabling and supporting collaborative contributions to this work.

None of this would have been possible without the financial support from funding sources. I must thank AHEPA 5th District Cancer Research Foundation, the Stacy Goldstein Faculty Scholar Award for Dr. Kim M. Hirshfield, established by Suzann and Edwin Goldstein, National Institutes of Health Grant P30CA072720, through a generous gift to the Genetics Diagnostics to Cancer Treatment Program of the Rutgers Cancer Institute of New Jersey and Rutgers University Cell and DNA Repository (RUCDR) Infinite Biologics, and Shared Resources of the Rutgers Cancer Institute of New Jersey.

I would like to thank the graduate program, especially Dr. Nancy Walworth, Dr. Rick Padgett, Dr. Janet Alder and Tina Cicolella for enhancing learning opportunities and ensuring a well-rounded, positive experience.

Ultimately, I would like to thank my family, whose endless support and encouragement throughout life has made this a possibility for me. This is dedicated to my parents and my sister for always motivating me to achieve my goals and to my husband, Saikiran Chaluvadi, who has been instrumental to my decision of pursuing doctoral research and has been a true partner, by supporting and sharing my passion for science and accompanying me in this journey.

I acknowledge that this work includes material, which is accepted for publication as an original research article in Paratala BS, Chung JH, Williams CB, Yilmazel B,

Petrosky W, Williams K, . . . Hirshfield KM, (2018) RET rearrangements are actionable alterations in breast cancer. *Nature Communications*: Accepted on 25 October 2018, under the Creative Commons Attribution 4.0 International License. License can be viewed in this link: http://creativecommons.org/licenses/by/4.0/

TABLE OF CONTENTS

LIST OF TABLES

LIST OF FIGURES

CHAPTER ONE: Introduction

Breast Cancer

Breast cancer is the leading cancer among women in 2018, with an estimated 266,120 new cases to be diagnosed in United States alone[1]. It is the second leading cause of cancer related deaths (14%) in women following lung cancer (25%)[1]. Mortality rates have consistently declined since 1990s and are largely attributed to improvements in effective systemic therapies, such as hormonal and other targeted treatments, increased understanding of the complexity and heterogeneous nature of the disease and early detection[2]. As a result, ~320,000 breast cancer deaths are estimated to have been averted as of 2015. Overall survival rates are optimistic at 91% for 5 years after diagnosis and 80% after 15 years. However, more than 450,000 deaths from breast cancer are expected annually worldwide[3] with 40,000 from the United States alone. Part of this is due to intrinsic or acquired resistance to standard therapies, especially in advanced/metastatic breast cancer where median survival is 3 years, as well as the lack of effective targeted treatments for all subtypes, which underscores the need for alternative therapeutic strategies.

Although breast cancer is often referred to as a single disease, it is a collection of up to 21 distinct histological subtypes and at least five molecular subtypes that in turn guide differences in risk factors, presentation, response to treatment and outcomes[4-6]. Most breast cancers (80%) are invasive, where tumor cells infiltrate walls of the ducts or glands in which they originate. Pathology-based assays used to routinely subtype breast cancer rely on three biological markers including the presence or absence of hormone

(estrogen or progesterone) receptors (HR+/HR-) and whether there are elevated levels of human epidermal growth factor receptor 2 (HER2) protein and/or extra copies of *HER2 (*or *ERBB2)* gene (HER2+/HER2-). In addition, gene expression profiling and proliferation markers allow stratification of newly diagnosed cases into five intrinsic groups[7]: luminal A, luminal B, HER2-enriched, and triple negative breast cancer (TNBC), which is further divided into basal-like and claudin-low[8-10] (**Figure 1**).

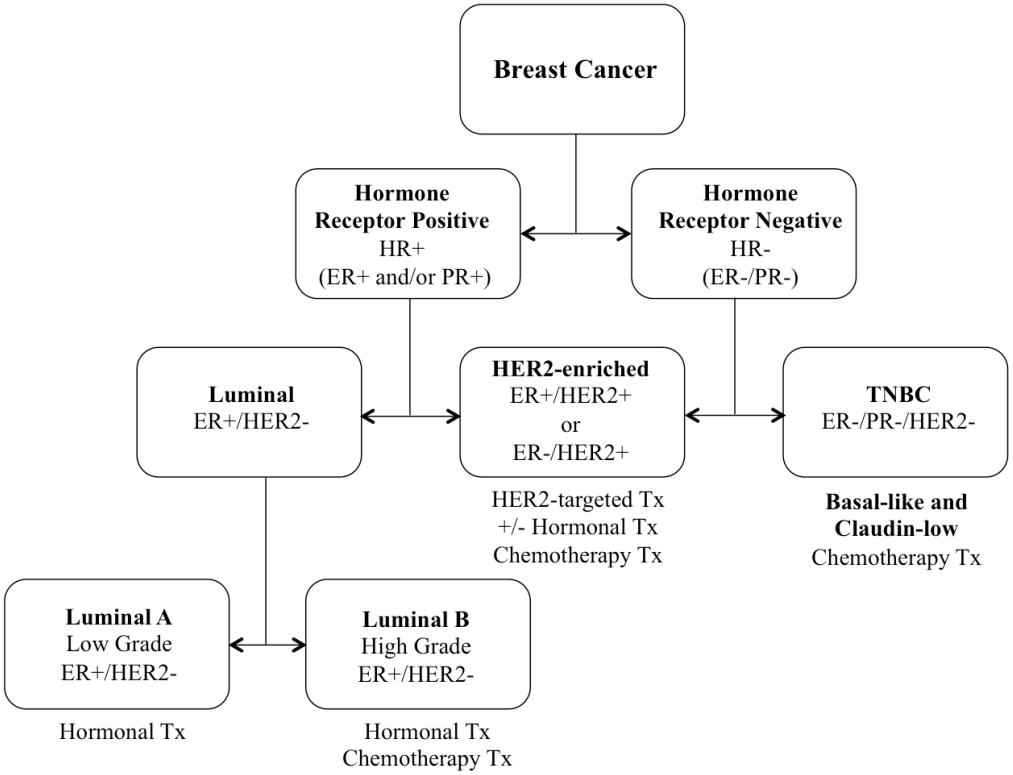

Figure 1. Broad classification of breast cancer subtypes.

Hormone receptor (HR) positive cancers include ER+ (estrogen receptor), and/or PR+ (progesterone receptor) cancers. HR+/HER2- cancers are classified as luminal cancers. Low grade are considered luminal A; high grade are mainly luminal B. Cancers positive for HER2 are HER2-enriched cancers. Cancers negative for all three receptors, ER-/PR-HER2- are triple negative breast cancers (TNBC). Adapted from Hirshfield et al., 2014[8]

Although TNBC is referred to as a separate subtype, it is a collection of diverse cancers with different gene expression patterns, histology and genomic profiles.

In addition to surgery and radiotherapy, hormone therapy and/or chemotherapy are used to treat luminal ER+ cases, while HER2-targeted therapy is used in combination with hormone therapy and/or chemotherapy for HER2+ cases. For early stage TNBC, chemotherapy remains as the primary option. There are currently no effective targeted therapies for TNBC as for the other breast cancer subtypes apart from the recent approval of PARP inhibitors for advanced cases carrying mutations in either *BRCA1* or *BRCA2* genes. The TNBC subtype is also associated with poorer short-term prognosis, higher recurrence, and higher metastasis rate compared to the non-TNBC subtypes[11]. Even within each subtype, variable responses to targeted therapies and chemotherapy is often observed and is attributable to tumor heterogeneity and/or intrinsic or acquired drug resistance[12]. Massively parallel sequencing and 'omics' technologies have revealed a high degree of heterogeneity within TNBCs, now driving investigation of actionable drivers in subsets of TNBC[8,13-15]. In addition to targeted therapies, early stage clinical trials with immunotherapy and combination with existing treatments are being evaluated in TNBC and in metastatic breast cancers[15-18].

In spite of significant advances in the treatment of hormone receptor positive breast cancers with targeted endocrine therapies, the intrinsic or frequent development of resistance and its overall prevalence results in it being the most common subtype among breast cancer deaths. Crosstalk between ER and other growth factor receptor pathways such as EGFR (HER1)/HER2, changes to transcription or activity of ER-α, and mutations in ER are frontrunners in current understanding of mechanisms of endocrine resistance[19-21]. Similar mechanisms have been proposed for HER2-targeted treatment resistance, with evidence of gene amplifications, crosstalk with other receptor pathways (e.g. IGFR, ER),

heterodimerization of the HER2 receptor, HER2 kinase domain mutations, and activation of compensatory or bypass signaling pathways[22,23]. Recent studies comparing the genomic landscape of drug-resistant ER+ cancers to that of primary cancers have revealed significant differences, with frequent genomic alterations in *ESR1*, *ERBB2*, *PIK3CA*, *PTEN*, and *AKT* among others[24].

Emerging strategies in treatment of advanced or metastatic breast cancers based on molecular and clinical findings are now focused on tyrosine kinase inhibitors, PARP inhibitors for *BRCA1/2* mutations, CDK4/6 inhibitors, PI3K/mTOR inhibitors, and immunotherapy. In each case, evaluation of the combination of these drugs with existing treatment modalities to overcome resistance by blocking tumor survival pathways is underway. Many of these novel approaches seek to target known vulnerabilities within an individual breast cancer to optimize patient outcome.

Tailoring optimal treatment approaches based on individual responses, where genomic analysis is applied to explore approved targeted therapies or promising alternative strategies is the cornerstone of precision medicine. In addition to identification of new and potential markers for targeted treatment, characterization of biomarkers predictive of response is needed. Aligned with this effort, this dissertation describes a precision medicine-based approach focused on the identification and characterization of *RET* alterations in breast cancer. The initial identification of *RET* rearrangements in several independent index cases of breast cancer, sequenced through a precision medicine protocol, further warranted an in-depth analysis of *RET* genomic alterations, including their functional and therapeutic relevance as predictive biomarkers in selected breast cancers. These topics are discussed in the following chapters.

Patient Index breast cancer cases with *RET* alterations

As part of a study to assess the clinical actionability of comprehensive genomic profiling in patients with rare or refractory cancers by the Precision Medicine Oncology group at the Rutgers Cancer Institute of New Jersey, *RET* alterations in several breast cancer cases were initially identified[25]. The observations form these index cases motivated our further inquiry into the frequency of *RET* alterations, functional characterization of selected *RET* alterations, and the therapeutic relevance of *RET* alterations in breast cancer, which is presented in this dissertation. The clinical and genomic detail of *RET* from each case is further described here. Two *RET* rearrangements and *RET* amplification were detected in three separate breast cancers using targeted sequencing on formalin-fixed paraffin embedded tumor tissue (FFPE).

Index case #1:

NCOA4-RET fusion in an ER+/PR-/HER2+ metastatic breast cancer

A 63-year-old female with a remote history of a stage I, ER- breast cancer (first occurrence, 24 years prior) followed by a more recent stage I, ER+/HER2- breast cancer (second occurrence, 13 years prior) was found to have stage IV disease in 2014. The patient had a lumpectomy followed by adjuvant radiation for the first occurrence, and required a mastectomy with axillary lymph node dissection for the second occurrence which was in the same breast. This was followed by four cycles of doxorubicin and cyclophosphamide and five years of tamoxifen. In 2014, a regional/distant recurrence of ER+/HER2+ disease (by immunohistochemistry) was confirmed on ultrasound-guided biopsy of the right axillary tail and both MRI and PET/CT imaging showed findings

consistent with bony metastasis. Palliative radiation to the thoracolumbar spine followed by trastuzumab plus pertuzumab for HER2-targeted treatment and anastrazole, a non-steroidal aromatase inhibitor, was initiated. Subsequently, progression in the axilla and bone was noted in addition to rising tumor markers.

Prior to progression, the 2014 recurrent biopsy was sent for genomic profiling (FoundationOne, Foundation Medicine) which identified the presence of an *NCOA4-RET* fusion. Based on the breakpoints of the intrachromosomal translocation, the fusion was found to include exons that code for the dimerization motifs from NCOA4 (nuclear receptor coactivator 4) and kinase domain for RET. Histology of the recurrent breast cancer tissue revealed a papillary architecture which is characteristic of *RET* fusion-positive thyroid cancers. For second line therapy after progression, trastuzumab, exemestane (a steroidal aromatase inhibitor), and cabozantinib, a multi-kinase inhibitor, were initiated.

Cabozantinib inhibits tyrosine kinases, such as VEGFR-1, 2, 3 (vascular endothelial growth factor receptor), MET, and RET. *NCOA4-RET* fusions have been identified as driver mutations previously in papillary thyroid and non-small cell lung cancers (PTC and NSCLC) and several pre-clinical and clinical studies are investigating anti-RET multikinase inhibitors such as cabozantinib in patients with advanced RET fusion positive NSCLC, including *NCOA4-RET* cancers[26-29]. Based on this and early safety data for the combination of cabozantinib and trastuzumab for metastatic breast cancer in an ongoing phase II study (clinicaltrials.gov, NCT02260531), cabozantinib was added to the treatment as a genomic-guided targeted therapy due to the presence of the *NCOA4-RET* fusion observed in the recurrent tumor.

Index case #2:

***RASGEF1A-RET* rearrangement in a triple negative breast cancer**

A 66-year-old female was diagnosed with a stage I, grade 3, ER-/PR-/HER2- invasive ductal carcinoma in 2014 after an ultrasound-guided biopsy in the right breast. She underwent a right skin-sparing mastectomy, followed by a regimen of docetaxel plus cyclophosphamide, which was planned for 6 cycles. Due to severe side effects including neurologic symptoms (altered personality, headache, balance issues), hand and foot erythema with desquamation, palpitations and compromised quality of life requiring hospitalization, treatment was discontinued after 3 cycles.

Comprehensive genomic profiling (FoundationOne, Foundation Medicine) of primary tumor revealed the presence of a novel *RET* rearrangement, *RASGEF1A-RET*. Based on detected breakpoints, which predicted the preservation of kinase domain coding exons of *RET*, that are similarly retained in other oncogenic *RET* fusions, *RASGEF1A-RET* was listed as an actionable alteration. Since the patient was considered to be at high risk of relapse due to treatment discontinuation, primary recommendations by molecular tumor board included further investigation of the novel *RET* alteration for functional characterization and if applicable, when relapse occurs, consideration of RET inhibitors beyond conventional therapies.

Index case #3:

***RET* amplification detection after development of acquired resistance to HER2-targeted treatments for a HER2+ breast cancer**

A 49-year-old female with a history of locally advanced, intermediate grade, ER+/HER2+ invasive ductal carcinoma (IDC) of the breast underwent deferred intermittent treatment with HER2-targeted therapy starting approximately one year after biopsy-confirmed diagnosis in 2012. Based on an excellent response initially over 11 months to nab-paclitaxel/trastuzumab/pertuzumab, her tumor was considered sensitive to trastuzumab. However, after subsequent T-DM1 and then the combination of vinorelbine, trastuzumab, and pertuzumab, with progression observed after 3 months with each therapy, limited response was consistent with acquired resistance to HER2-targeted therapy. At that time, she received 5 months of capecitabine and lapatinib, another HER2-targeted agent, before clear evidence of disease progression was noted. She then underwent palliative mastectomy in late 2015, including resection of a large pectoral mass and partial resection of bulky lymph nodes. Pathology showed an 11cm, high grade IDC that was ER-/PR-/HER2+.

PET/CT showed residual disease in axilla but no evidence of distant metastatic disease. After completion of 7 weeks of radiation to the chest wall and nodal regions, concomitantly with trastuzumab and carboplatin (carboplatin for only first 5 weeks), trastuzumab alone was continued for another 3 months, owing to evidence indicating benefit of trastuzumab despite progression[30,31]. Disease progression was observed while on trastuzumab and PET-CT revealed new hepatic masses, bilateral mediastinal

adenopathy, pulmonary nodules, and left axillary adenopathy. Treatment was switched to pegylated liposomal doxorubicin and trastuzumab to reduce risk of cardiotoxicity.

Given the progressively refractory nature of this patient's cancer and to further evaluate treatment options, comprehensive genomic profiling (FoundationOne, Foundation Medicine) of tumor from both 2012 (primary, HER2-sensitive) and 2015 (recurrent, HER2-resistant) was performed. While *ERBB2* amplification was confirmed in both the 2012 breast primary and the trastuzumab-resistant progressive disease, consistent with the history of HER2+ disease, only the tumor tissue from 2015 revealed the presence of a *RET* amplification. As the *RET* amplification was not present in the 2012 tumor, prior to initiating HER2-targeted therapy, this suggested a potential contribution of the *RET* amplification in the acquired resistance to HER2-targeted therapy.

Based on results from a phase II clinical study[32] reporting tolerable combinations of sunitinib, a RET-targeting multikinase inhibitor, with trastuzumab and docetaxel, the treating physician appealed to insurance for sunitinib in order to treat with this combination. However, the patient died before she was able to receive this treatment.

RET proto-oncogene

RET signaling for normal tissue development and maintenance

RET (*RE*arranged during *T*ransfection) is a known proto-oncogene located in the pericentromeric region of chromosome 10q11.2. It encodes a single-pass transmembrane tyrosine kinase, RET, which is a receptor for a family of four soluble glial cell line-derived neurotrophic factor (GDNF) ligands (GFLs). Each of these ligands, GDNF, neurturin (NRTN), artemin (ARTN) and persephin (PSPN) interact indirectly with RET via one of four cell surface co-receptors belonging to the group of the GDNF family receptor-α (GFRα, 1-4)[33-35]. RET signaling is essential for the normal development of the nervous system and kidney and is critical for maturation and maintenance of neurons and spermatogonial stem cells[36-39].

Typical of other receptor tyrosine kinases, RET has a large extracellular domain, a transmembrane region, and an intracellular kinase domain (**Figure 2**). Four repeats of cadherin-like domains that contribute in stabilizing RET dimers and a cysteine-rich region essential for ligand interaction and intramolecular disulfide bonding, make up the extracellular region. Unlike other RTKs, RET does not have a ligand-binding domain. The extracellular domain also contains several glycosylation sites. Nascent RET protein in the endoplasmic reticulum is glycosylated to an immature 155kDa glycoprotein, which is further processed through the secretory pathway into a mature, plasma membrane-localized 175kDa protein.

RET also has a cytosolic juxtamembrane (JM) region N-terminal to the kinase domain. Although this domain is associated with autoinhibitory signaling in other receptor tyrosine kinases, its contribution to RET catalytic function via an allosteric input from JM-segment elements, such as Y687, was only recently suggested[40].

Upon binding with the ligand-co-receptor complex, RET undergoes dimerization and autophosphorylation of tyrosine residues on the intracellular kinase domain, in turn recruiting adaptor and signaling proteins to stimulate multiple downstream pathways (**Figure 2**). A primary hub for docking of multifunctional signal proteins is the phosphotyrosine 1062 (pY1062), which can lead to activation of RAS-MAPK and PI3K-AKT signaling pathways or recruitment of CBL ubiquitin ligases that downregulate RET functions. In addition, other known signaling consequences of RET includes protein kinase C (PKC) pathway, SRC kinase binding and RET-associated STAT3 activation.

Consistent with its early role during development, RET expression is at its highest level during embryogenesis and reduces to relatively low levels in normal adult tissues [41,42]. RET remains expressed in several adult nerve cells, thyroid C cells, and germ cells in testes driving tissue maintenance and morphogenesis[43-45]. Homozygous mice with targeted deletion of RET kinase develop to term but die within a day of birth due to enteric neuron and renal defects[46]. It has been shown that *Ret* null mice can be rescued by RET9, the short isoform but not by the longer isoform RET51[44,47]. Given its important roles in development and maintenance of organ systems, known germline loss-of-function *RET* mutations are associated with human pathologies such as Hirschsprung disease (HSCR) affecting the enteric nervous system and congenital abnormalities of kidney and urinary tract (CAKUT) phenotypes[48,49].

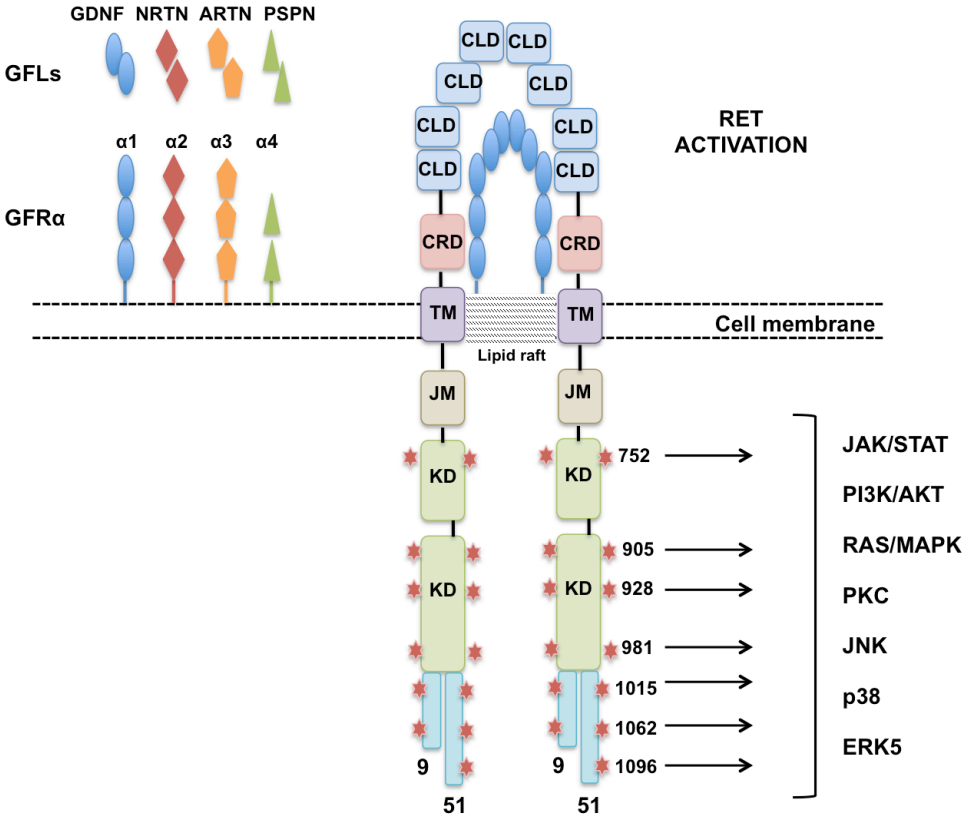

Figure 2. RET receptor tyrosine kinase activation and signaling

RET is a single-pass, transmembrane protein that has an extracellular domain with four cadherin-like domain (CLD) repeats and a cysteine rich domain (CRD) that interact with a ligand-co-receptor complex (GFL-GFRα). The ligand-co-receptor complex is a heterodimer consisting of one of four GFLs (GDNF, NRTN, ARTN, PSPN) interacting with one of four GFRα (GFRα1-4). The complex can recruit RET into lipid raft membrane subdomains. Once bound to the complex, conformational changes facilitate RET monomer association via CLD followed by receptor dimerization and results in autophosphorylation of key tyrosine residues in the intracellular kinase domain (KD). This facilitates interaction with signaling proteins or adaptor molecules leading to activation of multiple signaling pathways promoting cell growth, proliferation, survival, and differentiation. TM (Transmembrane domain), JM (Juxtamembrane domain)

Aberrant RET activation and cancer

The role of RET in initiation and progression of multiple cancers is well documented. Germline gain-of-function RET mutations, primarily resulting in single amino acid substitutions, are observed in patients with multiple endocrine neoplasia 2 (MEN2), a multi-tumor syndrome characterized by early onset of medullary thyroid cancer (MTC)[50-52]. These mutations drive ligand-independent, constitutive kinase activation and downstream oncogenic signaling. Although several pathogenic variants are reported, these changes tend to affect key residues belonging to the extracellular and kinase domains. In addition, genotype-phenotype correlations have been established for many *RET* missense mutations and MEN2 clinical phenotypes. For example, extracellular domain mutations affecting cysteine residues are mostly found in MEN2A subtype and familial MTC, while MEN2B is observed predominantly in patients with specific amino acid substitutions in the kinase domain. Cysteine residue mutations tend to drive aberrant activation by receptor dimerization; whereas, kinase domain mutations are associated with more complex functional outcomes such as protein conformational changes that have increased kinase activity or reduced autoinhibition and may be activated as either monomers or dimers[53-55]. Some of these intracellular mutations have also been found in 40 – 65% of sporadic MTC, affecting later events such as tumor progression[56].

Somatic chromosomal rearrangements affecting the *RET* locus have resulted in a special class of RET oncoproteins and have been described in ~7% of papillary thyroid cancers (PTC) and 1-2% of non-small cell lung cancers (NSCLC) [57,58]. More recently, they have been reported in smaller numbers in chronic myelomonocytic leukemia, colorectal cancer, salivary gland cancer and breast cancer[59-62]. Chromosomal inversions,

duplications or translocation events involving *RET* can result in juxtaposing 3' intracellular kinase domain coding *RET* sequences with 5' upstream partner genes which may contribute regulatory or dimerization domains to the fusion gene[63] (**Figure 3**). *KIF5B-RET* fusions are observed more frequently in NSCLC while *CCDC6-RET* and *NCOA4-RET* are most prevalent in PTC though not limited to this cancer type[64,65]. Breakpoints in the *RET* gene have been known to preferentially occur at defined regions. Intron 11 is the most commonly observed breakpoint for *RET* fusions. As a result, active RET fusions mostly tend to incorporate *RET* sequences beginning from exon 12, thus encoding only the cytosolic kinase domain and c-terminal regions of RET. Other breakpoints in introns 7 and 10 have also been reported, including additional *RET* residues coding for the transmembrane region.

RET rearrangements resulting in kinase domain fusions induce oncogenic pathway activation through one of two main mechanisms. The rearrangement results in placing the *RET* kinase under the transcriptional control of the N-terminal partner gene. RET expression is relatively low in adult tissues and restricted to specific cell types, whereas the partner gene, depending on the tissue type, may be more ubiquitously expressed, thus driving increased expression of a RET fusion kinase in tumor tissue[66]. Secondly, upstream partner genes may contribute to dimerization motifs such as coiled-coil, cysteine rich, or leucine zipper domains leading to ligand-independent dimerization, followed by constitutive kinase activation of downstream oncogenic pathways. In addition to lacking the normal N-terminal RET domains, most RET fusions also tend to lack the transmembrane domain and may undergo aberrant localization, avoiding normal trafficking and degradation.

Other alterations of RET include increased activity and overexpression of the wildtype RET, which is observed more broadly in a wider variety of cancers, with

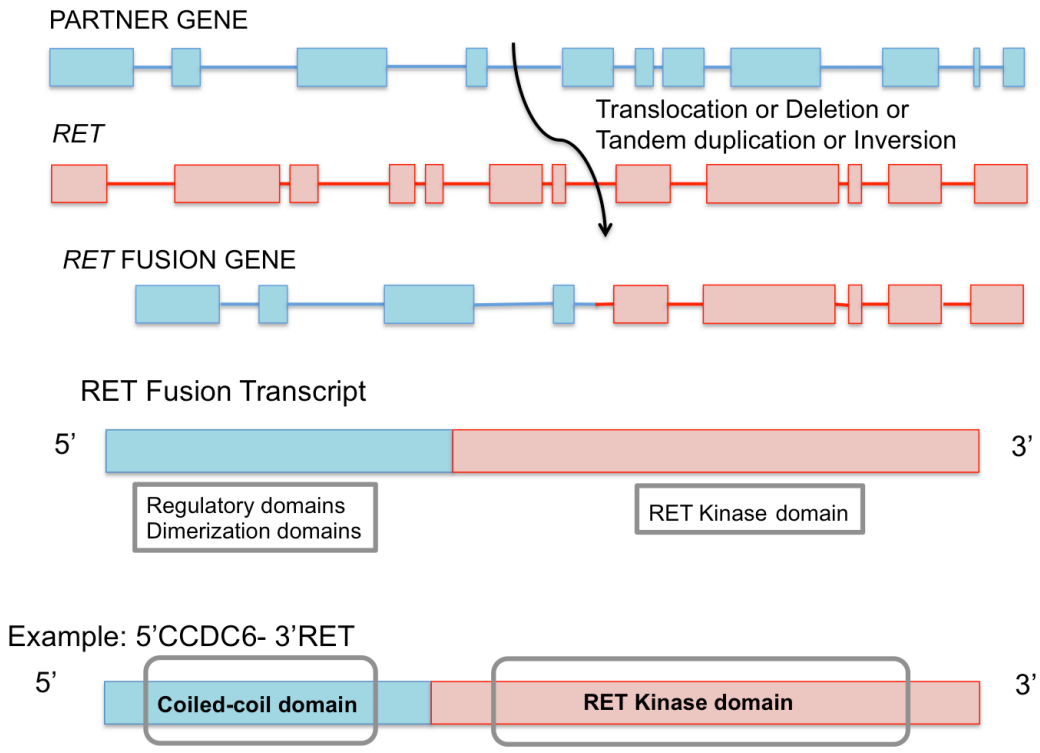

Figure 3. Illustration of a genomic rearrangement leading to a *RET* fusion

Chromosomal events such as translocation, inversion, deletion or duplication may place portions of two independent genes together resulting in a gene fusion. Oncogenic *RET* fusions tend to include kinase domain coding exons from *RET* fused with exons from partner genes. An example of CCDC6-RET fusion, which includes a coiled-coil dimerization domain from CCDC6 and kinase domain from RET. Adapted from Paratala et al., 2016[63]

implications for tumor progression and resistance to therapy. RET expression is seen in 50-65% of pancreatic ductal carcinomas and more frequently in metastatic and higher-grade tumors, where it is associated with poor outcomes[67]. It is also expressed in 30-70%

of invasive breast cancers, more frequently observed in ER+ tumors, and is associated with endocrine resistance[68,69]. In recurrent breast cancers, expression is increased significantly compared to the primary breast tumor or normal breast tissue and correlates with reduced metastasis-free survival and overall survival[70]. Other cancers where RET expression is reported and clinical relevance is being investigated include prostate cancer, acute myeloid leukemia, melanoma, renal cell cancers and head and neck cancers[34].

RET in breast cancer

RET overexpression at the RNA level and elevated protein levels have been reported in different breast cancer subtypes, predominantly in ER+ cases, and is correlated with reduced metastasis-free and overall survival[69-71]. In particular, the role of RET in the biology of ER+ breast cancers has been under significant investigation revealing high levels of RET in ER+ breast cancer cell lines and tumors[68-70]. A crosstalk between RET and ER pathways implicate RET's contribution to endocrine therapy resistance and preclinical evidence suggest RET as a potential target to resensitize resistant tumors to respond to endocrine therapies[70]. Studies have shown that estrogen can upregulate RET expression and consistent with the finding, the RET promoter region contains Estrogen Response Elements (ERE)[69,72]. Expression of RET ligand, ARTN can be induced by estrogen and GDNF by inflammatory cytokines secreted by tumor associated macrophages in the breast cancer microenvironment[68,73]. Concomitantly, when RET signaling is activated by GDNF-treatment of MCF7 breast cancer cells, which express high levels of RET and co-receptor GFRα1, an increase in ER phosphorylation is

observed. In these cells, siRNA inhibition of RET enhances response to the anti-estrogen drug, tamoxifen and restores sensitivity in tamoxifen-resistant cells[70].

In addition to the RET-ER association, an estrogen/ER-independent interaction was described between RET and the cytokine IL6 in the presence of an endocrine agent in RET-positive cells. In this setting, activated IL6 and RET lead to a positive feed-forward loop that induced migration and invasion of breast cancer cells[71]. Further, RET inhibition revealed a reduction in growth and migration/metastatic potential of cells and xenograft tumors.

In light of these findings, several other groups have investigated the use of RET-targeting kinase inhibitors either alone or in combination with endocrine therapies (selective estrogen receptor modulators, downregulators, and aromatase inhibitors) in preclinical and clinical studies of breast cancer[72,74-77].

RET-targeting multi-kinase inhibitors in clinic and research

Several small molecule tyrosine kinase inhibitors targeting multiple kinases are also active against RET and have been extensively explored in preclinical and clinical studies for RET-directed therapies in thyroid, lung, and breast cancers. Four such inhibitors, cabozantinib, vandetanib, lenvatinib and sorafenib, are now approved for the treatment of advanced MTC and differentiated thyroid cancers[78-80]. Although patients in thyroid cancer trials were enrolled irrespective of whether their tumors carried an alteration in *RET,* subgroup analyses for both cabozantinib and vandetanib trials revealed a positive association between presence of a *RET* mutation and specific clinical outcomes. Longer progression free survival (PFS) for cabozantinib and vandetanib and

increased overall response rates (ORR) for vandetanib were observed in patients with *RET*-mutated tumors as compared to those lacking *RET* mutations.

In the case of *RET*-rearranged lung cancers, confirmed responses and durable disease control has been reported in selected cases. Recent completion of three prospective phase II trials (one for cabozantinib, two for vandetanib) in molecularly defined cohorts of *RET*-rearranged NSCLC reveal an ORR of 16 – 53% with disease control ranging from a few months to >3 years from some patients[29,81,82]. This aligns with both preliminary results from a lenvatinib phase II trial in *RET*-fusion positive lung cancer patients and a retrospective series of *RET*-fusion positive lung cancer patients that received multikinase, RET-targeting inhibitors[83,84]. The wider range of response rates from different trials has been considered somewhat modest in comparison to more recent targeted therapy approvals for other inhibitors matched to molecular targets such as crizotinib for *MET* or *ALK* alterations, alectinib for *ALK* fusions, or gefitinib for *EGFR* mutations in lung cancer.

In breast cancer, several ongoing clinical trials are assessing if approved endocrine therapies combined with tyrosine kinase inhibitors are effective in re-sensitizing resistant breast cancers or preventing development of endocrine resistance. Within the group of agents being evaluated, RET-targeting inhibitors are also included. Sorafenib, a VEGFR, BRAF, and RET inhibitor, was used in a Phase II trial in combination with the aromatase inhibitor anastrazole, and was found to be effective in 23% of postmenopausal breast cancer patients who had relapsed on aromatase inhibitors previously, attributing this effect to restoration in sensitivity. Based on promising anti-tumor activity in preclinical studies[75,77], a phase II trial comparing vandetanib (VEGFR2,

EGFR and RET inhibitor) in combination with docetaxel to docetaxel alone in pretreated metastatic breast cancer was found to be well tolerated, but a clinical benefit was not observed. However, patients were not preselected for participation based on detection of RET overexpression or *RET* genomic alteration in their tumors. Other studies with vandetanib in unselected cohorts of breast cancer also reveal similar results[85]. Cabozantinib monotherapy, with activity against MET, VEGFR2, AXL, and RET, demonstrated objective response and disease control in a phase II trial for heavily pretreated metastatic breast cancer patients[86]. Cabozantinib, either alone or in combination with trastuzumab, is being evaluated in a phase II study in advanced breast cancer patients with brain metastases (clinicaltrials.gov, NCT02260531). More recently, a phase II trial is accruing patients for investigating immunotherapy in combination with cabozantinib for metastatic triple negative breast cancer (clinicaltrials.gov, NCT03316586).

With the exception of *RET*-rearranged lung cancers, thyroid and breast cancer trials with multikinase inhibitors have been thus far conducted in patient populations that are unselected for any RET aberration, such as *RET* mutation, overexpression or active signaling. Although these studies have informed on toxicity and general efficacy, their clinical applicability in targeted-treatment of *RET*-altered breast cancers remains unclear.

Genomic profiling and detection of rearrangements

In the past decade, the success of targeted therapies combined with the advent of sophisticated next generation sequencing has revolutionized our concept of cancer classification. More recently, cancers are being catalogued based on shared molecular drivers and related tumor biology rather than solely being based on histology. This has also fostered a change toward the approach and applicability of precision medicine to improve clinical outcomes by applying targeted treatments.

RET rearrangements, which were first detected in and associated solely with papillary thyroid cancers are now increasingly reported in several other cancers. Standard techniques previously used for detection of rearrangements such as fluorescent in situ hybridization (FISH), array based comparative genomic hybridization (CGH), PCR based techniques, although powerful, are limited in efficient detection of potentially unknown fusions[63]. FISH is used for detecting specific rearrangements and is clinically applied in detecting *BCR-ABL* in leukemia and *EML4-ALK* in lung cancers[87,88]. However, it is not suitable for detecting fusions with unknown gene partners or small intrachromosomal fusions. An improved technique, break-apart FISH, can detect fusions even if only one of two genes involved in the fusion are known but may result in false negatives and cannot identify breakpoints, if the partner is not already known. Array-based CGH can detect larger inter- and intra-chromosomal rearrangements but not intergenic rearrangements. If breakpoints are known, PCR-based techniques can detect intron rearrangements, but may miss small insertion/deletion events if allele-specific primers are not used. These techniques that were previously applied across cancers may have underrepresented the

presence of certain rearrangements, which are now detectable by advanced genomic profiling tools.

The development of efficient, high-throughput sequencing methods has made detection of such rearrangements across several types of cancers more affordable and accessible. Some of the next-generation sequencing techniques are better equipped to identify rearrangement events, such as exome sequencing with targeted intron capture and hybrid capture enriched RNA-sequencing. While whole-exome sequencing can identify rearrangements, fusion junctions occurring outside the coding region will be missed. More recently, deep sequencing comprehensive platforms that are certified for clinical detection of 'actionable' genomic alterations include 'targeted intron capture' that can identify previously undetected events by exome-sequencing only. Newer technologies to further improve sensitivity such as single primer enrichment technology for detection of novel fusions and anchored-multiplex PCR designed for target-enrichment are being explored.

RATIONALE

Aberrant activation of RET signaling caused by changes at the gene or the protein level contributes to the development and progression of several cancers and correlates with response to RET-targeting therapies. Evidence implicating RET in endocrine treatment resistance raises its potential as a therapeutic target in breast cancer. Given the preliminary finding of *RET* gene alterations in three index cases and the absence of comprehensive mutational analysis for *RET* in breast cancer, we identified the need and feasibility for such an analysis, which is the primary objective of this work.

Consequently, based on sequencing data, we hypothesized that the *RET* alterations detected in these index cases are functional and tumorigenic, which is evaluated in our secondary objective. In addition to understanding the *RET* genomic landscape and functional characterization of the index breast cancer *RET* alterations, which includes a canonical *RET* fusion *NCOA4-RET*, a non-canonical *RET* fusion, *RASGEF1A-RET,* and *RET* amplification, of direct relevance to the first two objectives is the impact of therapeutically targeting RET in *RET*-altered cases.

As the third and final objective, we evaluated if RET-targeting inhibitors sensitize the cells and tumors bearing *RET* alterations, and, if *RET* alterations may serve as predictive biomarkers of response in the breast cancers in which they are found. Ultimately, our findings, models and clinical reports would lay the foundation for a deeper analysis into RET's role in intrinsic or acquired resistance to existing targeted therapies and the potential for alternative treatments in *RET*-positive, treatment refractory cancers, by either targeting RET alone or in combination with existing therapies.

CHAPTER TWO: Materials And Methods

Mutational analysis of *RET* in breast cancers

Targeted next-generation sequencing was performed in a Clinical Laboratory Improvement Amendments (CLIA)-certified, New York State-accredited, and College of American Pathologists (CAP)-accredited laboratory (Foundation Medicine, Inc., Cambridge MA) between May 2012 and Sept 2016. Technical details and validation of genomic profiling assays, FoundationOne, Version 1(v1) and Version 2(v2) have been extensively described in Frampton, G.M., et al. 2013 and Hartmaier, R.J., et al. 2017[89,90]. Approval for this study, including a waiver of informed consent and a HIPAA waiver of authorization, was obtained from the Western Institutional Review Board (Protocol No. 20152817). Formalin-fixed, paraffin-embedded (FFPE) tissue samples obtained from 9,693 patients with breast cancer were submitted by clinicians for targeted next generation sequencing as part of routine clinical care. The pathologic diagnosis of each submitted case was confirmed and tumor content was determined on routine hematoxylin- and eosin-stained slides. Specimens were submitted with limited accompanying clinical information; pathology reports were reviewed to determine ER status. HER2 *(ERBB2* amplification) status, based on genomic profiling, was available for all cases. At least 50ng DNA was extracted from 40-µm FFPE sections with at least 20% tumor cells. Adaptor-ligated DNA underwent hybrid capture for all coding exons of 236, 315, or 405 cancer-related genes plus select introns from 19, 28, or 31 genes frequently rearranged in cancer, including *RET*. Captured libraries were sequenced to a median exon coverage depth of 637× (Illumina HiSeq). Resultant sequences were analyzed for short variants [base substitutions, insertions/deletions (indels)], copy number

alterations (focal amplifications and homozygous deletions), and select gene fusions. RNA sequences were analyzed for the presence of rearrangements only. Custom filtering was applied to report genomic alterations and remove benign germline events[89,90]. Copy number detection and validation was obtained by normalizing the reads in the tumor against a process-matched normal control and further corrected for tumor purity[89]. Comparative analysis between available breast cancer status of RET altered cases was presented using the oncoprint software[91,92].

Index case study participants evaluated at the Rutgers Cancer Institute of New Jersey provided informed consent for point-of-care tumor genomic profiling and were part of a prospective trial for patients with rare or refractory tumors. Relevant clinical history, pathology, and genomic profiling results were reviewed at a formal molecular tumor board. Discussions of genomic profiling results were in the context of clinical course, tumor type, mutational frequency, cancer biology/behavior, and considerations for therapy. Based on consensus recommendations, cases with actionable alterations were referred for clinical trials, FDA-approved therapies (on- or off-label), and were followed for clinical course. The molecular tumor board did not provide recommendations for non-targeted therapies and therapeutic approach was ultimately the treating physician's choice. The protocol (CINJ001209) was approved by the Institutional Review Board of Rutgers Robert Wood Johnson Medical School.

Generation of expression plasmids

***NCOA4-RET* fusion and *ΔRET* open reading frames (ORFs).** The fusion cDNA sequences for *NCOA4* (exon 2 – exon 7) and *RET* (exon 12 – exon 19) were

amplified from cDNA derived from MCF7 (ATCC® HTB-22™) cell line whereas *ΔRET* (exon 11 ATG – exon 19) cDNA was amplified from plasmid pDONR223-RET, a gift from William Hahn & David Root (Addgene, 23906) using Platinum High Fidelity *Taq* DNA polymerase enzyme (Invitrogen, 11304-011) with fusion-specific primers (**Table 1**). Fusion-specific primers were designed to be suitable for gateway cloning technology. RNA was extracted from MCF7 using manufacturer's protocol (Qiagen, 74104) and cDNA was prepared using a reverse transcription PCR (RT-PCR) kit (Applied Biosystems, N8080234). Using a DNA ladder (Invitrogen, 1006211) and diagnostic agarose electrophoresis, all PCR products were verified at expected sizes and then extracted from gels using manufacturer's protocol for QIAquick Gel Extraction Kit (Qiagen, 28704). Gel extracted PCR products for *NCOA4-RET* were ligated using T4 DNA ligase enzyme (Invitrogen, 15224-017). To amplify the fusion product, Platinum High Fidelity *Taq* DNA polymerase enzyme (Invitrogen, 11304-011) with fusion-specific primers was used again and then purified using QIAquick PCR Purification kit (Qiagen, 28104).

Table 1. RET gene-fusion specific PCR primers

NCOA4-RET	
NCOA4 exon_2_Forward	ATGAATACCTTCCAAGACCAGAG
NCOA4 exon_7_Reverse	CTGACTGTTCTCCAAGGTCTGCT
RET exon 12_Forward	GAGGATCCAAAGTGGGAATTC
RET exon 19_Reverse	GAATCTAGTAAATGCATGGGAAATTC
RASGEF1A-RET (ΔRET)	
RET exon 11 ATG_Forward	ATGACCTTCCGGAGG
RET exon 19_Reverse	GAATCTAGTAAATGCATGGG

Generation of expression vectors using gateway cloning. In order to be able to easily move DNA sequences between multiple vector systems based on the experimental

need, gateway-cloning technology was employed. The ORFs obtained for *NCOA4-RET* and *ΔRET* were used to generate entry vector clones using the PCR cloning system (Invitrogen, 12535029) protocol. For full-length, wildtype *RET (RET^{amp}),* pDONR223-RET (Addgene, 23906) was used as the template. The donor vector map (pDONR-221, Invitrogen, 12536017) for generating the entry vector is described in **Appendix B**. At this stage all the entry vectors were confirmed to have the correct full-length sequences using Sanger sequencing. In case of the *NCOA4-RET* fusion, where HindIII restriction enzyme sequence was used for ligation of the two gene fragments, and in cases where base changes were observed, site-directed mutagenesis (Agilent technologies, 2105185) was employed to rectify the sequence back to the correct bases. Entry vectors were then used to transfer sequences to any choice of expression vector as described further. In order to generate expression plasmids, the sequence-confirmed entry clones were then transferred into gateway destination vectors pLenti6.3/V5–DEST and pEF-DEST51 (Invitrogen, V53306 and 12285-011), where both include a c-terminal V5-tag, using the LR clonase II enzyme kit (Invitrogen, 11791-020). The vector maps are described in **Appendix B**. pLenti6.3/V5–DEST, which contains the human CMV promoter (cytomegalovirus immediate-early), was chosen to allow high-level, constitutive expression in human cell lines. Due to reports of transcriptional silencing of CMV in mouse cell lines[93], pEF-DEST51 with the human EF-1α subunit promoter was used for expression in the mouse NIH-3T3 cell line. Constitutively kinase active (corresponding to M918T mutation) and kinase inactive (corresponding to K758M mutation) full-length variants were generated using QuikChange II XL Site-Directed Mutagenesis Kit (Agilent, 2105185). Empty expression vector for CMV promoter was purchased and propogated from Addgene

(pLenti CMV Blast empty (w263-1) was a gift from Eric Campeau & Paul Kaufman, Addgene plasmid #17486) and *lacZ* control vector for EF-1α promoter, pEF/GW-51/*lacZ*, was available from the kit for the destination vector (Invitrogen, 12285-011). All full-length sequences are described in **Appendix C**.

Cell culture and reagents

All mammalian cell lines were cultured in American Type Culture Collection (ATCC) recommended media and protocols as described in **Table 2** and at 37°C in a humidified atmosphere containing 5% CO_2. Authentication of all cell lines was performed by ATCC using short tandem repeat analysis and mycoplasma contamination tested negative. For all cell line experiments and growth curves, cells were counted using Vi-CELL XR (Beckman Coulter) cell analyzer using trypan blue die exclusion method. For most experiments, cells were counted and plated at a density that would reach 80% confluence on the day of protein isolation or measurement.

Table 2. Cell lines used and culture conditions

Cell line	Species	Source	Type	Culture Media	Trypsin-EDTA (%)
NIH-3T3	Mouse	ATCC® CRL -1658™	fibroblast	DMEM+10% BCS	0.05
MCF10A	Human	ATCC® CRL 10317™	breast epithelial	MEGM™ Bulletkit™	0.25
MCF7*	Human	ATCC® HTB -22™	breast cancer epithelial	DMEM+10% FBS	0.05

ATCC, American Type Culture Collection
DMEM, Dulbecco's Modified Eagle Medium from Sigma, D5796
BCS, Iron fortified Bovine Calf Serum from ATCC, 30-2030
MEGM™ Mammary Epithelial Cell Basal Medium from Lonza, CC-3150 plus SingleQuots™, CC-4136
SingleQuots™ include bovine pituitary extract, human epidermal growth factor, insulin, hydrocortisone
FBS, heat inactivated (55°C, 30 minutes) Fetal Bovine Serum from ATCC, 30-2020

Trypsin-EDTA (Ethylenediaminetetraacetic Acid) from Thermo Fisher 25200-056 (0.25%) and 25300-054 (0.05%)
*No mutations in MCF7 for NCOA4 and RET as confirmed by Broad Institute Cancer Cell Line Encyclopedia

Plasmid transfections

For transient transfections, the pLenti6.3 vectors were expressed in MCF10A using Fugene HD transfection (Promega, E2311) and in NIH/3T3 cells using Lipofectamine 3000 reagents (Invitrogen, L3000-015) according to manufacturer's protocols. To generate stable cell lines, pEF-DEST51 vectors were transfected into NIH/3T3 using Lipofectamine LTX (Invitrogen, 15338030) according to manufacturer's protocols and selected with the antibiotic blasticidin S (Thermo Fisher Scientific, R21001) at a final concentration of 4ug/ml for 2 weeks. Stable expression was confirmed by immunoblot.

Immunoblot analysis

Protein samples were extracted from cells and tumor xenografts using NETN lysis buffer (NaCl 150mM pH7.5, EDTA 1mM, Tris 20mM pH 8.0, NP40 0.5%) supplemented with protease inhibitor cocktail (Sigma-Aldrich, P8340) and phosphatase inhibitor 2 and 3 cocktails (Sigma-Aldrich, P5726 and P0044). For measurements involving phosphorylated proteins, cells were serum starved for 24 hours in Dulbecco's modified Eagle Medium prior to protein isolation. Cells were gently rinsed with cold PBS and the cell monolayer was briefly coated with cold lysis buffer prior to scraping. Samples were collected in tubes, vortexed for 5 seconds every 5 minutes while incubating on ice for 15 minutes. This was followed by centrifugation at 14,000 rpm for 10 minutes at 4°C. For lysates from xenografts tumors, frozen tissue was sliced on dry ice with a scalpel,

weighed and approximately 20 mg was homogenized in 200µl NETN lysis buffer with inhibitor cocktails in individual tubes on ice. After homogenization, samples were briefly sonicated twice for 20 seconds each and incubated on ice for 30 minutes, followed by centrifugation at 14,000 rpm for 15 minutes at 4°C. Supernatants were then collected and protein concentrations were determined by the Bradford colorimetric assay (Bio-Rad 500-0205). Based on the concentrations, samples were prepared by mixing with distilled water, 4x Laemmli sample buffer (Bio-Rad 161-0747) and β-mercaptoethanol (Sigma-Aldrich, M3148) and heated at 95°C for 5 minutes on a heat block, cooled at room temperature for 5 minutes and then spun down at 12,000rpm for 2 minutes. 10 to 30 µg of protein were separated in precast Mini PROTEAN TGX gradient (4-15%) gels (Bio-Rad, 456-1085) by sodium dodecyl sulphate-polyacrylamide gel electrophoresis (SDS-PAGE, (Bio-Rad 1658006)) under reducing conditions and transferred (Bio-Rad 1703930) onto 0.45µm polyvinylidene fluoride membrane (Millipore, IPVH00010) for detection. Dual-color protein standard was added next to samples to estimate molecular weights on all gels (Bio-Rad 161-0374). Membrane blots were incubated for 1 hour in blocking buffers containing 5% non-fat dry milk or 5% bovine serum albumin (Sigma, A9647) in 1X TBS-T (Tris buffered saline with 0.1% tween-20)(10X TBS, BioRad, 170-6435). Blots were then incubated overnight with primary antibodies (**Table 3** for full list and dilutions) at 4°C on a gentle shaker followed by washing in 1X TBS-T and incubation with a horseradish peroxidase secondary antibody for 1 hour. After washing, enhanced chemiluminescence (ECL) reagent (Perkin Elmer, NEL104001EA) was added to the membrane and protein bands were detected on the ChemiDoc™ Imaging System. In cases that required blots to be probed again, Restore PLUS Western Blot Stripping

Buffer (Thermo Fisher Scientific, 46430) was used for 15 minutes at room temperature with gentle shaking followed by blocking and antibody incubation. Image densitometry was performed using the Image Lab software (Bio-rad, version 5.2.1). Relative phosphorylated protein expression was calculated by dividing the signal intensity value of the phosphorylated protein bands by that of the corresponding total protein band. Relative expression compared to control was obtained by dividing the relative phosphorylation expression of each condition by that of the control. Relative expression compared to control was subsequently plotted on the y-axis.

Table 3. Antibody list and dilutions

Primary Antibody	Company	Catalog#	Dilution
phospho-Ret (Y905)	Cell Signaling Technology	3221	1,000
phospho-Ret (Y1062)	Santa Cruz Biotechnology	20252-R	250
phospho-Akt (S473)	Cell Signaling Technology	4060	1,000
phospho-Erk (T202/Y204)	Cell Signaling Technology	4370	1,000
phospho-Mek	Cell Signaling Technology	9154	1,000
phospho-p70-S6	Cell Signaling Technology	9234	500
Ret	Cell Signaling Technology	14698	1,000
V5 tag	Cell Signaling Technology	13202	1,000
Akt	Cell Signaling Technology	9272	1,000
Erk	Cell Signaling Technology	9102	1,000
Mek	Cell Signaling Technology	9126	1,000
p70-S6	Cell Signaling Technology	2708	500
Actin	Sigma-Aldrich	clone AC-15	10,000
Ki-67	Spring Biosciences	M3062	400
cleaved-caspase 3 (D175)	Cell Signaling Technology	9661	200
Secondary Antibody	**Company**	**Catalog#**	**Dilution**
rabbit IgG HRP conjugated	Cell Signaling Technology	7074	1,000
mouse IgG HRP conjugated	Santa Cruz Biotechnology	sc-2005	10,000

Clonogenic assay

Cells were counted and seeded at 150 cells per well in 6-well plates and incubated for 14 days. Fresh media was supplemented every 3-4 days. After 14 days, cells were washed with 1X phosphate buffered saline and colonies were stained with crystal violet solution (2% crystal violet dissolved in 20% methanol, Sigma-Aldrich, C6158) for 20 minutes. Wells were gently rinsed with distilled water, plates were allowed to dry and colonies were visualized using ChemiDoc™ Imaging System (Bio-rad, 12003153). Colonies greater than 50 cells were counted using a cell counter (National Institutes of Health, ImageJ program) for comparison between groups.

Drug response assays

Drugs. ATP competitive multi-kinase inhibitors with activity against RET based on published IC-50 values were evaluated and cabozantinib (S1119), sorafenib (S1040), and vandetanib (S1046) were purchased from Selleck Chemicals. The chemical structures are shown in **Figure 4**. *In vitro* stock solutions were prepared in DMSO at concentrations of 10 mM (or 5 mM for vandetanib) and further serially diluted in cell culture media to prepare working solutions based on the experiment. Stock solutions were aliquoted and stored at -80°C. *In vivo* cabozantinib stocks were freshly formulated as 6 mg/ml suspensions in sterile 0.9% sodium chloride (saline) by bath sonication for each use. Trastuzumab was obtained from the Rutgers Cancer Institute of New Jersey Research Pharmacy in solution that was ready to use *in vivo* and was stored at 4°C and used within 2 weeks after opening.

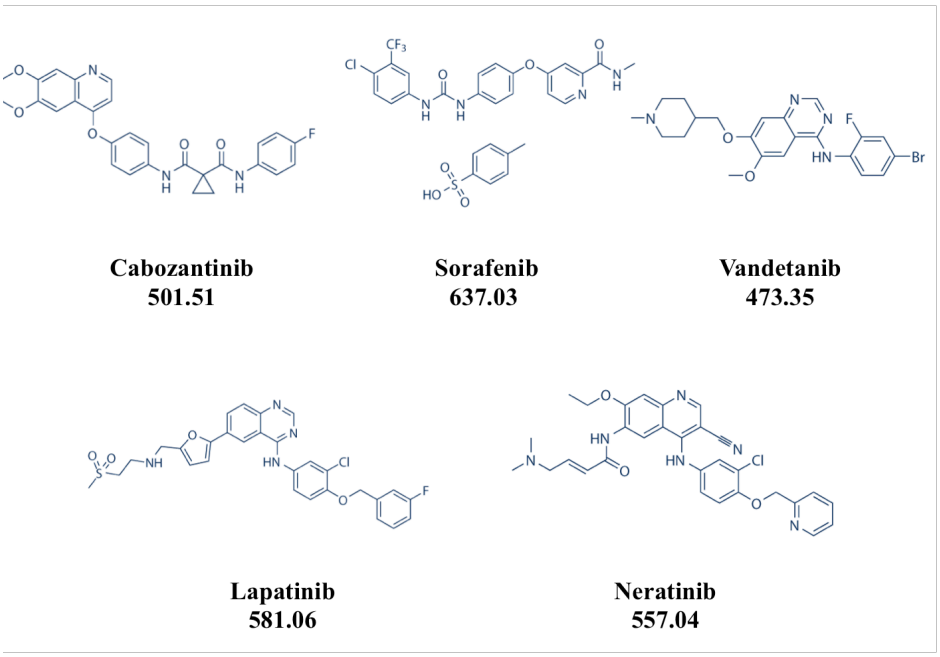

Figure 4. Chemical structures of RET and HER2 inhibitors with molecular weights

Drug sensitivity. Cell viability was measured using the CellTiter 96 Aqueous Non-Radioactive Cell Proliferation reagent (Promega G5430). After optimizing based on growth rates and time duration of experiment, 5,000 MCF10A cells expressing RET alterations or 1,000 NCOA4-RET and 2,000 vector, RET^{amp}, and ΔRET cells for NIH/3T3 stable cells were allowed to attach per well in clear, flat bottom 96-well plates overnight under normal culture conditions. Cells were then treated with increasing concentration of inhibitors in the range of 0 – 20 μM for 72 hours. After incubating with 20 μl of the MTS reagent per well for 2-4 hours at 37°C, absorbance was measured at 490 nm on a plate reader (Infinite 200 PRO NanoQuant, Tecan). For each plate, cells were treated with each drug concentration in triplicate. After subtraction of background signal from the blank wells (containing media alone, no cells), viability of cells was calculated by dividing the average absorbance of treatment wells by that of vehicle DMSO-treated

wells. Data was analyzed and dose-response curves were generated using GraphPad Prism version 7 software.

Clonogenic inhibition in response to drugs. For experiments involving inhibitor treatment, cells were incubated with inhibitor (cabozantinib or vandetanib (Selleck Chemicals)) at increasing concentrations or DMSO control media for 10 – 14 days prior to crystal violet staining using the aforementioned protocol. Fresh media with drug was replaced every 3-4 days.

Ret kinase and signaling inhibition. To study changes in fusion signaling under the influence of Ret inhibitor cabozantinib (Selleck Chemicals), cells were counted and plated at a density enough to reach 80% confluence on the day of treatment. Cells were serum-starved for 24 hours in DMEM media, treated with increasing concentrations of cabozantinib up to 1 μM for 1 hour unless mentioned otherwise and isolated for immunoblotting. Protein bands and image densities were compared to vehicle DMSO-treated controls.

Xenograft generation and drug treatment

All experiments were performed under the approval of the Rutgers Institutional Animal Care and Use Committee, approval# 15-080.

Cell line derived xenografts. Transduced NIH/3T3 cells were suspended in a 1:1 ratio in high concentration Matrigel basement membrane matrix (Corning, 354248) and injected subcutaneously in 6-8 week old, female, athymic nude mice (Taconic, CrTac: NCr-Foxn1^{nu} (NCr Nude) or NOD/SCID/interleukin 2 receptor γ null mice (The Jackson Laboratory, NOD.Cg-Prkdc^{scid} Il2rg^{tm1Wjl} /SzJ (NSG)). For tumor formation, 1 x 10^6 cells

were injected for all three RET altered cell lines in nude mice. For RET^{amp}, tumor formation was further examined at 4.5 x 10^6 cells in NSG mice. Tumors were monitored twice weekly by palpation and tumor dimensions were measured using digital calipers (VWR). Tumor volumes were calculated using the formula ½ x (length x $width^2$), where width is the smaller of the two measurements by calipers. For drug treatment, 0.5 x 10^6 NCOA4-RET cells and 5 x 10^6 ΔRET and RET^{amp} cells were injected bilaterally into dorsal flanks of athymic nude mice and were allowed to form palpable tumors before randomization. Allocation to treatment groups (n=5 for NCOA4-RET and n=7 for ΔRET and RET^{amp} studies per group) was performed when average tumor volumes measured about 300mm^3 using simple randomization with stratification and blinding to group allocation. Cabozantinib was dosed orally at 30 mg kg^{-1} or 60mg kg^{-1} once daily for 14-16 days and was formulated in sterile saline as described previously. Tumor measurements and body weights were recorded thrice weekly for each animal upon initiating treatment. At the end of the treatment, all mice were euthanized and tumors were weighed. A portion of the tumor was snap frozen in liquid nitrogen and then stored at -80°C for future protein analysis as described in the Immunoblotting methods. Remaining portion of the tumor was preserved for histology and immunohistochemistry analysis as described further below.

Patient-derived xenograft. Rutgers Institutional Review Board approved generation of xenograft from patient tumor tissue. A viable portion of resected tumor tissue obtained from index case #3 after palliative mastectomy was divided into samples of equal size, minced, suspended in high concentration Matrigel basement membrane matrix (Corning, 354248) and implanted into the left and right mammary fat pads of three

immunodeficient NSG mice (The Jackson Laboratory). This was repeated for two successive generations to generate adequate tumor for sufficient number of mice for the drug treatment experiment. Tumor formation was monitored twice a week and dimensions were measured using digital calipers (VWR). Tumor volume was calculated using the formula ½ x (length x width^2). Prior to the random assignment of mice to treatment groups, mice were allowed to form palpable tumors with volume in the range of 100 – 200mm^3. Depending on the assigned groups, mice were dosed daily by oral gavage with cabozantinib at 60 mg kg^{-1} for 30 days or received 50 mg kg^{-1} of trastuzumab by intraperitoneal injections twice weekly, every 3-4 days or received a combination of both the cabozantinib (60 mg kg^{-1}) and trastuzumab (50 mg kg^{-1}) treatments. Control mice did not receive any drug treatment. Mice not receiving cabozantinib received an equal volume of sterile saline orally. Tumor and body weight measurements were recorded thrice weekly for each animal. After the completion of treatment duration, the remaining mice were euthanized and tumors were measured and weighed. A portion of the tumor was snap frozen in liquid nitrogen and then stored at -80°C for protein analysis as described in the Immunoblotting methods. Remaining portion of the tumor was preserved for histology and immunohistochemistry analysis as described below. **Patient-derived cell line** was generated and validated using methods described in Pham et al.[94] Tumorigenicity of cell lines was verified by injecting 200µl containing 3 x 10^6 cells suspended in a 1:1 ratio with high concentration Matrigel basement membrane matrix (Corning, 354248) into flanks of three 8 week-old female NSG mice.

Histology and Immunohistochemistry

Xenograft tumors were excised and fixed in 10% buffered formalin overnight and then stored in cold 70% ethanol at 4°C before paraffin embedding. Hematoxylin and eosin (H&E) staining and immunohistochemistry (IHC) were performed on 5-μm-thick formalin-fixed paraffin-embedded sections prepared by the Rutgers Cancer Institute of New Jersey Biospecimen Repository and Histopathology Service. Immunohistochemical staining was prepared using a Ventana XT Discovery automated staining device according to manufacturer's protocol. Primary antibodies Ki-67 (Spring Biosciences M3062), Cleaved-Caspase 3 (Cell Signaling Technology 9175) were used at 1:400 and 1:200 dilutions respectively.

Statistical analysis

Data is expressed as mean ± standard deviation (s.d.), unless otherwise indicated. Statistical analysis was performed using Prism, version 7.0d (GraphPad software). All experiments including three or more groups were analyzed using one-way ANOVA or two-way ANOVA for two variables. Multiple comparisons were performed using Tukey's test. Results with p-value < 0.05 was considered statistically significant in all experiments.

CHAPTER THREE: Results

Genomic profiling identifies recurrent alterations of *RET* in breast cancers

The landscape of *RET* genomic alterations in 9,693 breast cancer samples was assessed as part of hybrid capture-based next-generation sequencing of up to 405 cancer-related genes including select introns of up to 25 genes. Samples were sequenced to a high uniform depth of coverage (median exon coverage, 637x). Median patient age was 54 years (range: 20-88) (**Table 4**) and all samples were from female patients. Tissue for genomic profiling was obtained from the breast for 3,859 patients (40%) and from metastatic sites for 5,834 patients (60%).

RET genomic alterations were observed in 1.2% (121/9,693) of independent breast cancer cases. One case harbored two *RET* alterations (*RET* amplification and *RET* rearrangement), resulting in a total of 122 *RET* genomic alterations were identified including 16 rearrangements, 25 missense mutations, and 81 amplifications (median copy number = 8, copy number range = 6-21) (**Figure 5, Table 4, Supplementary Table 1**). ER status, based on immunohistochemistry, was available for 81% (98/121) of *RET* altered cases and HER2 *(ERBB2* amplification) status, based on genomic profiling, was available for all cases (**Figure 5, Table 4**). *RET* genomic alterations were detected across all breast cancer subtypes although a majority were ER- (65%) or *ERBB2* non-amplified (82%). In comparison to cases with other types of *RET* genomic alterations (**Table 4**), the subset of cases with *RET* missense mutations were more frequently ER+ (71%) (p=0.0002*,* Fisher's exact test, two-tailed). *RET* rearrangements were more frequently ER- (75%) (p=0.1615, Fisher's exact test, two-tailed), as were *RET* amplifications (75%) (p=0.0077, Fisher's exact test, two-tailed). For the 121 *RET*-altered cases, the most

frequent altered genes that co-occurred with *RET* were *TP53* (80%), *MYC* (32%), *PIK3CA* (26%), *ERBB2* (20%), *MCL1* (20%), and *PTEN* (17%), which are known to be frequently altered in breast cancer (**Table 5**).

Table 4. Clinicopathologic characteristics of *RET* altered breast cancers

Characteristics		**All breast cancer cases**	***RET* altered cases**	***RET* activating rearrangement**	***RET* uncharacterized rearrangement**	***RET* missense mutation**	***RET* amplification-on**
Number of cases (n)		9693	121	8	8	25	81
Median age (range), years		54 (20-88)	56 (31-85)	61.5 (54-66)	60 (48-69)	52 (33-71)	54 (28-85)
Median Tumor Mutational Burden (range), mutations/Mb		3.6 (0-251.4)	4.5 (0-36.6)	5.2 (0.9-7.2)	4.5 (1.8-17.1)	3.6 (0-36.6)	4.5 (0-16.2)
Sequenced sample: site of origin	Breast (n)	3859	49	4	4	7	34
	Metastasis (n)	5834	72	4	4	40	47
ER	Positive	N.A.	34 (34.7%)	2 (25%)	2 (25%)	15 (71.4%)	16 (25%)
	Negative	N.A.	64 (65.3%)	5 (75%)	5 (75%)	6 (28.6%)	48 (75%)
	Unknown	8221	23	1	1	4	17
ERBB2	Amplified	1019 (10.5%)	22 (18.2%)	1 (12.5%)	1 (12.5%)	5 (20.0%)	15 (18.5%)
	Non-amplified	8674 (89.5%)	99 (81.8%)	7 (87.5%)	7 (87.5%)	20 (80.0%)	66 (81.5%)

ER, Estrogen Receptor status measured by routine clinical immunohistochemistry
ERBB2 gene amplification status by genomic profiling
ER and *ERBB2* represented as numbers (%)
N.A. not applicable; Mb, megabase

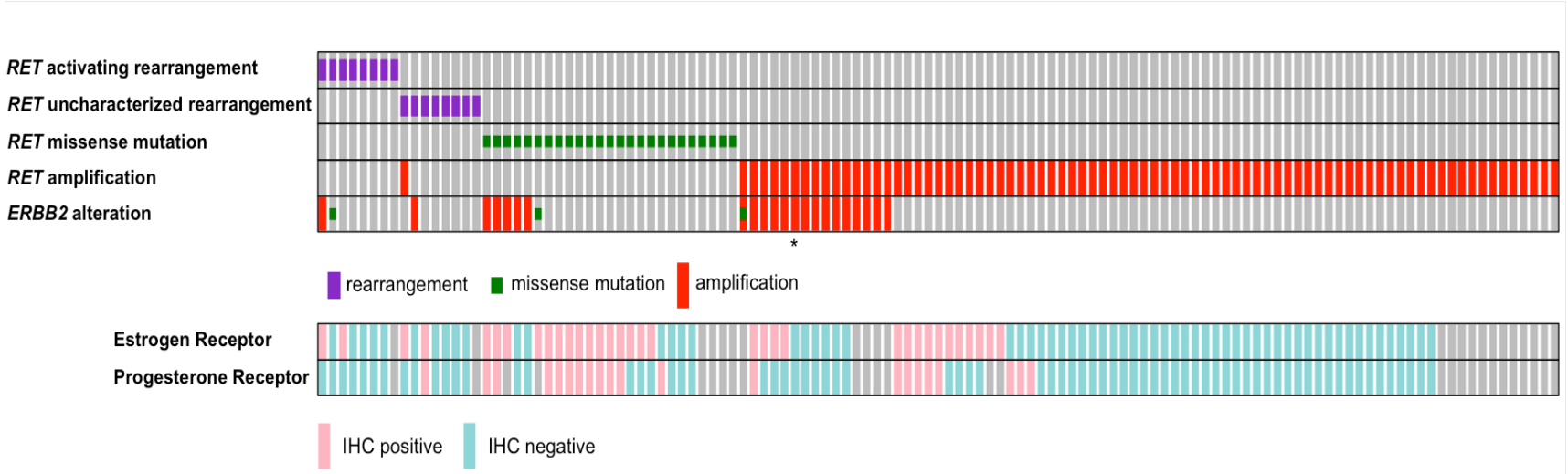

Figure 5. Recurrent RET genomic alterations in breast cancer

OncoPrint of *RET* alterations in breast cancer. A case-by-case comparison of 121 independent breast cancers (column) carrying either a *RET* activating or uncharacterized rearrangement, missense mutation or amplification (rows) to their *ERBB2* amplification status (row) by clinical genomic profiling and available ER (Estrogen Receptor), PR (Progesterone Receptor) status (rows) from routine immunohistochemistry, generated using the oncoprint software[91,92]. Only one case harbored both a *RET* rearrangement and a *RET* amplification. * RET protein expression in tissue from case with *RET* amplification in an ER-/PR-/HER2+ breast cancer is verified by western blot (**Figure 23**).

Table 5. Co-event status in *RET* altered breast cancers

Details	**All breast cancer cases**	***RET* altered cases**	***RET* activating rearrangement**	***RET* uncharacterized rearrangement**	***RET* missense mutation**	***RET* amplification**
n	9693	121	8	8	25	81
Median age, years (range)	54 (20-88)	56 (31-85)	61.5 (54-66)	60 (48-69)	52 (33-71)	54 (28-85)
Median TMB, mutations/Mb	3.6	4.5	5.2	4.5	3.6	4.5
ER-positive, n (%)	N.A	34 (34.7%)	2 (25%)	2 (25%)	15 (71.4%)	16 (25%)
ER-negative, n (%)	N.A	64 (65.3%)	5 (75%)	5 (75%)	6 (28.6%)	48 (75%)
ER-unknown, n (%)	N.A	23	1	1	4	17
HER2-positive, n (%)	1019 (10.5%)	22 (18.2%)	1 (12.5%)	1 (12.5%)	5 (20%)	15 (18.5%)
HER2-negative, n (%)	8674 (89.5%)	99 (81.8%)	7 (87.5%)	7 (87.5%)	20 (80%)	66 (81.5%)
Rank-ordered co-occurring genomic alterations: GENE (%, number of altered cases)	*TP53* (56.5%, 5481)	*TP53* (80%, 97)	*TP53* (75%, 6)	*TP53* (87.5%, 7)	*TP53* (72%, 18)	*TP53* (90%, 73)
	PIK3CA (32.5%, 3155)	*MYC* (32%, 39)	*MYC* (38%, 3)	*11q13* (50%, 4)	*ERBB2* (24%, 6)	*MYC* (37%, 30)
	MYC (23.4%, 2269)	*PIK3CA* (26%, 31)	*11q13, ERBB2, GATA3, LYN, PIK3CA, PTEN, RB1 (25% each; 2)*	*FGFR1* (37.5%, 3)	*GATA3* (24%, 6)	*PIK3CA* (30%, 24)

	11q13 (17.4%, 1688)	*ERBB2* (20%, 24)			*MYC* (20%, 5)	*MCL1* (26%, 21)
	ZNF703 (14.2% 1376)	*MCL1* (20%, 24)		*MYC, MYST3, NOTCH1, PIK3CA, PIK3R1, ZNF703* (25% each, 2)	*MAP2K4* (16%, 4)	*ERBB2* (19%, 15)
	FGFR1 (13.9%, 1346)	*PTEN* (17%, 20)			*ZNF217* (16%, 4)	*PTEN (19%, 15)*

n, number of cases; TMB, Tumor Mutation Burden; ER, Estrogen Receptor; HER2, Human Epidermal Growth Factor Receptor 2; N.A not applicable

Rearrangements were identified by hybrid capture using probes for selected hotspot introns (introns 9-11) and all exons of *RET*. Based on detection of breakpoints, all rearrangements retaining intact sequences for *RET* kinase domain coding exons (12-19), with or without N-terminal fusion partner genes were included for the analysis. Out of the 16 *RET* rearrangements identified, 8 were defined as activating fusions, and the other 8 as uncharacterized rearrangements (**Figure 6 and 7**). Of the 8 activating fusion events predicted to contain the kinase domain of RET, seven cases were either *CCDC6-RET* (n=6) or *NCOA4-RET* (n=1) that have been previously characterized as oncogenic[35,95,96] and are recurrent in NSCLC[97] and PTC; one case, Index case#2, harbored the *RASGEF1A-RET* fusion which is subsequently characterized here as functional and activating.

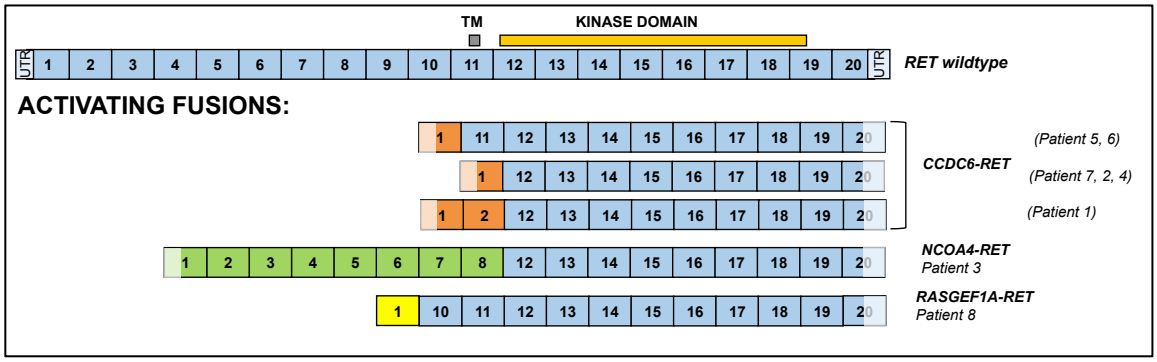

Figure 6. Activating RET fusions

Exon composition comparing full-length, wildtype *RET* with activating fusions identified in this study. Activating fusions maintain the exons (12-19) required for an intact kinase domain. Six patient samples carried the *CCDC6-RET* fusion. *NCOA4-RET* and a novel *RASGEF1A-RET* fusion initially detected in the index cases 1 and 2 and full-length RET were functionally characterized. UTR, untranslated region, TM, Transmembrane domain.

Of the total 8 unique uncharacterized rearrangements identified, novel gene partners, duplications, and truncations were observed (**Figure 7**). One case harbored a

RET-RASGEF1A rearrangement. Although this rearrangement did not include the exons encoding the kinase domain, the similarity of the genomic breakpoints to the *RASGEF1A-RET* fusion (**Figure 6**) suggest the potential for a reciprocal rearrangement event that was not detected but could potentially lead to an activating fusion. One case harbored a *ZNF485-RET* rearrangement where ZNF485 is a putative novel fusion partner; four cases harbored full length *RET* (including the 3' untranslated region or UTR) followed by tandem duplication of the *RET* 3' exons including exons 12-19 that encode the kinase domain; two cases harbored rearrangements with a breakpoint at *RET* intron 11 with exons encoding the kinase domain juxtaposed with intergenic space.

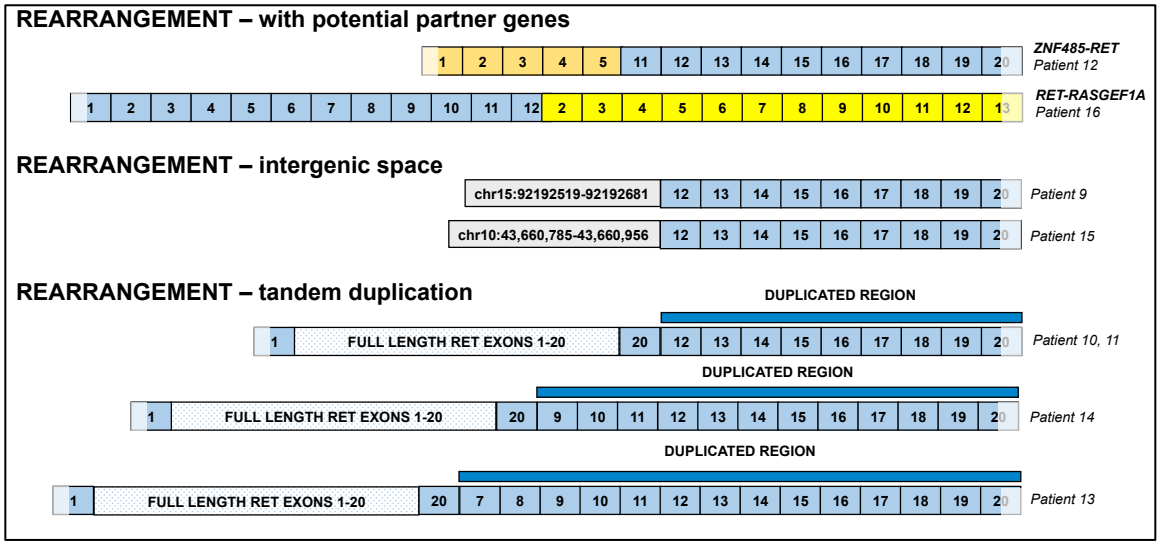

Figure 7. Uncharacterized *RET* rearrangements

Exon composition of rearrangements including *RET* exons fused with novel partner genes (*ZNF485, RASGEF1A*), rearrangements of kinase domain coding exons 12-19 of *RET* into intergenic space, rearrangements resulting in tandem duplications that involve exons 12-19 of *RET*.

Missense mutations in *RET* were detected in 25 cases (**Figure 8**) and the majority were characterized as activating (64%, 16/25). Observed recurrent, *RET* activating point

mutations included the E511K extracellular domain mutation (n=5)[98] and V804M kinase domain mutation (n=4)[99]; other activating mutations that were observed include extracellular domain mutation C611R, C620F, L633V, C634R, C634F, T636M, and the kinase domain mutation M918T[99,100]. The remaining missense mutations have been previously described as somatic in cancer but have not been characterized[101]. *RET* missense mutations are known to be causally associated with MEN2 syndrome (multiple endocrine neoplasia type 2). Using a computational method, missense mutations were analyzed to determine germline versus somatic variant status based on allele frequencies, altered copy number, and tumor purity and further verified using a second algorithm in cases where ploidy was two (**Table 6**)[102,103]. Out of 25 missense mutations, 12 were germline and 7 were somatic. The remaining 6 were categorized as ambiguous and require further analysis using other approaches.

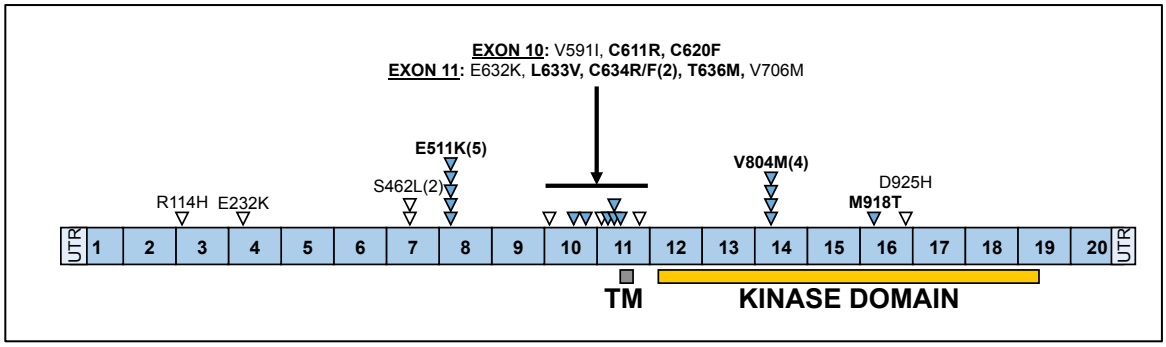

Figure 8. *RET* point mutations

Schematic depicting location and number of the 25 *RET* mutations. Filled triangles and bold font indicate characterized activating mutations based on literature and open triangles represent uncharacterized mutations that have been described as somatic in cancer. Number in bracket represents number of cases.

Table 6. Germline versus somatic variant status of RET missense mutations

Case#	*RET* point mutation	TN %	Allele freq.	Total copies	Altered copies	Status based on SGZ model*	Reported germline associations (level of risk of aggressive MTC) §
17	C634R	30	0.42	2	1	**somatic**	pheochromocytoma, hyperparathyroidism, MTC (Level C)
18	R114H	20	0.5	1	1	ambiguous, CNAmodel	
19	E632K	30	0.4	3	1	germline	
20	C634F	70	0.63	3	1	ambiguous both G, S	pheochromocytoma, hyperparathyroidism, MTC (Level C)
21	V804M	40	0.51	4	2	germline	MEN 2A, MTC (Level A)
22	D925H	40	0.21	2	1	**somatic**	
23	V706M	30	0.59	4	2	ambiguous neither G, S	
24	R600Q	80	0.62	4	3	germline	MTC Level A
25	V591I	30	0.47	2	1	germline	
26	L633V	40	0.46	2	1	germline	
27	S462L	20	0.5	3	2	germline	
28	M918T	25	0.16	2	1	**somatic**	MEN2B, MTC (Level D), either somatic or germline
29	E511K	30	0.35	3	1	ambiguous both G, S	
30	E511K	70	0.46	2	1	germline	
31	E511K	70	0.64	3	2	germline	
32	E511K	20	0.88	2	2	germline	
33	C620F	40	0.31	2	1	ambiguous, CNAmodel	MEN 2A, FMTC, HSCR1
34	S462L	80	0.04	3	1	**subclonal somatic**	
35	V804M	70	0.52	2	1	germline	MEN 2A, MTC (Level A)
36	E511K	70	0.44	4	2	ambiguous, CNAmodel	
37	E232K	60	0.15	4	2	**subclonal somatic**	
38	C611R	60	0.13	2	1	**subclonal somatic**	MTC Level B
39	V804M	25	0.48	2	1	germline	MEN 2A, MTC (Level A)
40	T636M	20	0.03	4	2	**subclonal somatic**	
41	V804M	20	0.51	2	1	germline	MEN 2A, MTC (Level A)

TN=Tumor Nuclei; SGZ=somatic-germline-zygosity; MEN=multiple endocrine neoplasia; MTC= medullary thyroid cancer; FMTC= familial medullary thyroid cancer; HSCR1= hirschsprung's; CNA=copy number alteration; References for *[102,103] and §[104]

Analysis of publically available breast cancer datasets through cBioPortal confirmed similar trends in frequency of *RET* alterations (**Figure 9**)[91,92]. Overall, 1.7% *RET* altered cases were reported from 5,931 sequenced breast cancer cases. A majority of amplifications, followed by missense mutations and other alterations were reported. One fusion (*ERC1-RET*), three truncating mutations, three in-frame mutations, and eight deep deletions were reported. In cases where ER status was available, *RET* amplifications were frequently ER- (78%, $p = 0.005$) and *RET* mutations were frequently ER+ (70%, $p = 0.02$, Fisher's exact test, two-tailed). No significant associations were observed for *ERBB2* status in *RET* altered cases.

Figure 9. RET-altered breast cancer cases from The Cancer Genome Atlas, cBioPortal

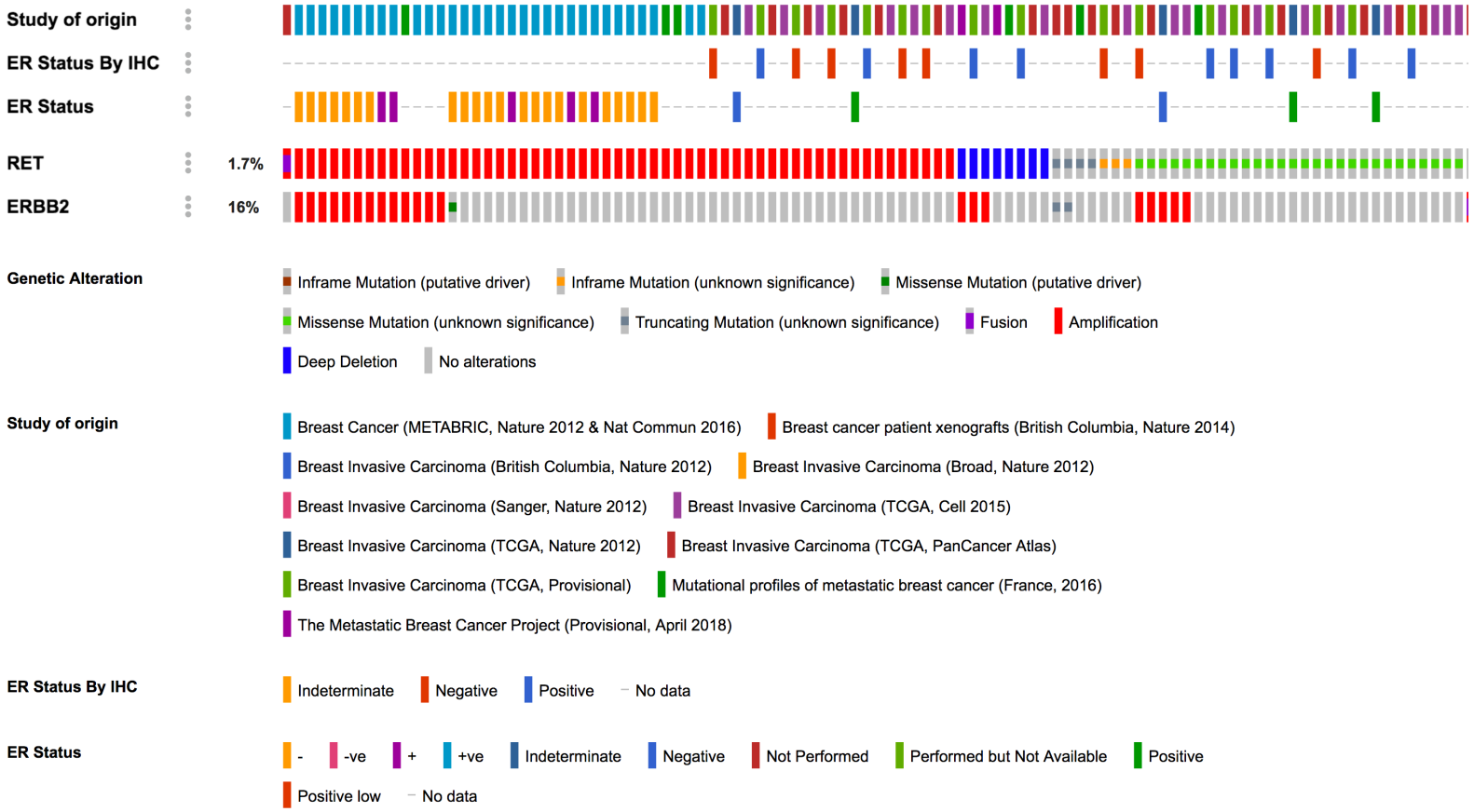

Generation of *RET* fusion constructs for functional analysis

Two *RET* fusions were further analyzed in detail (**Figure 10**). The *NCOA4-RET* fusion detected in Index case #1, in an ER+/PR-/HER2+ breast cancer results from tandem duplication with breakpoints in *NCOA4* exon 8 and *RET* intron 11; includes the *NCOA4* exons encoding a putative coiled-coil domain and the *RET* exons encoding the kinase domain and therefore retains all the functional domains characteristic of an activating NCOA4-RET fusion proteins that have been studied in PTC and NSCLC[95,97,99,105].

The novel *RASGEF1A-RET* fusion detected in Index case #2, in an ER-/PR-/HER2- breast cancer results from an inversion event on chromosome 10 with breakpoints in *RASGEF1A* intron 1 and *RET* intron 9 that juxtaposes the 5'UTR of *RASGEF1A* upstream of the *RET* kinase domain. To characterize the novel *RASGEF1A-RET* fusion, exons 10-19 of *RET* were analyzed for the presence of an alternate internal start site. A methionine codon in exon 11 was identified that could potentially translate an N-terminally truncated RET protein with an intact RET kinase domain and this variant was designated as *ΔRET*. *RASGEF1A* does not contribute to the amino-acid sequence of ΔRET as it only encompasses the 5' UTR of *RASGEF1A*.

ΔRET may also serve to model some of the intergenic *RET* rearrangements depicted in **Figure 7** which are missing exons 1-10 but preserve kinase domain coding exons 12-19. If using an internal methionine codon in exon 12, the intergenic rearrangements would also be N-terminal truncation mutants, similar to *ΔRET*, but missing more N-terminal residues from exon 11 and some kinase domain residues from exon 12. Since they are intergenic rearrangements, unlike *RASGEF1A-RET*, they could

also potentially use alternate transcription initiation mapping prior to *RET* exons and if in-frame, may include an intact RET kinase domain.

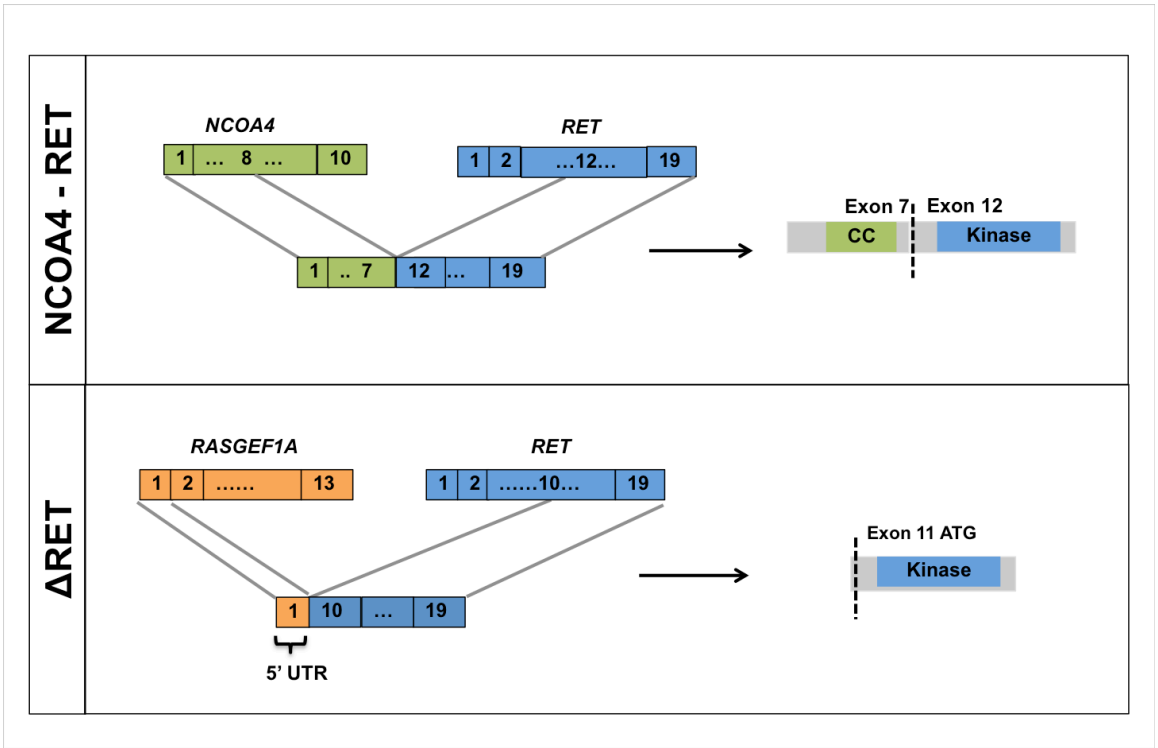

Figure 10. Illustration of index case *RET* fusions, *NCOA4-RET* and *RASGEF1A-RET*

Figure depicting breakpoints in exon 8 for *NCOA4* and intron 11 for *RET* resulting in a product encoding *NCOA4* (exons 2-7) fused to *RET* (exons 12-19). Breakpoints in intron 1 of *RASGEF1A* and intron 9 of *RET* modeled to result in an N-terminally truncated product **ΔRET**, as exon 1 of *RASGEF1A* is part of 5' UTR and exon 11 of *RET* contains a potential alternate start site.

Breast cancer RET alterations constitutively activate RET kinase

NCOA4-RET and *ΔRET* (product of *RASGEF1A-RET*) constructs were expressed in immortalized mouse fibroblasts NIH/3T3 and non-tumorigenic MCF10A human epithelial mammary cells. Full-length, wildtype *RET* was ectopically expressed in order to model *RET* amplification leading to overexpression and is hereby referred to as RET^{amp}. Western blot analysis using an antibody against C-terminus of RET detected NCOA4-RET and ΔRET bands at predicted sizes of 68kDa and 46kDa in the transduced cells respectively and full-length RET^{amp} as expected at 155/175kDa (**Figure 11**).

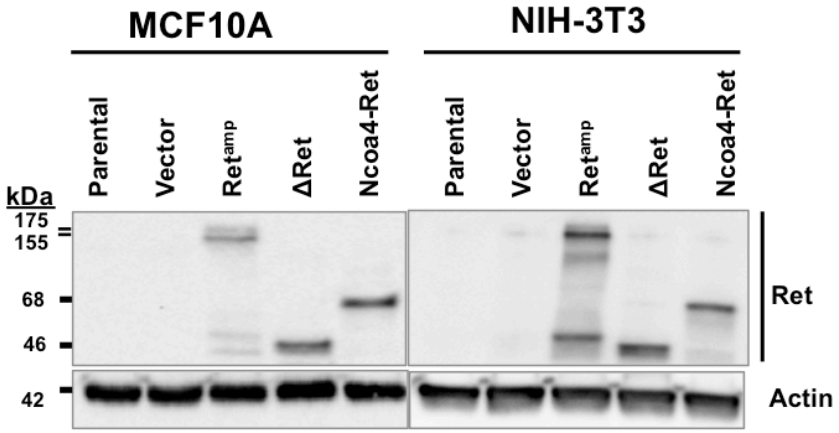

Figure 11. Expression and detection of RET alterations in cell lines

MCF10A (human breast epithelial) and NIH/3T3 (immortalized mouse fibroblasts) cells transiently expressing RET wildtype (RET^{amp}), NCOA4-RET, and ΔRET. Expressed proteins were detected using a C-terminal RET antibody at predicted sizes of 175/155, 68, and 46 kDa respectively. Both MCF10A and NIH/3T3 parental and empty vector cells were negative for RET expression by western blot.

In the absence of growth factor stimulation, expression of NCOA4-RET, ΔRET, and RET^{amp} resulted in phosphorylation at tyrosine 905 (kinase activation loop tyrosine of RET) and tyrosine 1062 (major signaling hub of RET kinase to MAPK and PI3K-AKT pathways) consistent with constitutive kinase activation (**Figure 12**).

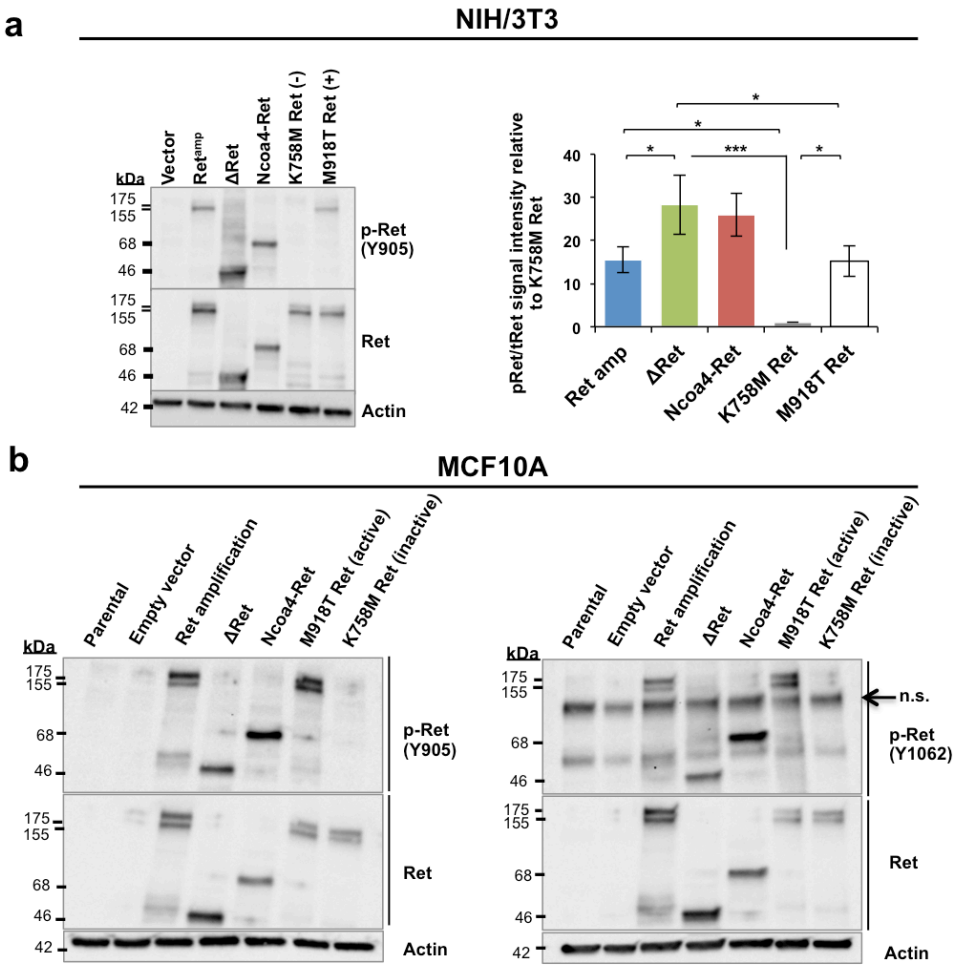

Figure 12. Constitutive kinase activation of RET alterations

Immunoblot analysis of (**a**) NIH/3T3 cells transiently expressing RET^{amp}, ΔRET, and NCOA4-RET reveal phosphorylation at tyrosine residue 905 (**b**) MCF10A cells transiently expressing RET^{amp}, ΔRET, and NCOA4-RET reveal phosphorylation of tyrosine residue 905 (left blot) and tyrosine residue 1062 (right blot). Both cells were harvested in the absence of serum/growth factor stimulation and after serum starvation overnight. Cells expressing constitutively kinase active (M918T) and kinase inactive (K758M) full-length RET variants serve as positive and negative controls respectively. Graph is representative of experiments performed thrice and error bars indicate s.d. (n=3). $p \leq 0.05$ (*), ≤ 0.01(**), ≤ 0.001(***) are statistically significant and analyzed by ANOVA and Tukey's multiple comparisons test. Open-ended brackets depict comparison between the indicated group(s) and each of the groups under the bracket. n.s. in represents non-specific band around 100kDa for the blot on the right in (**b**).

The kinase inactive mutant, K758M-RET, was used as a negative control and the constitutively active kinase mutant, M918T-RET, was used as a positive control[106]. Both mutants were generated by site-directed mutagenesis of the full-length wildtype RET sequence and confirmed by Sanger sequencing. In NIH/3T3 cells, increased signaling in the presence of RET alterations was confirmed for either RAS-MAPK pathway by phosphorylation of MEK or PI3K-AKT pathway by downstream phosphorylation of p70 S6 kinase, thus revealing functional activation of oncogenic pathways (**Figure 13**).

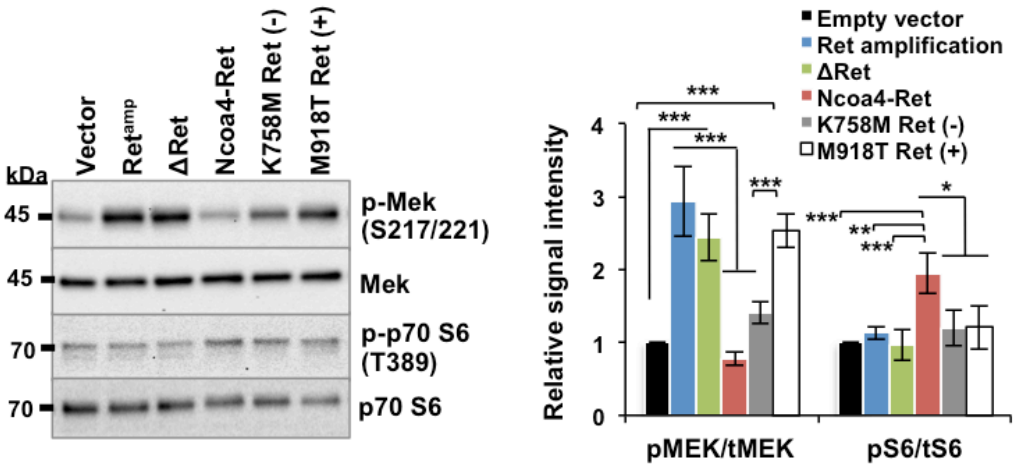

Figure 13. RET alterations are functional

Downstream signaling measured after serum starvation for 24h in transiently expressing NIH/3T3 cells (same lysates as in Figure 11a). Kinase inactive mutant (K758M) and constitutively active mutant (M918T) used as negative and positive controls respectively. Results shown are representative of experiments performed thrice and error bars indicate s.d. (n=3). $p \leq 0.05$ (*), ≤ 0.01(**), ≤ 0.001(***) are statistically significant and analyzed by ANOVA and Tukey's multiple comparisons test. Open-ended brackets depict comparison between the indicated group(s) and each of the groups under the bracket

RET altered cells exhibit increased growth rates and transforming potential

To assess the oncogenic potential, non-tumorigenic NIH/3T3 and MCF10A cells expressing empty vector, RET^{amp}, ΔRET, or NCOA4-RET were evaluated for cell growth and colony formation (**Figure 14**). Expression of both fusions and RET^{amp} resulted in a significantly increased growth capacity in both cells. Increased clonogenic expansion was observed in 3T3-transduced cells when compared to vector control.

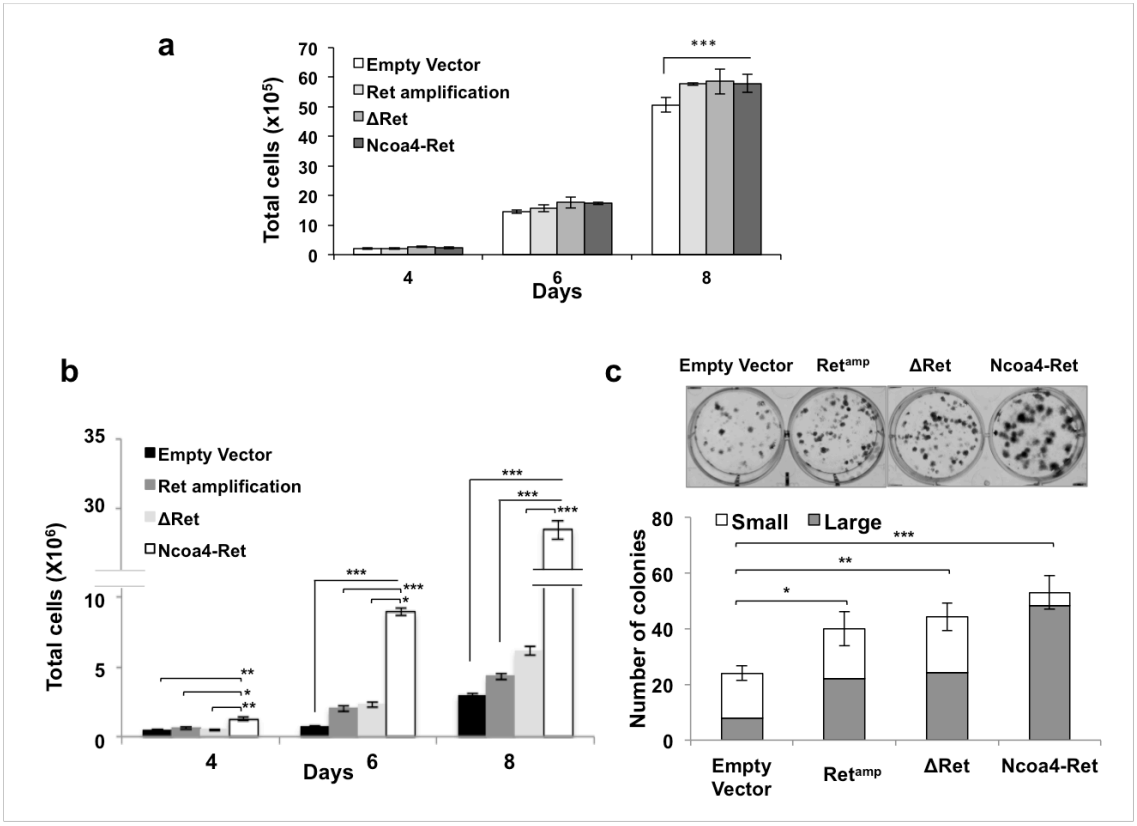

Figure 14. Increased growth and transforming potential of RET altered cells

(a) Growth rates of MCF10A cells transiently expressing RET alterations. Cells at 25,000 per dish were plated in triplicate and counted on days 4, 6, and 8. Stably expressing NIH/3T3 cells show increased (**b**) growth rates and (**c**) clonal expansion compared to cells transduced with vector alone. For growth, 20,000 cells were plated per dish in triplicate and counted at days 4, 6, and 8. For clonogenic analysis, 150 cells were plated per well in triplicate and stained with crystal violet at the end of 14 days. Data represented as mean ± s.d. for n=3 experiments, $p \leq 0.05$ (*), ≤ 0.01(**) and ≤ 0.001(***) between indicated groups after ANOVA (two-way for growth, one-way for colonies) and Tukey's multiple comparison test.

Breast cancer RET fusions are tumorigenic

NIH/3T3 cells stably expressing RET fusions formed tumors in athymic nude mice within 2 weeks of subcutaneous injections (1 million cells, bilateral flank injections) for NCOA4-RET and 5 weeks for ΔRET, whereas vector and RET^{amp} cells did not form tumors when examined for 10 weeks (**Figure 15a**). To further explore tumor formation for RET^{amp} cells, higher numbers (4.5 million cells, bilateral flank), were injected into NOD/SCID/interleukin 2 receptor γ null mice, which is a more powerful immunodeficient model compared to athymic nude mice. RET^{amp} mice formed tumors within 7 weeks whereas matched vector cells did not form tumors when examined for 10 weeks (**Figure 15b**). This suggests that while RET fusions are tumorigenic, constitutive activation of the RET kinase by RET overexpression alone (RET^{amp}) is also capable of driving tumor growth under sufficiently permissive conditions. Immunohistochemistry revealed positive staining for the proliferation marker Ki-67 for RET^{amp}, ΔRET, and NCOA4-RET tumor tissues (**Figure 15c**). Tumor protein was verified for the expression of RET fusions by immunoblot and activation of PI3K-AKT and MAPK pathways was observed (Figure 14d). Based on results from NIH-3T3 stable cell line experiments, all three alterations were confirmed to be tumorigenic. However, NCOA4-RET was observed to be the fastest growing cell line and this translated to tumor formation in less than 2 weeks; whereas, ΔRET and RET^{amp} were slower in comparison, taking longer than a month (**Figures 14b and 15a**).

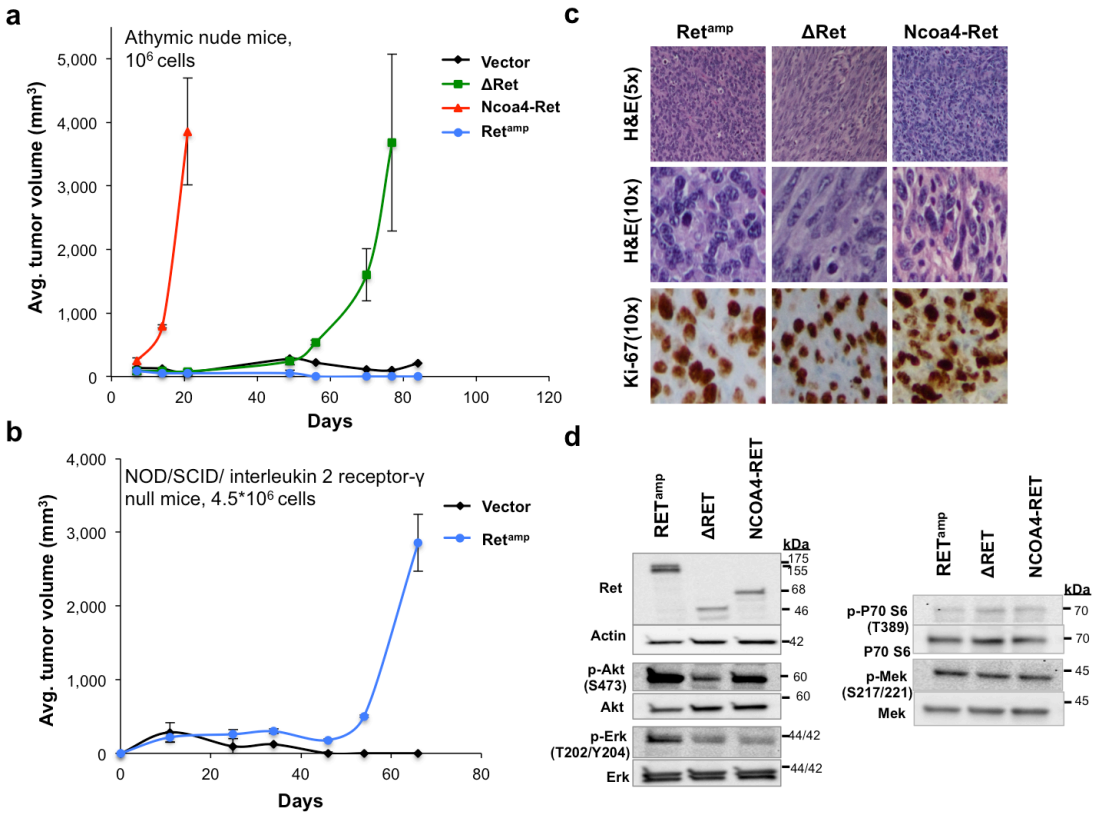

Figure 15. Tumorigenicity of RET altered NIH/3T3 cells

Growth curve of tumors formed upon subcutaneous injection of transduced NIH/3T3 cells at (**a**) 1 x 10^6 cells, bilateral flank injections in athymic, nude mice (n= 4 injection sites for vector, ΔRET, and RET^{amp} and n= 6 injection sites for NCOA4-RET) and (**b**) 4.5 x 10^6 cells, bilateral flank injections in NOD/SCID/ interleukin 2 receptor γ null mice (n= 4 injection sites per group) for vector and RET^{amp} cells. Error bars represent mean ± s.d. (**c**) Representative staining for hematoxylin and eosin (H&E) demonstrates a packed population of tumor cells (top row, x5 magnification). At higher power (middle row, x10 magnification) tumor cells reveal mitoses. Tumor cells stain positive after immunohistochemistry for proliferation marker Ki-67 (bottom row, x10 magnification). (**d**) Immunoblot of tumor protein lysates from NIH/3T3 xenografts for verifying expression using the C-terminal RET antibody and activation of downstream signaling proteins.

Breast cancer RET fusions confer sensitivity to RET inhibition

RET fusions were evaluated for sensitivity to FDA approved kinase inhibitors known to have activity against RET. Cabozantinib and sorafenib effectively reduced viability of both 3T3 stable cell lines and MCF10A breast cell lines transiently expressing RET fusions in a 72-hour antiproliferative MTS assay (**Figure 16**). In order to account

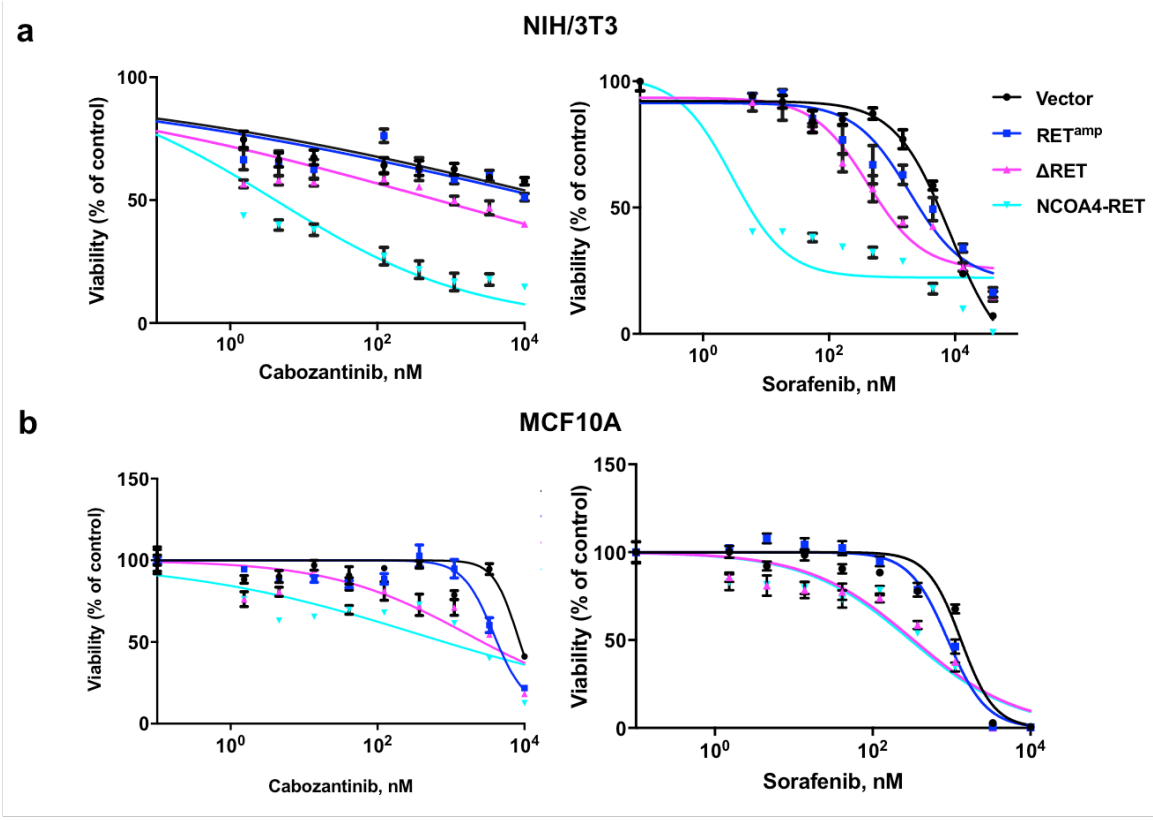

Figure 16. RET fusion expressing cell lines are sensitive to RET inhibitors

Dose-response curves after 72 hours of drug treatment with cabozantinib or sorafenib in: (**a**) NIH/3T3 cells stably and in (**b**) MCF10A cells transiently expressing RET^{amp}, ΔRET, NCOA4-RET, and vector. Cell viability normalized to vehicle (DMSO) treated cells. Error bars indicate s.d. of three replicates and are representative of three independent experiments (n=3).

for differences in growth rate, cell numbers were plated differentially for the 3T3 stable cells to ensure 80% confluence in vehicle-treated wells on the day of viability measurement. In case of MCF10A, equal numbers were plated for all cell lines since

growth differences were not observed between the cell lines at day 4 of the MCF10A growth assay, which coincides with the time duration from plating to reading of the MTS assay and does not confound the drug response results observed (**Figure 14a**). In addition, cabozantinib and another RET inhibitor, vandetanib, were able to effectively inhibit the enhanced colony forming abilities of stable NIH/3T3 RET fusion cell lines and resulted in a significant reduction in size and number of colonies in a dose-dependent fashion in comparison to no-drug treatment and vector control cell lines (**Figure 17**).

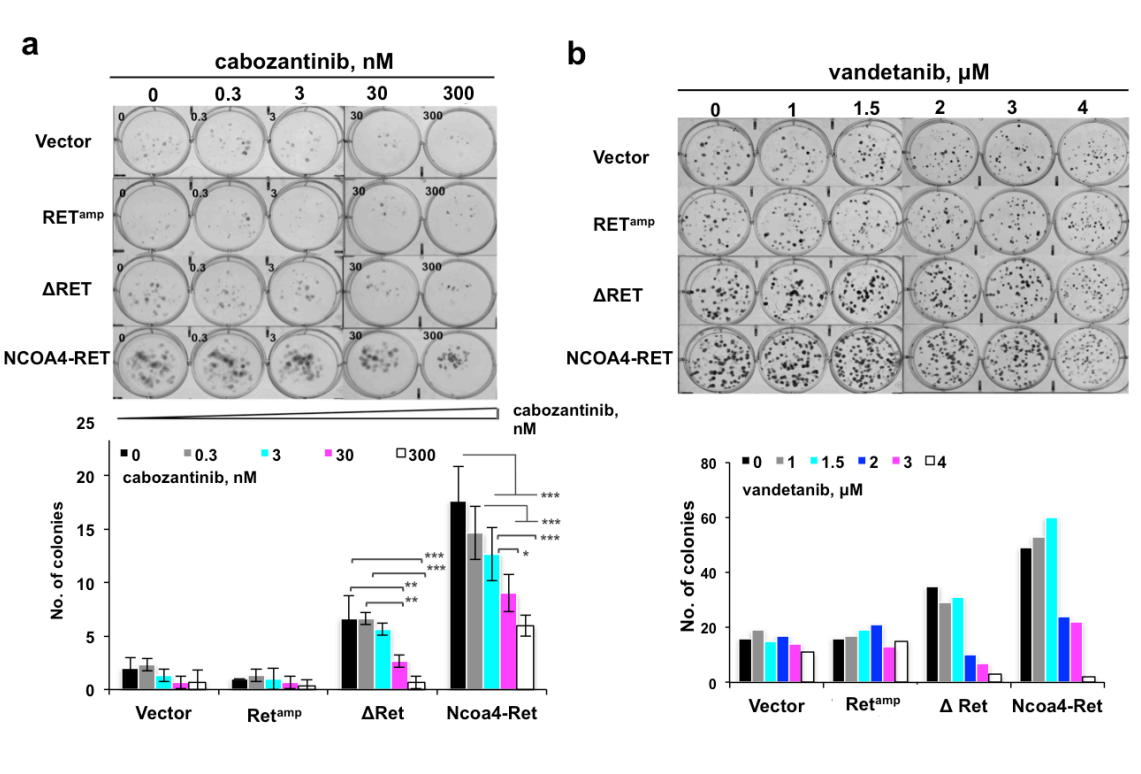

Figure 17. Dose-dependent reduction in ΔRET and NCOA4-RET colony numbers

NIH/3T3 stable cells after 14 days or 10 days of treatment with cabozantinib or vandetanib respectively. 0 represents DMSO controls. All cells were plated at equal numbers per well in triplicates per experiment. Graphs show quantification of colony numbers. Error bars in (**a**) indicate s.d. of three replicate measurements per condition (n=3) and are representative of experiments performed thrice. $p \leq 0.05$(*), ≤ 0.01(**) and ≤ 0.001 (***) by ordinary two-way ANOVA with Tukey's multiple comparisons test. Graph in (**b**) represents average of three replicates per condition in one experiment.

Evaluation with cabozantinib in RET fusion cell lines revealed a dose-dependent reduction in phosphorylation of RET fusion kinase and downstream signals MEK and p70 S6 by western blot (**Figure 18**) suggesting that the effect was driven by RET inhibition. Although tNCOA4-RET decreased slightly in MCF10A cells, a finding shown by others with alternative tyrosine kinase inhibitors (TKIs) in the setting of *RET* point mutations[107], and may be attributable to indirect or an off-target effect of multi-kinase inhibitors, a significant decrease in pNCOA4-RET was verified after normalization to tNCOA4-RET. In order to verify the contribution of off-target signals, comparison to vector cells, which are negative for RET expression by western blot, revealed an increased inhibition of downstream signals in NCOA4-RET which was absent in vector cells at the same conditions, thus suggesting the effect was mainly driven by targeting the RET fusion (**Figure 19).**

Figure 18. Dose-dependent reduction in RET fusion driven signaling Western blot indicating inhibition of RET fusion kinase, MEK and p70 S6 signaling with increasing concentration of cabozantinib in (**a**) NIH/3T3 and (**b**) MCF10A cells transiently expressing NCOA4-RET or ΔRET. Measurements were made after overnight serum/growth factor starvation and 1h incubation with cabozantinib in the absence of serum/growth factor. 0 represents vehicle DMSO treated cells. Graphs represent image densitometry analysis of western blots from three independent experiments (n=3). Ratio of phosphorylated to total proteins is measured at each concentration and mean values with error bars indicating s.d. are plotted relative to DMSO treated control. $p \leq 0.05$(*), ≤ 0.01(**) and ≤ 0.001(***) by ordinary one-way ANOVA with Tukey's multiple comparisons test. Open-ended brackets depict comparison between the indicated group and each of the groups under the bracket. Where brackets are absent, comparison is with DMSO control.

Figure 18. Dose-dependent reduction in RET fusion driven signaling

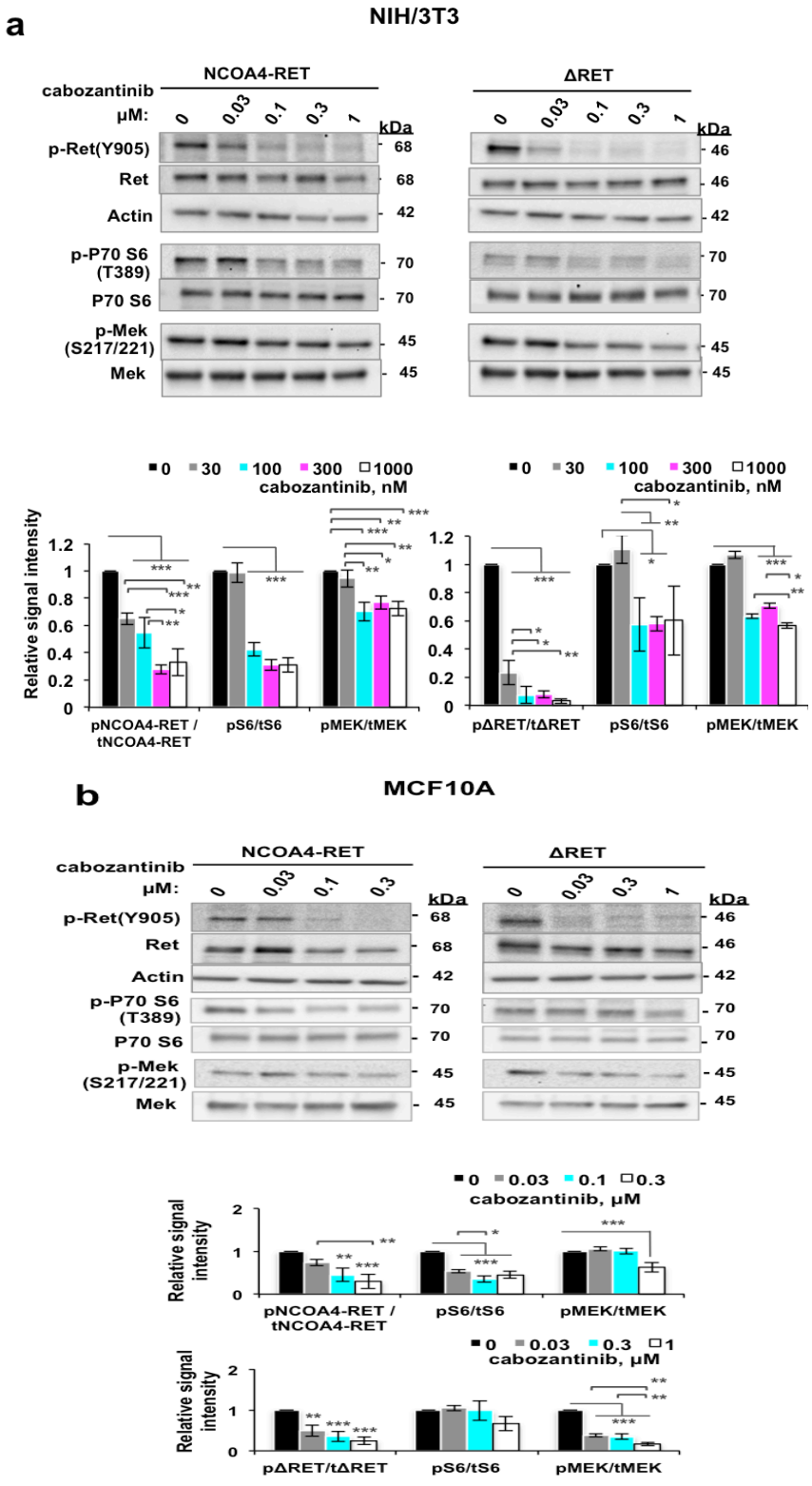

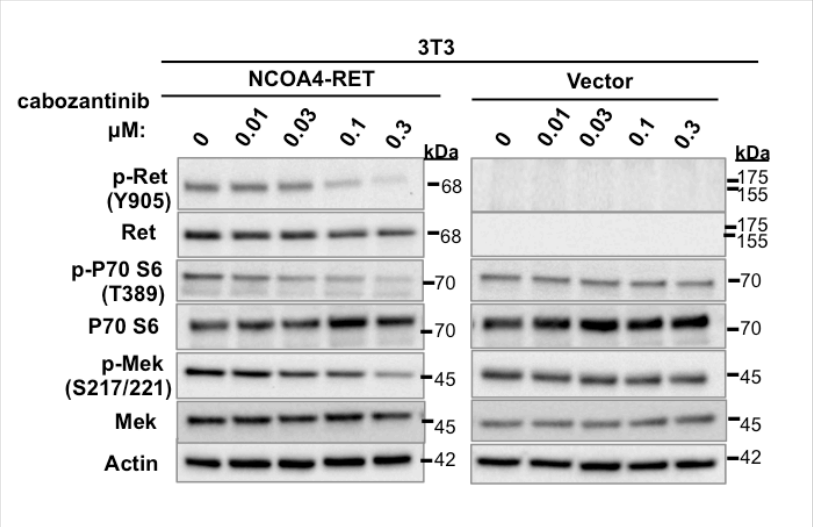

Figure 19. Fusion-specific inhibition of downstream signaling

Immunoblot of NIH-3T3 cells stably expressing NCOA4-RET or vector and dose-dependent inhibition of phosphorylation of RET kinase and downstream signaling with cabozantinib for NCOA4-RET. Measurements were made after 15 minutes of incubation with compound in the absence of serum after serum starvation overnight.

RET-fusion driven tumors respond to anti-RET, multi-kinase inhibitor, cabozantinib

Cabozantinib was used in xenograft models for NCOA4-RET, ΔRET, and RET^{amp} to determine drug response *in vivo.* In order to offset the time for tumor formation, $0.5x10^6$ NIH/3T3 stable cells were used per injection for the NCOA4-RET model, and $5x10^6$ cells for ΔRET and RET^{amp} models in athymic nude mice. In each case, upon tumor formation, mice were randomized into three groups and treated with either a low dose (30mg/kg), high dose (60mg/kg) of cabozantinib, or vehicle saline. Treatment with 60mg/kg and 30mg/kg effectively inhibited tumor growth for NCOA4-RET xenografts and resulted in rapid regression of the tumor within two weeks (**Figure 20a**). In case of ΔRET, both doses inhibited tumor growth and a dose-dependent effect was observed, with the higher dose of 60mg/kg resulting in a more significant reduction when compared to 30mg/kg at the end of two weeks (**Figure 20b**). RET^{amp} xenografts also showed significant reduction in tumor volumes with both doses of cabozantinib in comparison to vehicle, despite increased variability between mice from the same treatment group (**Supplementary Figure 1**). Overall, results indicated that all three RET alterations are sensitive to cabozantinib as evidenced by significant tumor volume reduction.

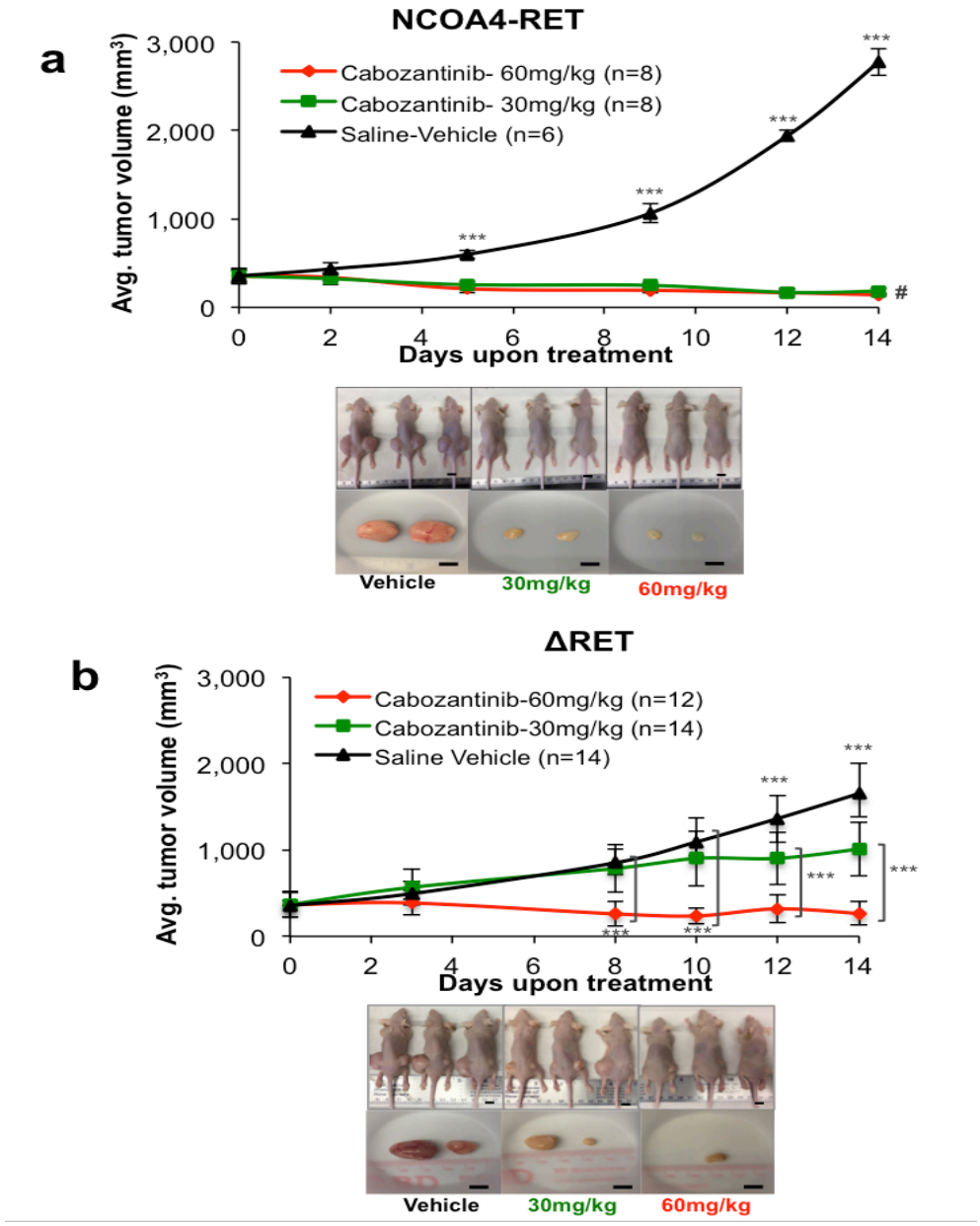

Figure 20. Cabozantinib is effective in inhibiting tumor growth driven by RET fusions in xenograft models

Mean tumor volume was measured in NIH/3T3 xenograft tumors driven by (**a**) NCOA4-RET (n= 8 or 6 injection sites per group) or (**b**) ΔRET (n= 14 or 12 injection sites per group) under treatment with either cabozantinib at 30mg/kg, 60mg/kg, or saline vehicle control for 14 days. Treatment started at day 0. Error bars represent mean ± s.d., ***($p \leq 0.001$) represent comparisons between both treatment groups and vehicle treated controls when depicted above the vehicle curve or between indicated groups and # ($p \leq 0.001$) represents comparisons between day 0 and day 14 for the treatment groups (two-way ANOVA with Tukey's multiple comparison test). Mouse and tumor images are

representatives from each treatment group at the end of study after 14 days of treatment. Scale bars indicate 10mm.

Tumor protein collected at the end of treatment on day 14 for NCOA4-RET and ΔRET revealed significant reduction in the fusion protein levels and downstream AKT signaling for cabozantinib-treated groups as measured by western blot (**Figure 21a**). Histological analysis of the xenograft tissue for NCOA4-RET and ΔRET shows a stark contrast in tumor cellularity between vehicle and treatment groups (**Figure 21b**), supporting the reduction of fusion proteins observed in Fig. 21a. A packed population of highly proliferative cells as revealed by Ki-67 stain in vehicle tissue is efficiently cleared in treatment groups in a dose-dependent manner. The treated tumors reveal hyalinization and apoptosis. Treated tumor tissues stained positive for Cleaved-Caspase 3 whereas vehicle tissue was relatively negative verifying activation of the apoptotic pathway for tumors treated with cabozantinib (**Figure 21b**). Xenograft data with RET^{amp} is suggestive of a benefit; however the large confidence intervals and smaller differences compared to control should be interpreted more cautiously and warrants further exploration (**Supplementary Figure 1**).

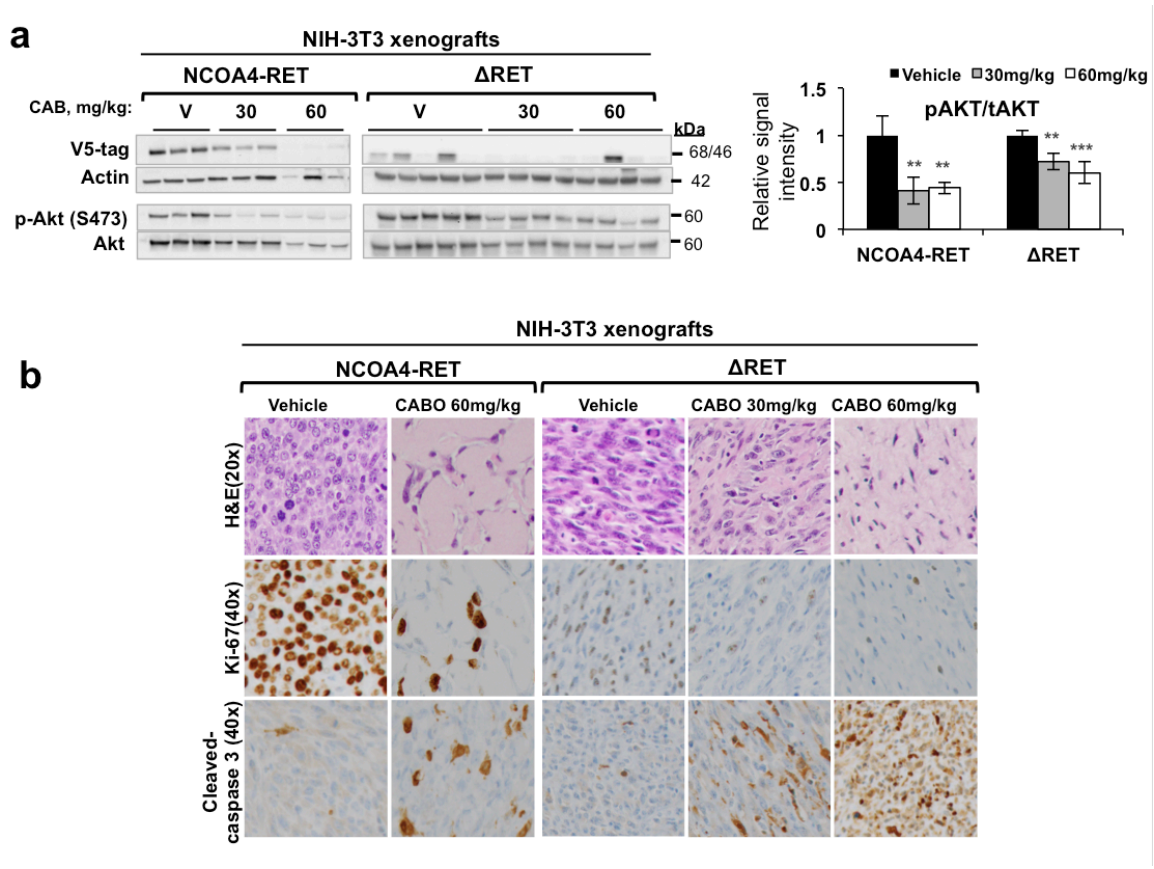

Figure 21. Tumor protein analysis and immunohistochemistry of RET fusion xenografts

(**a**) Immunoblot of tumor protein lysates collected at the end of 14 days of drug treatment reveals reduction in NCOA4-RET, ΔRET (detected by V-5 tag antibody, actin as loading control) and downstream AKT signaling. Mice were treated on the day of tumor harvest for 4 hours with vehicle (V) or cabozantinib (CAB, 30mg/kg or 60mg/kg) and sacrificed. n=3 xenograft samples per treatment condition for NCOA4-RET. n=5 for vehicle, n=4 for 30mg/kg or 60mg/kg for ΔRET. Graph represents image densitometry analysis of western blots. Averages of phosphorylated/total AKT levels with error bars indicating s.d. are plotted relative to average of vehicle. $p \leq 0.01$(**), ≤ 0.001(***) after ordinary one-way ANOVA with Tukey's multiple comparisons test represent comparisons between the vehicle and treatment groups. (**b**) Representative hematoxylin and eosin (H&E) staining of tumor tissue revealing a high grade sarcoma distribution (top row, x20 magnification) and immunohistochemistry of markers Ki-67, Cleaved Caspase-3 for comparison between vehicle and cabozantinib treatment groups in NCOA4-RET and ΔRET xenograft experiments (middle and bottom row, x40 magnification).

Index case#1: NCOA4-RET positive breast cancer responds to cabozantinib

When Index case #1 patient progressed on HER2-targeted treatment with pertuzumab, trastuzumab, and anastrazole, second line therapy including trastuzumab, exemestane, and cabozantinib was initiated. Cabozantinib was added as a genomic-guided targeted therapy based on the *NCOA4-RET* fusion observed in the recurrent tumor (**Figure 22**). The patient was treated initially with 140mg/day of cabozantinib but due to side effects such as shortness of breath, intermittent treatment and dose reduction to 100mg/day was required, and ultimately, treatment had to be discontinued (**Figure 22c**). For a total of 67 days on cabozantinib, which amounts to 80% of duration for second-line treatment, there was a rapid radiographic and clinical response along with improvement in dyspnea and epistaxis. Representative PET/CT images of the thoracic spine lesion (**Figure 22d**), which was present prior to cabozantinib, showed a significant reduction in PET avidity after treatment. Whether the response was due solely to cabozantinib, a change in hormone treatment, or the combination of these therapies cannot be determined with certainty. However, addition of a RET inhibitor to treatment of an ER+/HER2 treatment-refractory, *NCOA4-RET* positive breast cancer resulted in a clinical response.

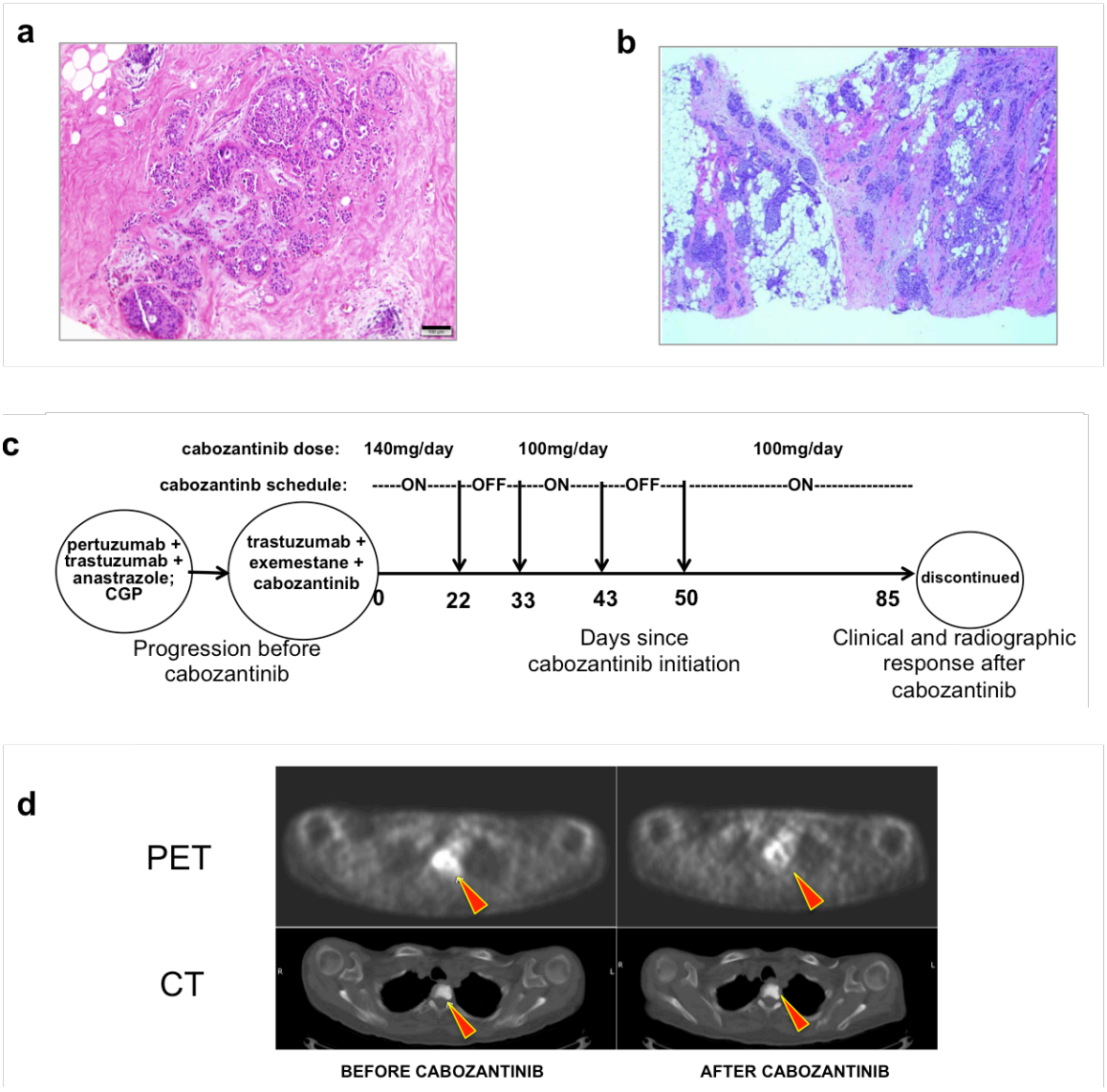

Figure 22. Clinical response to RET targeted therapy in a patient with recurrent, metastatic breast cancer carrying the *NCOA4-RET* fusion

(**a**) Histology image of stage I ER+/HER2- tumor. Scale bar indicates 100µm. (**b**) Histology of the regional/distant recurrence of ER+/PR-/HER2 3+ tumor from the right axillary tail. Genomic profiling on this tissue revealed *NCOA4-RET* fusion (same as patient 3 in Fig.1b). (**c**) Treatment schematic and timeline showing initiation of cabozantinib (day 0) after progressing on HER2-targeted treatment (pertuzumab, trastuzumab) and anastrazole. Targeted genomic profiling identified the presence of *NCOA4-RET* fusion. Based on the finding, cabozantinib, a RET inhibitor, was added along with trastuzumab and exemestane as second-line treatment. Intermittent treatment and dose reduction was required due to side effects. Clinical and radiographic response was observed 85 days after cabozantinib initiation. (**d**) Representative PET (top row) and CT (bottom row) images of thoracic spine lesion (arrows) present before and after cabozantinib treatment. PET signal avidity is reduced after treatment.

Index case #3: RET^{amp} patient -derived xenograft model responds to cabozantinib

RET expression in patient tumor, patient-derived xenograft, and patient-derived cell-line model

Viable patient tumor tissue obtained after palliative mastectomy from index case#3 was implanted into mammary fat pad of three immunodeficient NSG female mice for the generation of patient-derived xenografts (PDX). Successful tumor formation was observed from first-generation and the xenograft tissue was further implanted for a successive passage and also used to generate a patient-derived cell line (PDC) in parallel. The cell line was further validated by subcutaneously injecting cells into NSG mice, which also resulted in tumor formation, referred to as patient-derived cell line xenografts (PDC-X). Comparative histology of tumors from PDX and PDC-X, confirmed the establishment of the patient derived cell line (**Figure 23a**).

Tumor protein harvested from original frozen patient tissue (RET^{amp}–patient), patient-derived xenograft (PDX) and patient- derived cell line (PDC) revealed relatively similar levels of RET protein expression across all samples and confirmed expression of RET in the RET- amplified patient sample and its derivatives (**Figure 23b**). Detection of phosphorylated-RET levels in the same lysates also revealed constitutive activation of the RET kinase in the PDX, PDC and PDC-X models, with very high levels for the patient-derived cell line. Notably, phospho-RET levels in the patient tumor tissue lysate were relatively weak and hard to detect. Of necessary mention critical to this analysis is the difference in freezer storage duration between all the tissue samples before processing for protein, which could be a contributor to phosphorylated protein viability and detection.

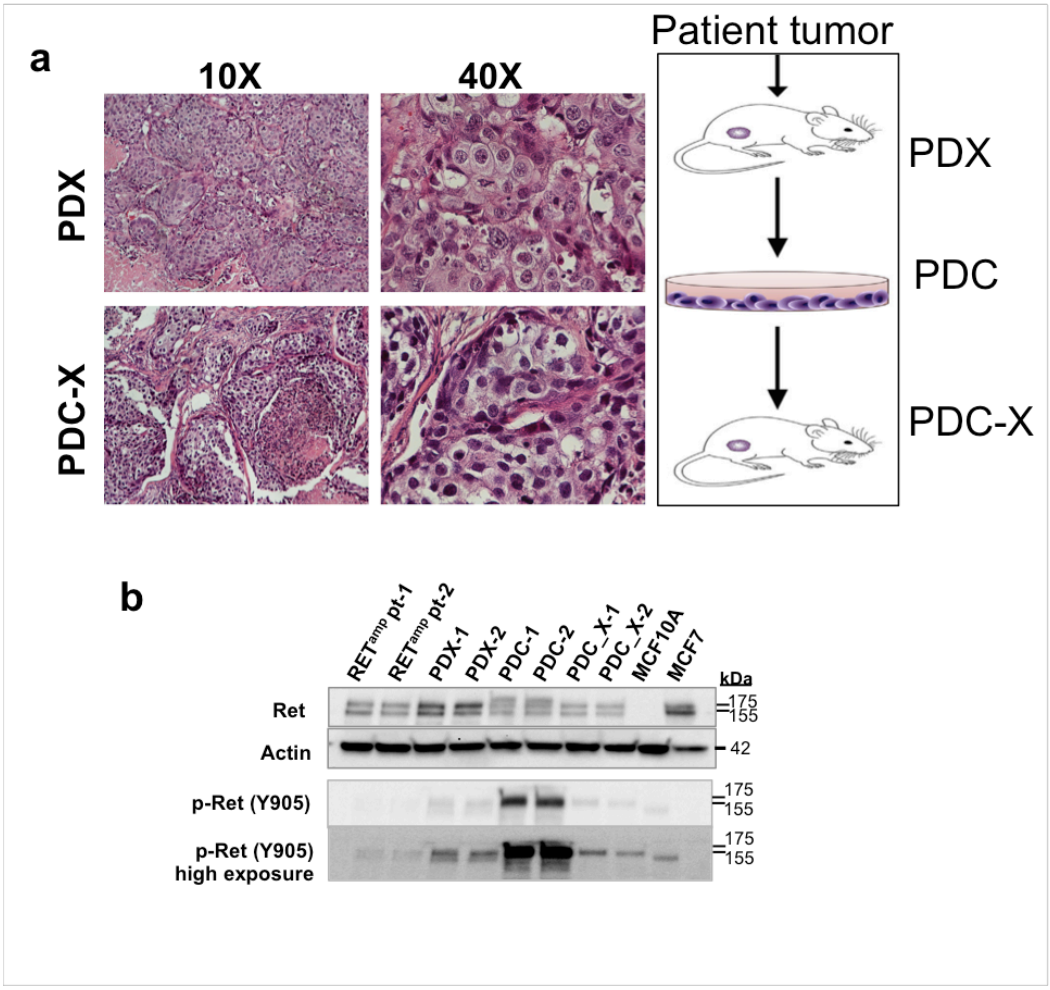

Figure 23. Patient derived xenograft and cell line models for Index case #3

(**a**) H&E analysis comparing patient derived xenograft (PDX) and patient-derived cell line xenograft (PDC-X). 10X and 40X indicate magnification. (**b**) RET protein verification in a patient tissue with RET amplification (RET^{amp} pt, Index case #3, * in Figure 5), RET^{amp} patient-derived xenograft (PDX), RET^{amp} patient-derived cell line (PDC), RET^{amp} patient- cell line derived xenograft (PDC-X); (n=2, where lysates are derived from different location of the same tumor, xenograft, or different passages of cell line), MCF10A breast cells as negative control, MCF7 breast cancer cells as positive control. Actin used as loading control.

Patient tissue sample was frozen at -80 degrees for ~two years before the protein was evaluated, however, other lysates were processed for protein within 1 - 6 months after harvesting. Due to this limitation in this analysis, although the positive phospho-RET signal for the patient-derived samples is present, the absence of the signal in the

patient tissue lysate does not necessarily rule out activated RET signaling in the patient tissue. Further validation with immunohistochemistry may help verify this. Nevertheless, the patient-derived samples revealed activated RET signaling, which is potentially a consequence of the RET amplification.

Cabozantinib elicits tumor growth inhibition in a RET^{amp} patient-derived xenograft model

Second-generation PDX tissue was implanted into mammary fat pads of ten female NSG mice (two implants per mouse) to evaluate the effect of cabozantinib on tumor growth. Mice were treated with cabozantinib (60mg/kg, n=4 tumor sites), trastuzumab (50mg/kg, n=4), a combination of both (n=6), or no treatment (to serve as a control, n=4) for 30 days. In consideration of the small sample size, the combination treatment consisted of full doses of trastuzumab and cabozantinib to mimic the dosing administered in the clinic.

As shown in **Figure 24**, mice receiving no treatment demonstrated the fastest tumor growth and greatest increase in tumor volume. Mice treated with trastuzumab were observed to have a mild reduction in relative tumor size and growth rate in comparison to the control. Cabozantinib alone was able to significantly reduce relative tumor growth in comparison to both the control and trastuzumab groups. The combination of trastuzumab and cabozantinib treatment did not result in any appreciable difference in relative tumor volume compared to treatment with cabozantinib alone.

Additionally, two mice treated with the combination were found dead on day 9 and day 13, and on day 14, a third mouse from the combination was sacrificed due to its poor health. While tumors extracted from these mice were found to have low relative

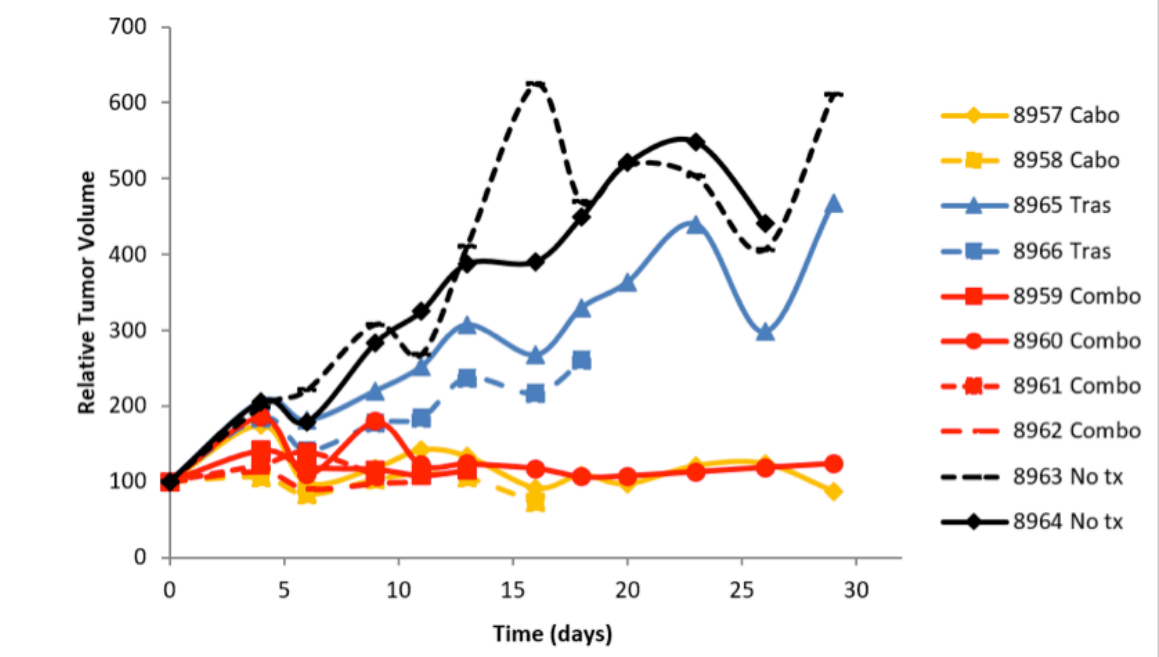

Figure 24. Response to cabozantinib ± trastuzumab in a HER2+/RET^{amp} patient-derived xenograft model from Index case # 3

Each mouse carried two tumors. Mean tumor volume is normalized to day 0 for each mouse. Time indicates days upon treatment. Mice received either biweekly treatment with 50mg/kg of trastuzumab via IP injection, daily 60mg/kg cabozantinib via oral gavage, the combination, or no treatment as a control.

tumor size, the reduction in overall survival suggests toxicity of the combination treatment at the maximal dosage used. Of note, trastuzumab is a monoclonal antibody and, among the multitude of mechanisms that potentially contribute to its therapeutic action and clinical significance, the activation of the immune system is one of them. Since this contribution is lacking in the immunodeficient PDX model, results from this study do not reflect the benefit or lack thereof of combining trastuzumab to cabozantinib in the clinical setting. This could also potentially explain the modest effect seen in the trastuzumab group. Nevertheless, results from this experiment suggest a clear benefit of a RET-targeting inhibitor in the setting of a trastuzumab-resistant, HER2^{amp}/RET^{amp} breast cancer model. It also suggests that the combination at non-adjusted doses may result in

toxicity. It is intriguing to note that Index case #1 received both trastuzumab and cabozantinib at full doses, and although had clinical benefit, had to discontinue combination due to toxicity with reduction in left ventricular ejection fraction. No clear etiology for mouse death was noted in the combination group on dissection, but death was preceded by weight loss.

Hematoxylin and eosin staining of tumor tissue revealed clearance and dying or dead tumor cells in cabozantinib and combination groups, consistent with results from tumor volume measurements (**Figure 25**). Control and trastuzumab tissues showed a relatively healthy and packed population of tumor cells.

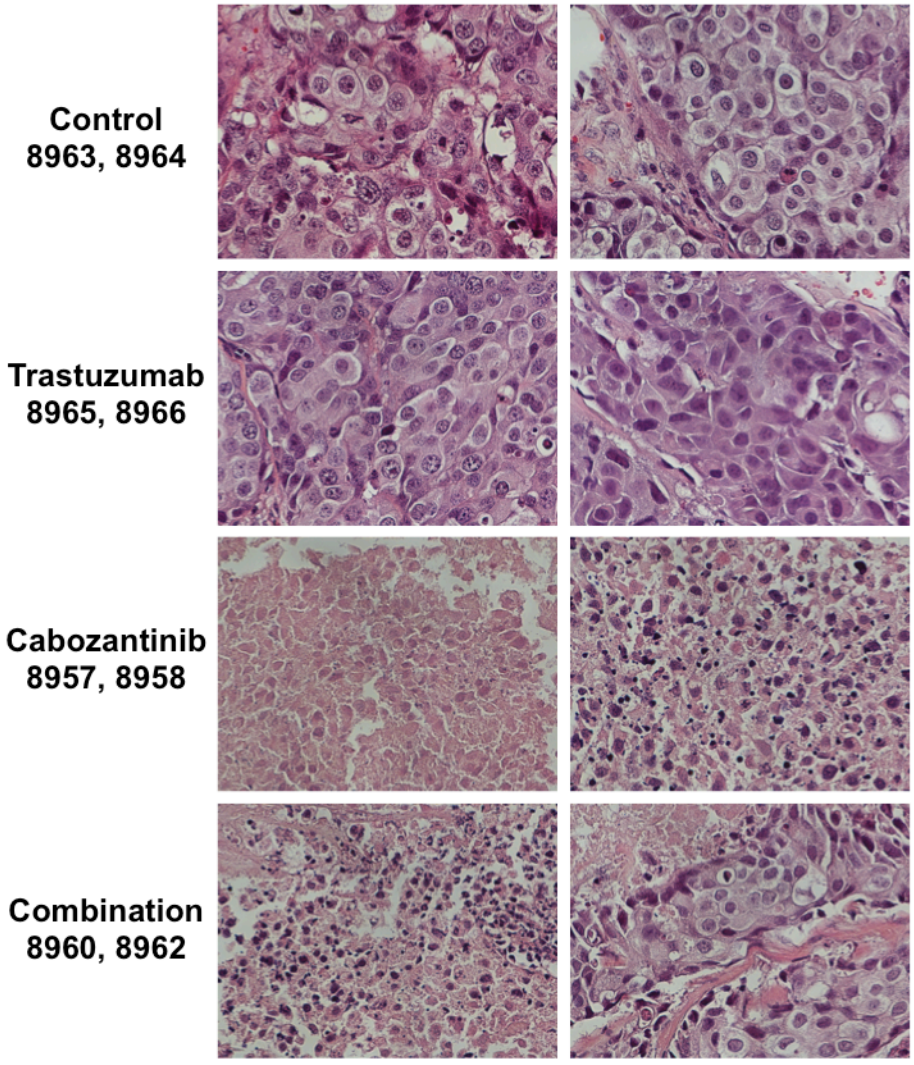

Figure 25. Histology by H&E comparing representative tumor tissues from patient-derived xenograft drug experiment

All images are at 40X magnification. Numbers indicate mouse id and represent tumors harvested from the right side of each mouse.

Drug response to HER2 kinase inhibitors and cabozantinib in patient-derived cell line model

The effect of cabozantinib and HER2 inhibitors on the viability of the patient-derived cell line was assessed in a 72-hour drug response assay. Equal cell numbers were plated in triplicate in collagen I- coated 96-well plates for each concentration per condition. Cells were treated with increasing concentrations of cabozantinib, lapatinib or neratinib alone, or a 1:1 fixed ratio combination of lapatinib + cabozantinib or neratinib + cabozantinib. While cells displayed sensitivity to both HER2 inhibitors, neratinib, an irreversible pan-HER inhibitor, was more effective in comparison with lapatininb, a reversible, dual kinase inhibitor of HER2 and EGFR (HER1) (**Figure 26**). This is not unexpected, especially with reference to the origin of the cell line, which is derived from the patient tumor after the patient had experienced resistance to both trastuzumab and lapatinib. Surprisingly, cabozantinib did not demonstrate sensitivity in this assay, especially considering the positive response observed in the PDX model. In case of combinations, cabozantinib did not add further to the effect observed by using either HER2 inhibitors alone. Apart from *in vitro* versus *in vivo* differences and the duration of exposure to the drug, another explanation is the changes acquired in signaling and contribution of culture conditions in the cell line model. Based on western blot data from **Figure 23**, it is also evident that although RET expression levels are comparable, pRET signaling is very strong for the cell line in comparison to the xenografts, which could be a contribution of cell line establishment and culture/growth factor conditions. Further evaluation in other drug response assays, genomics of PDC, and signaling evaluation may explain the discrepancy between cell line response and xenograft response.

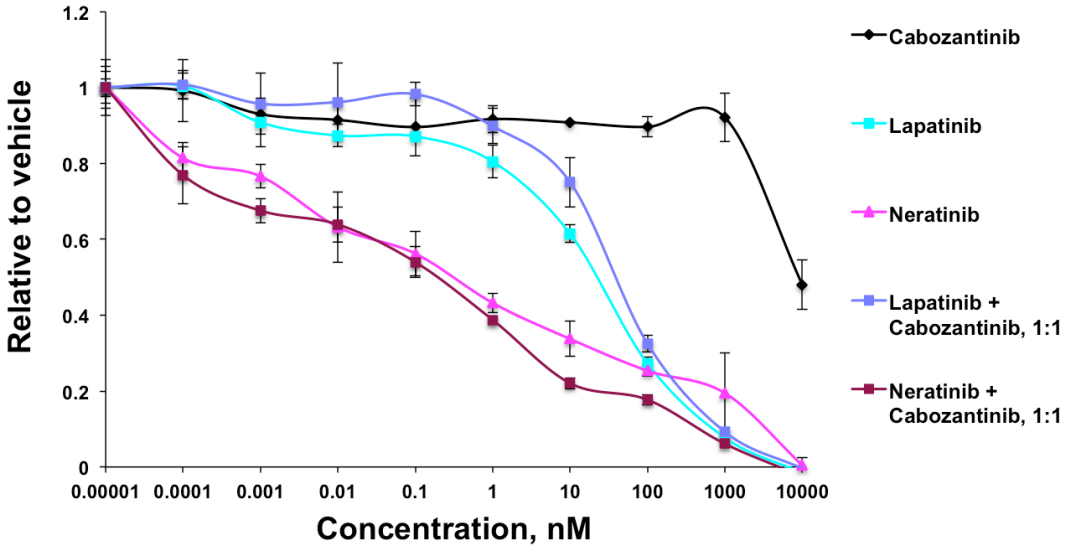

Figure 26. Patient-derived cells (PDC) are sensitive to HER2 targeting kinase inhibitors

Dose-response curves after 72 hours of drug treatment in HER2+/RET^{amp} patient-derived cell line model. Cell viability normalized to vehicle (DMSO) treated cells. Error bars indicate s.d. of three replicates (n=3) from one experiment.

CHAPTER FOUR: Discussion

The clinical benefit of targeted agents in ER+ and HER2+ cases has significantly improved outcomes and survival for patients with these breast cancer subtypes. However, ER+ and HER2+ metastatic breast cancers eventually develop resistance to their targeted therapies resulting in the need for alternative approaches. Similarly, other breast cancer subtypes, such as TNBC, still remain without identifiable therapeutic targets by routine immunohistochemistry or limited targets found with amplicon-based tumor genomic profiling[13,108]. In addition to these challenges, inherent heterogeneity of the disease and response to treatments has rendered breast cancer as one of the leading causes of cancer deaths in women worldwide[109,110].

RET is considered a targetable alteration and although the role of RET overexpression in ER+ breast cancers has been under investigation, a comprehensive analysis of the presence and frequency of recurring *RET* genomic alterations has not been reported. Initial detection of *RET* rearrangements and a *RET* amplification in three independent breast cancers led us to investigate the landscape of *RET* genomic alterations in breast cancers. We conducted an in-depth analysis in a variety of breast cancer subtypes using results from targeted genomic profiling with hybrid capture which includes details of introns 9, 10, and 11 of *RET,* enabling a higher sensitivity for the detection of rearrangements. A total of 9,693 breast cancers were genomically profiled for routine clinical care and were evaluated for the presence of *RET* rearrangements as well as missense mutations and copy number changes. Large sample size, high sequencing depth (>600x), and hybrid capture to identify select introns in *RET*, ensured accurate detection of all classes of genomic variants, robust statistical analyses as well as

validation of rare variants. This resulted in an overall hit rate of 1.2% for *RET* gene alterations in breast cancer. While this may be a relatively small fraction of patients, given that roughly 250,000 new cases of invasive breast cancer are diagnosed in the U.S. alone, annually[111], this extrapolates to roughly 3,000 new cases each year in which *RET* alterations may become potentially relevant therapeutic targets. This is similar to the frequency of *ALK* fusion positive non-small cell lung cancers diagnosed in the U.S. annually[112], which is a highly relevant target in NSCLC. Though we report that 60% of the tumor tissues in this analysis were from metastasis sites, the fraction of advanced disease in this cohort is likely underestimated (**Table 4**) as these assays are often performed on primary breast tumor tissue when distant site tumor tissue is insufficient in quality, quantity, or is inaccessible. Considering the advanced or refractory nature of cases that undergo genomic profiling, identifying a targetable alteration holds promise for these patients who may face diminishing options using standard approaches.

Of all variant classes, *RET* amplifications were the most commonly observed (67% of *RET* alterations) followed by missense mutations and rearrangements. A better understanding of whether this amplification translates into increased mRNA and protein levels in cases where it is detected was needed given its overall frequency in breast cancer. The minimally amplified region around *RET* in this cohort cannot be determined from targeted genomic profiling alone. Therefore, the presence of an amplicon that encompasses another oncogene surrounding *RET* on chromosome 10 cannot be ruled out. Array comparative genomic hybridization (array CGH) studies have previously demonstrated that structural changes such as chromosomal gains or losses occur in all subtypes of breast cancer. 8q24 (*MYC*), 11q13 (*CCND1*), and 17q12 (*ERBB2*) for high-

grade ER+ cancers, and numerous low amplitude gains and losses for triple negative breast cancers are some commonly observed chromosomal features[113-115]. Notably, while *RET* is the only compelling oncogene from the Cancer Gene Census on the 10q11 segment, additional evaluation of this region will be required. A recent study demonstrated that chronic overexpression of *RET* wildtype sequence in an inducible, transgenic mouse model results in luminal mammary tumors that are also responsive to a RET kinase inhibitor[116]. This is highly relevant in case of active *RET* amplifications that will consequently result in chronic overexpression of *RET* wildtype. Our study highlights that the frequent finding of *RET* amplification, its near exclusivity with respect to other *RET* alterations reported here and the known involvement of RET overexpression in tumorigenesis and resistance to hormonal therapies is worthy of follow-up in future clinical datasets and currently available databases with access to detailed genomic, and expression data, treatment, and drug response history.

RET amplifications were mainly found in ER- and *ERBB2*- (*ERBB2* wildtype/HER2-) breast cancers. Conversely, *RET* missense mutations were more frequently associated with ER+ breast cancers. *RET* missense mutations are found as germline mutations in cancer susceptibility syndromes such as MEN2, but may also be somatic as seen in sporadic MTC cases [43]. In each case, algorithms using allele frequency, tumor purity, and ploidy may suggest whether or not a missense mutation is likely germline or somatic, which was evaluated in our cohort. However, clinical care guidelines would include genetic counseling and testing based on the strength of the patient's personal medical and family history[25].

The presence of *RET* missense mutations in ER+ breast cancers, a subset which may be hormone therapy resistant, becomes highly relevant and merits further study given known associations between RET expression levels and resistance to hormonal therapies[77,117]. As genomic profiling cases may be biased toward more aggressive or refractory breast cancers and this cohort was restricted to cases with available ER status, the distribution of *RET* alterations across the subtypes may be skewed and limited in generalization to specific breast cancer subtypes. However, these trends were confirmed to be similar upon analysis of publically available breast cancer datasets through cBioPortal (**Figure 9**).

Our analysis shows that activating *RET* fusions may be more frequent in breast cancer than previously reported. While interchromosomal rearrangements leading to *RET* fusions have been reported in other cancers, all *RET* fusions detected in this cohort reflect intrachromosomal rearrangements in chromosome 10 and were mostly found in ER- breast cancers. The exclusive presence of chromosome 10 partners here may reflect loss of specific DNA damage and repair mechanisms particular to basal-like breast cancers, that have been known to exhibit numerous intrachromosomal rearrangements when compared to luminal subtypes[118].

With *RET* being considered a cancer-relevant gene and a targetable alteration, in case of *RET* rearrangements, there is a need to model and characterize novel structural variants to determine functional significance before their identification can be incorporated appropriately for tailoring therapeutic approaches. Importantly, the novel fusion, *RASGEF1A-RET* that was detected in Index case #2 and functionally characterized as *ΔRET* in our study also serves to model a number of novel

rearrangements identified in this cohort (**Figure 7**). Other rearrangements that need further evaluation are *RET* tandem duplications. Detailed enquiry including intronic sequences and scoring of potential splice regulator sites using validated splice prediction tools may be needed to computationally evaluate if alternative splicing in such cases results in kinase domain duplications at the RNA and protein level. However, that there is a precedent for functional and therapeutically actionable EGFR, MET, BRAF kinase domain duplications in other cancers[119-121] is suggestive that a similar mechanism may be applicable to the observed RET kinase duplications in breast cancer.

Molecular characterization to assess the activity and tumorigenicity of *NCOA4-RET*, *RASGEF1A-RET* and *RET* amplification from three index cases revealed that all three alterations are functional by constitutively activating the kinase and inducing signaling downstream of RET. NCOA4-RET is a known oncogenic alteration of RET based on its prevalence and characterization in the context of PTC and NSCLC. Depending on the breakpoints in the gene, several variants of *NCOA4-RET* have been reported previously[122]. Modeling of the breast cancer *NCOA4-RET* detected in Index case #1 revealed preservation of the key functional domains typical of NCOA4-RET fusions, which includes a putative coiled-coil protein-protein interaction domain contributing to dimerization of the fusion arising from the N-terminal NCOA4 and the intact kinase domain from C-terminal RET. The functional consequence of expressing this fusion confirmed the suspected oncogenic profile in our cell-line and xenograft models, which revealed a highly potent phenotype, driving significantly increased cell and tumor growth and a highly sensitive response to kinase inhibition by RET-targeting drugs, including cabozantinib. In the clinical context for Index case #1, *NCOA4-RET* was detected in an

ER+/*ERBB2*-amplified breast cancer tissue prior to the observed resistance to primary treatment with anastrazole (aromatase inhibitor), trastuzumab, and pertuzumab. Resistance to cancer treatment can arise from tumor evolution resulting in development of fusions, mutations, or amplifications and alternative, by-pass signaling pathways driven by other tyrosine kinases including other receptor tyrosine kinases[123,124]. Due to the lack of an initial response to first-line HER2 targeted treatment, one can speculate that the presence of *NCOA4-RET* contributed to an intrinsic resistance to treatment in Index case #1. Intriguingly, co-existence of *NCOA4-RET* with another HER family member, EGFR (HER1), has been shown as a mechanism of resistance in an *EGFR*-mutated lung cancer treated with afatinib[125]. While Index case #1 patient had a clinical response after switching to second-line, which included cabozantinib, trastuzumab, and an alternative aromatase inhibitor, exemestane, one cannot determine with certainty, based on case information alone, whether that clinical benefit was primarily attributable to initiation of cabozantinib, the new aromatase inhibitor, or the combination of these drugs (**Figure 22c**). In addition, despite a response to second-line treatment, the cabozantinib treatment had to be discontinued due to cardiomyopathy and this suggested adverse effects from the combination. Of relevance to this observation, our PDX model for Index case#3 included a combination arm for cabozantinib and trastuzumab at maximal dose. Although relative tumor growth inhibition was observed in mice from this group, poor health and weight loss leading to death or sacrifice before study completion suggested toxicity from the full-dose combination (**Figure 24**).

By modeling and characterization of the novel and non-canonical *RET* fusion from Index case #2, our work revealed that *RASGEF1A-RET* could employ alternative

transcription initiation, internal to the *RET* exon 11, and lead to an N-terminally truncated protein with an RET kinase domain that is constitutively active, functional, oncogenic and targetable. Although *ΔRET* is missing protein contribution from the partner gene *RASGEF1A,* it would still be under the control of the *RASGEF1A* promoter, a ubiquitously expressed gene, unlike RET, and, its expression level in breast is reported to be high based on human protein atlas data[126]. Modification of transcriptional control, leading to deregulated expression levels of the kinase is a well-known mechanism that contributes to oncogenic activation of fusions, including *RET* fusions[66]. The N-terminally truncated ΔRET, which includes residues 674 to 1072 of RET, includes a portion of the juxtamembrane region, an intact kinase domain and the C-terminal tails. The juxtamembrane (JM) domain is functionally important in regulating auto-inhibitory roles of RTKs[127,128]. For RET, it was recently reported that JM domain contributes toward allosteric catalytic input for kinase activation. Loss or changes in the JM region of RET have been associated with cancer. In-frame insertion/deletion mutations and single base changes in JM domain (666 and 691) have been reported to cause gain-of-function, constitutively active, monomeric RET in familial and sporadic medullary thyroid cancer[55,98,129]. In addition, precedence for activated and targetable, N-terminally truncated tyrosine kinases has been reported for HER2[130] in breast, ALK[131] in melanoma, c-KIT[132] in prostate cancers, and EGFR[133] in gliomas, which lack the extracellular and transmembrane regions, similar to ΔRET. Characterization of *RASGEF1A-RET* (*ΔRET*) also serves to model other intergenic rearrangements of *RET* as those identified in this cohort that may place kinase domain coding exons under the influence of alternate start

sites, promoters, and enhancers, and could potentially render a larger group of breast cancers therapeutically actionable.

Interestingly, characterization experiments that were performed in parallel for RET fusions also revealed a distinction in the degree of phenotypes. Comparison of *NCOA4-RET* and *RASGEF1A-RET* shows that although both fusions induce transformation of non-tumorigenic cells, *NCOA4-RET* has a greater oncogenic potential than *RASGEF1A-RET*. Similar to many *RET* missense mutations, where the oncogenic potential may differ between variants[134], preclinical modeling of *RET* rearrangements shows differing severity of phenotypes associated with expression of the canonical CCDC6-RET and NCOA4-RET fusions[135]. Additionally, even for RET fusions that are under control of dimerizing partners (NCOA4, CCDC6) distinctions in functional pathways employed is reported. This may further differentiate phenotypes of truncated kinases without fusion partners such as ΔRET from NCOA4-RET. The preference of one signaling pathway over another has been reported for NCOA4-RET (previously referred to as RET/PTC3 in thyroid cancer) where enhanced signaling occurs via AKT rather than ERK, although both pathways are activated[136]. This was also observed in our model as shown in **Figure 13**, where, while cells expressing RET^{amp} and ΔRET increased MEK signaling, NCOA4-RET increased S6 kinase signaling. Similarly, comparison of RET and ΔRET phenotypes in our models confirm a contribution from the loss of extracellular, TM, and JM domains in the N-terminally truncated kinase ΔRET, which exhibits a stronger phenotype than the full-length wildtype kinase, RET^{amp}.

Consistent with a recent study which revealed that chronic overexpression of *RET* wildtype sequence in the mammary gland induced tumors [116], our modeling of active

RET amplifications by upregulated expression of the *RET* wildtype sequence constitutively activated the kinase and resulted in tumor formation. Our results also validate that active RET amplifications, similar to RET fusions, lead to aberrant downstream signaling. In index case # 3, a HER2+ breast cancer revealed a *RET* amplification after acquiring resistance to multiple HER2-targeted agents and we verified expression of RET in the resistant tumor, the patient derived xenograft tumor and in the patient-derived cell line (Figure 23). Since an initial response to HER2 targeted therapy was observed, the presence of the RET amplification in the resistant tissue, but its absence prior to initiation of HER2 targeted therapy raises the role of RET amplification in acquired resistance in this case. Owing to crosstalk between RTKs, amplification of RTKs is a known mechanism of resistance to targeted kinase inhibitors in cancers, which enables bypass activation and maintenance of oncogenic signaling[137]. Although RET's involvement in resistance to HER2 treatment is less well characterized in comparison to endocrine resistance in ER+ cancers, crosstalk between RET and HER2 via SRC has been reported. RET mediated SRC hyperactivity induced resistance to trastuzumab while SRC inhibition increased sensitivity to trastuzumab in cell line and xenograft models[138]. This highlights the potential for RET inhibitors to combat resistance in RET+ cases. Our PDX model, which is established from the HER2-targeting treatment resistant tumor in Index case #3, revealed sensitivity to cabozantinib. In addition, mice receiving maximal dose combination of cabozantinib plus trastuzumab experienced weight loss and poor health resulting in death before completion of the study. This highlights the factor of toxicity in combination treatments, where, despite resensitization of resistant tumors, adverse effects may lead to discontinuation. In the *NCOA4-RET*+ index case #1, although

a clinical response from cabozantinib plus trastuzumab was observed after full dose and dose reduction schedules during second-line treatment, the combination was discontinued after 2.5 months due to cardiomyopathy, with reduction in left ventricular ejection fraction (**Figure 22c**). Evaluation of suitable dose-range combinations, combination index values and safety in preclinical models is needed to tailor combination approaches. Utilizing the PDX model, ongoing and future studies from our group aim to investigate if combination of HER2-targeting inhibitors with RET inhibitors further offers an additive or synergistic benefit in targeting resistant tumor growth.

Our drug response assays revealed reduced viability of cells and tumor growth inhibition with anti-RET targeting multikinase inhibitors. Due to the translational relevance of our work, we applied previously approved RET-targeting inhibitors, cabozantinib, vandetanib and sorafenib. Given that cabozantinib was applied in second-line treatment for Index case#1, we pursued our xenograft studies with cabozantinib after confirming sensitivity in RET-fusion expressing cell line models. The goal of these xenograft studies was to individually address response of tumors to cabozantinib (**Figure 20, Supplementary Figure 1**). Since the studies were conducted at the different times and under different conditions, such as number of cells injected per site, direct comparisons cannot be drawn for in vivo drug response studies between them. For instance, the difference in latency of tumor formation between the models guided us to inject 10X more cells for ΔRET and RET^{amp} xenograft drug assays in order to offset the time for tumor formation. This may have attributed to a further increase in variability in response to cabozantinib in comparison to the NCOA4-RET model. However, in each of these studies, the primary goals of the experiment were met and results revealed a

significant reduction in tumor growth in response to a RET-targeting agent, cabozantinib. Further evaluation of RET-specific effect of cabozantinib and the evaluation with more potent and selective RET inhibitors that are under development such as BLU-667, LOXO-292 is required[139,140]. Future testing of RET alterations with these agents is warranted as they report a broad preclinical activity against RET rearrangements and mutations, including gatekeeper mutations, which are resistant to many approved anti-RET inhibitors.

Summary and Conclusions

A detailed investigation into the *RET* genomic landscape of breast cancers using a high-depth, hybrid capture based genomic profiling assay identified recurrent canonical and non-canonical *RET* gene alterations across breast cancer subtypes. Functional characterization for three index case *RET* alterations*, NCOA4-RET*, a canonical fusion, *RASGEF1A-RET*, a non-canonical fusion, and *RET* amplification using non-tumorigenic mouse and human cell-line expression models revealed constitutive kinase activation and downstream signaling and resulted in increased growth rates and tumorigenic phenotypes *in vitro* and *in vivo*. Modeling of the novel *RET* fusion, *RASGEF1A-RET* (*ΔRET*) also identified the potential for a functional role of other non-canonical *RET* rearrangements that may be active and using alternative transcription initiation, leading to N-terminally truncated and active RET kinase. Such rearrangements may be currently underappreciated for their clinical and therapeutic relevance. Additionally, a patient-derived xenograft model for a resistant tumor carrying *RET* amplification revealed increased protein expression in the tumor and sensitivity to a RET inhibitor, highlighting the relevance of *RET* amplifications as an actionable target in refractory breast cancers.

Supporting clinical considerations for targeting *RET* alterations, our study found that RET alterations are sensitive to RET inhibitors, as demonstrated in *in vitro* and *in vivo* models as well as in a patient with an *NCOA4-RET*+ve breast cancer, suggesting that they are potentially actionable in the subset of breast cancers in which they are found. Further studies are warranted to better understand the correlation of *RET* alterations with response to standard therapies and the ideal strategies to therapeutically target RET and improve patient outcomes.

Future Directions

This study details the presence and therapeutic relevance of *RET* gene alterations in breast cancer. With increased genomic profiling of cancers for improving and individualizing treatment strategies, the identification and functional analysis of such alterations recognizes *RET* as a predictive biomarker for RET-targeting alternative therapies in selected breast cancers. Although *RET* has been identified as an oncogene and a molecular target for almost three decades, small molecule inhibitors that have been clinically tested so far were not specifically designed to target RET, but repurposed. Currently approved anti-RET inhibitors are agents that can also effectively target other kinases such as VEGFR2, EGFR, and BRAF, making it difficult to dissect off-target versus RET-specific effects in observed responses. Although it can be argued that some of these effects, such as targeting VEGFR2 which results in anti-angiogenic effects, may offer an added benefit against the tumor, on a clinical level, these off-target effects might also contribute to modest responses and dose-reductions due to increased adverse side effects. Our work, which identifies the presence and relevance of *RET* alterations in breast cancer, further strengthens the case to develop and test more effective and selective RET inhibitors. Further, it also underlines the need to expand eligibility criteria of trials testing such agents in *RET*-rearranged lung cancers to also include *RET*-altered breast cancers.

Our finding of novel rearrangements and functionally active role of the N-terminally truncated ΔRET warrants further investigation into the mechanisms of kinase activation in such cases, which is atypical of known, activating *RET* mutations or fusions. Toward this end, mechanistic understanding of variant functionalities could aid design of

better drugs to target such aberrations. Drug response assays with new RET-targeting agents under development, which exhibit increased RET selectivity, could add more information on their utility against such rearrangements. Further, a better understanding of distinctions in functional pathway activation between such alterations could better predict treatment and potentially combination strategies to avoid or delay targeted treatment resistance. With increasing efficiency and accuracy of genome-editing tools such as CRISPR and inducible expression models, it is anticipated that it would be easier to assess complex genomic rearrangements at more endogenous levels of expression and in the context of tissue type.

Existing evidence for association of RET with endocrine resistance, our finding of RET alterations in the setting of intrinsic or acquired resistance to HER2 therapies in index cases and evidence for crosstalk between RET and ER or HER2 pathways, all warrant a deeper understanding of RET's role in breast cancer, resistance and response to treatment. Retrospective analysis of clinical datasets with access to detailed genomic, expression, treatment, and drug response data histories may provide insights on RET's mutational contribution to resistance for existing therapies. Using PDX models, ongoing and future studies from our group aim to investigate if the combination of HER2-targeted agents with RET inhibitors offers an additive or synergistic benefit over single-agent treatment in inhibiting resistant tumor growth. Overall, as an alternative strategy to existing treatments, our work signifies a role for *RET* genomic alterations as biomarkers for therapeutic response in *RET*+ or *RET*-altered breast cancers and warrants further investigation of resistance mechanisms involving *RET* and breast cancer.

REFERENCES

1. Cancer Facts & Figures 2018. *Atlanta: American Cancer Society* (2018).
2. Toriola, A.T. & Colditz, G.A. Trends in breast cancer incidence and mortality in the United States: implications for prevention. *Breast cancer research and treatment* **138**, 665-673 (2013).
3. Donepudi, M.S., Kondapalli, K., Amos, S.J. & Venkanteshan, P. Breast cancer statistics and markers. *Journal of cancer research and therapeutics* **10**, 506-511 (2014).
4. Comprehensive molecular portraits of human breast tumours. *Nature* **490**, 61-70 (2012).
5. Dieci, M.V., Orvieto, E., Dominici, M., Conte, P. & Guarneri, V. Rare breast cancer subtypes: histological, molecular, and clinical peculiarities. *The oncologist* **19**, 805-813 (2014).
6. Tamimi, R.M.*, et al.* Traditional breast cancer risk factors in relation to molecular subtypes of breast cancer. *Breast cancer research and treatment* **131**, 159-167 (2012).
7. Sørlie, T.*, et al.* Gene expression patterns of breast carcinomas distinguish tumor subclasses with clinical implications. *Proceedings of the National Academy of Sciences* **98**, 10869-10874 (2001).
8. Hirshfield, K.M. & Ganesan, S. Triple-negative breast cancer: molecular subtypes and targeted therapy. *Current Opinion in Obstetrics and Gynecology* **26**, 34-40 (2014).
9. Perou, C.M.*, et al.* Molecular portraits of human breast tumours. *Nature* **406**, 747 (2000).
10. Prat, A.*, et al.* Clinical implications of the intrinsic molecular subtypes of breast cancer. *Breast (Edinburgh, Scotland)* **24 Suppl 2**, S26-35 (2015).
11. Bianchini, G., Balko, J.M., Mayer, I.A., Sanders, M.E. & Gianni, L. Triple-negative breast cancer: challenges and opportunities of a heterogeneous disease. *Nature reviews. Clinical oncology* **13**, 674-690 (2016).
12. Gonzalez-Angulo, A.M., Morales-Vasquez, F. & Hortobagyi, G.N. Overview of resistance to systemic therapy in patients with breast cancer. *Advances in experimental medicine and biology* **608**, 1-22 (2007).
13. Lehmann, B.D.*, et al.* Identification of human triple-negative breast cancer subtypes and preclinical models for selection of targeted therapies. *The Journal of Clinical Investigation* **121**, 2750-2767 (2011).
14. Lehmann, B.D.*, et al.* Refinement of Triple-Negative Breast Cancer Molecular Subtypes: Implications for Neoadjuvant Chemotherapy Selection. *PLOS ONE* **11**, e0157368 (2016).
15. Marotti, J.D., de Abreu, F.B., Wells, W.A. & Tsongalis, G.J. Triple-Negative Breast Cancer: Next-Generation Sequencing for Target Identification. *The American journal of pathology* **187**, 2133-2138 (2017).
16. Adams, S.*, et al.* Phase 2 study of pembrolizumab (pembro) monotherapy for previously treated metastatic triple-negative breast cancer (mTNBC): KEYNOTE-086 cohort A. *Journal of Clinical Oncology* **35**, 1008-1008 (2017).

17. Nanda, R.*, et al.* Pembrolizumab in Patients With Advanced Triple-Negative Breast Cancer: Phase Ib KEYNOTE-012 Study. *Journal of clinical oncology : official journal of the American Society of Clinical Oncology* **34**, 2460-2467 (2016).
18. Vonderheide, R.H., Domchek, S.M. & Clark, A.S. Immunotherapy for breast cancer: what are we missing? *Clinical cancer research* **23**, 2640-2646 (2017).
19. Fan, W., Chang, J. & Fu, P. Endocrine therapy resistance in breast cancer: current status, possible mechanisms and overcoming strategies. *Future Medicinal Chemistry* **7**, 1511-1519 (2015).
20. Osborne, C.K. & Schiff, R. Mechanisms of Endocrine Resistance in Breast Cancer. *Annual Review of Medicine* **62**, 233-247 (2011).
21. Shou, J.*, et al.* Mechanisms of tamoxifen resistance: increased estrogen receptor-HER2/neu cross-talk in ER/HER2-positive breast cancer. *Journal of the National Cancer Institute* **96**, 926-935 (2004).
22. de Melo Gagliato, D., Leonardo Fontes Jardim, D., Marchesi, M.S.P. & Hortobagyi, G.N. Mechanisms of resistance and sensitivity to anti-HER2 therapies in HER2+ breast cancer. *Oncotarget* **7**, 64431-64446 (2016).
23. D'Amato, V.*, et al.* Mechanisms of lapatinib resistance in HER2-driven breast cancer. *Cancer Treatment Reviews* **41**, 877-883 (2015).
24. Cohen, O.*, et al.* Abstract S1-01: Whole exome and transcriptome sequencing of resistant ER+ metastatic breast cancer. *Cancer Research* **77**, S1-01-S01-01 (2017).
25. Hirshfield, K.M.*, et al.* Clinical Actionability of Comprehensive Genomic Profiling for Management of Rare or Refractory Cancers. *The oncologist* (2016).
26. Drilon, A.*, et al.* Response to Cabozantinib in patients with RET fusion-positive lung adenocarcinomas. *Cancer discovery* **3**, 630-635 (2013).
27. Li, G.G.*, et al.* Antitumor Activity of RXDX-105 in Multiple Cancer Types with RET Rearrangements or Mutations. *Clin Cancer Res* **23**, 2981-2990 (2017).
28. Sabari, J.K., Siau, E.D. & Drilon, A. Targeting RET-rearranged lung cancers with multikinase inhibitors. *Oncoscience* **4**, 23-24 (2017).
29. Yoh, K.*, et al.* Vandetanib in patients with previously treated RET-rearranged advanced non-small-cell lung cancer (LURET): an open-label, multicentre phase 2 trial. *The Lancet. Respiratory medicine* **5**, 42-50 (2017).
30. Gelmon, K.A.*, et al.* Use of trastuzumab beyond disease progression: observations from a retrospective review of case histories. *Clinical breast cancer* **5**, 52-58; discussion 59-62 (2004).
31. Waddell, T.*, et al.* Trastuzumab beyond progression in HER2-positive advanced breast cancer: the Royal Marsden experience. *British journal of cancer* **104**, 1675-1679 (2011).
32. Cardoso, F.*, et al.* An exploratory study of sunitinib in combination with docetaxel and trastuzumab as first-line therapy for HER2-positive metastatic breast cancer. *Breast (Edinburgh, Scotland)* **21**, 716-723 (2012).
33. Iwamoto, T.*, et al.* cDNA cloning of mouse ret proto-oncogene and its sequence similarity to the cadherin superfamily. *Oncogene* **8**, 1087-1091 (1993).
34. Mulligan, L.M. RET revisited: expanding the oncogenic portfolio. *Nature reviews. Cancer* **14**, 173-186 (2014).

35. Takahashi, M., Ritz, J. & Cooper, G.M. Activation of a novel human transforming gene, ret, by DNA rearrangement. *Cell* **42**, 581-588 (1985).
36. Airaksinen, M.S. & Saarma, M. The GDNF family: signalling, biological functions and therapeutic value. *Nat Rev Neurosci* **3**, 383-394 (2002).
37. Coulpier, M., Anders, J. & Ibanez, C.F. Coordinated activation of autophosphorylation sites in the RET receptor tyrosine kinase: importance of tyrosine 1062 for GDNF mediated neuronal differentiation and survival. *J Biol Chem* **277**, 1991-1999 (2002).
38. Jain, S., Encinas, M., Johnson, E.M., Jr. & Milbrandt, J. Critical and distinct roles for key RET tyrosine docking sites in renal development. *Genes Dev* **20**, 321-333 (2006).
39. Jijiwa, M.*, et al.* GDNF-mediated signaling via RET tyrosine 1062 is essential for maintenance of spermatogonial stem cells. *Genes Cells* **13**, 365-374 (2008).
40. Plaza-Menacho, I.*, et al.* RET Functions as a Dual-Specificity Kinase that Requires Allosteric Inputs from Juxtamembrane Elements. *Cell reports* **17**, 3319-3332 (2016).
41. Pachnis, V., Mankoo, B. & Costantini, F. Expression of the c-ret proto-oncogene during mouse embryogenesis. *Development (Cambridge, England)* **119**, 1005-1017 (1993).
42. Tsuzuki, T.*, et al.* Spatial and temporal expression of the ret proto-oncogene product in embryonic, infant and adult rat tissues. *Oncogene* **10**, 191-198 (1995).
43. Arighi, E., Borrello, M.G. & Sariola, H. RET tyrosine kinase signaling in development and cancer. *Cytokine & growth factor reviews* **16**, 441-467 (2005).
44. de Graaff, E.*, et al.* Differential activities of the RET tyrosine kinase receptor isoforms during mammalian embryogenesis. *Genes Dev* **15**, 2433-2444 (2001).
45. Santoro, M. & Carlomagno, F. Central role of RET in thyroid cancer. *Cold Spring Harbor perspectives in biology* **5**, a009233 (2013).
46. Schuchardt, A., D'Agati, V., Larsson-Blomberg, L., Costantini, F. & Pachnis, V. Defects in the kidney and enteric nervous system of mice lacking the tyrosine kinase receptor Ret. *Nature* **367**, 380-383 (1994).
47. Srinivas, S., Wu, Z., Chen, C.M., D'Agati, V. & Costantini, F. Dominant effects of RET receptor misexpression and ligand-independent RET signaling on ureteric bud development. *Development (Cambridge, England)* **126**, 1375-1386 (1999).
48. Hwang, D.Y.*, et al.* Mutations in 12 known dominant disease-causing genes clarify many congenital anomalies of the kidney and urinary tract. *Kidney international* **85**, 1429-1433 (2014).
49. Pini Prato, A.*, et al.* Hirschsprung disease and congenital anomalies of the kidney and urinary tract (CAKUT): a novel syndromic association. *Medicine* **88**, 83-90 (2009).
50. Donis-Keller, H.*, et al.* Mutations in the RET proto-oncogene are associated with MEN 2A and FMTC. *Human molecular genetics* **2**, 851-856 (1993).
51. Hofstra, R.M.*, et al.* A mutation in the RET proto-oncogene associated with multiple endocrine neoplasia type 2B and sporadic medullary thyroid carcinoma. *Nature* **367**, 375-376 (1994).
52. Mulligan, L.M.*, et al.* Germ-line mutations of the RET proto-oncogene in multiple endocrine neoplasia type 2A. *Nature* **363**, 458-460 (1993).

53. Asai, N., Iwashita, T., Matsuyama, M. & Takahashi, M. Mechanism of activation of the ret proto-oncogene by multiple endocrine neoplasia 2A mutations. *Molecular and cellular biology* **15**, 1613-1619 (1995).
54. Gujral, T.S., Singh, V.K., Jia, Z. & Mulligan, L.M. Molecular mechanisms of RET receptor-mediated oncogenesis in multiple endocrine neoplasia 2B. *Cancer Res* **66**, 10741-10749 (2006).
55. Cordella, D*., et al.* An in-frame complex germline mutation in the juxtamembrane intracellular domain causing RET activation in familial medullary thyroid carcinoma. *Endocrine-related cancer* **13**, 945-953 (2006).
56. Eng, C*., et al.* Heterogeneous mutation of the RET proto-oncogene in subpopulations of medullary thyroid carcinoma. *Cancer Res* **56**, 2167-2170 (1996).
57. Agrawal, N*., et al.* Integrated Genomic Characterization of Papillary Thyroid Carcinoma. *Cell* **159**, 676-690 (2014).
58. Wang, R*., et al.* RET Fusions Define a Unique Molecular and Clinicopathologic Subtype of Non–Small-Cell Lung Cancer. *Journal of Clinical Oncology* **30**, 4352-4359 (2012).
59. Ballerini, P*., et al.* RET fusion genes are associated with chronic myelomonocytic leukemia and enhance monocytic differentiation. *Leukemia* **26**, 2384-2389 (2012).
60. Hirshfield, K*., et al.* Abstract P3-07-02: Are we missing actionable targets in breast cancer? Novel insights into recurrent Ret alterations. *Cancer Research* **77**, P3-07-02-P03-07-02 (2017).
61. Pietrantonio, F*., et al.* RET fusions in a small subset of advanced colorectal cancers at risk of being neglected. *Annals of oncology : official journal of the European Society for Medical Oncology* **29**, 1394-1401 (2018).
62. Weinreb, I*., et al.* Recurrent RET Gene Rearrangements in Intraductal Carcinomas of Salivary Gland. *The American journal of surgical pathology* **42**, 442-452 (2018).
63. Paratala, B.S*., et al.* Emerging Role of Genomic Rearrangements in Breast Cancer: Applying Knowledge from Other Cancers. *Biomarkers in cancer* **8**, 1-14 (2016).
64. Romei, C. & Elisei, R. RET/PTC Translocations and Clinico-Pathological Features in Human Papillary Thyroid Carcinoma. *Frontiers in endocrinology* **3**, 54 (2012).
65. Kohno, T*., et al.* KIF5B-RET fusions in lung adenocarcinoma. *Nat Med* **18**, 375-377 (2012).
66. Richardson, D.S., Gujral, T.S., Peng, S., Asa, S.L. & Mulligan, L.M. Transcript level modulates the inherent oncogenicity of RET/PTC oncoproteins. *Cancer Res* **69**, 4861-4869 (2009).
67. Zeng, Q*., et al.* The relationship between overexpression of glial cell-derived neurotrophic factor and its RET receptor with progression and prognosis of human pancreatic cancer. *The Journal of international medical research* **36**, 656-664 (2008).
68. Esseghir, S*., et al.* A role for glial cell derived neurotrophic factor induced expression by inflammatory cytokines and RET/GFR alpha 1 receptor up-regulation in breast cancer. *Cancer Res* **67**, 11732-11741 (2007).

69. Boulay, A.*, et al.* The Ret receptor tyrosine kinase pathway functionally interacts with the ERalpha pathway in breast cancer. *Cancer Res* **68**, 3743-3751 (2008).
70. Plaza-Menacho, I.*, et al.* Targeting the receptor tyrosine kinase RET sensitizes breast cancer cells to tamoxifen treatment and reveals a role for RET in endocrine resistance. *Oncogene* **29**, 4648-4657 (2010).
71. Gattelli, A.*, et al.* Ret inhibition decreases growth and metastatic potential of estrogen receptor positive breast cancer cells. *EMBO molecular medicine* **5**, 1335-1350 (2013).
72. Morandi, A., Plaza-Menacho, I. & Isacke, C.M. RET in breast cancer: functional and therapeutic implications. *Trends in molecular medicine* **17**, 149-157 (2011).
73. Kang, J.*, et al.* Artemin is estrogen regulated and mediates antiestrogen resistance in mammary carcinoma. *Oncogene* **29**, 3228-3240 (2010).
74. Andreucci, E.*, et al.* Targeting the receptor tyrosine kinase RET in combination with aromatase inhibitors in ER positive breast cancer xenografts. *Oncotarget* **7**, 80543-80553 (2016).
75. Hatem, R.*, et al.* Vandetanib as a potential new treatment for estrogen receptor-negative breast cancers. *International journal of cancer* **138**, 2510-2521 (2016).
76. Spanheimer, P.M.*, et al.* Distinct pathways regulated by RET and estrogen receptor in luminal breast cancer demonstrate the biological basis for combination therapy. *Annals of surgery* **259**, 793-799 (2014).
77. Spanheimer, P.M.*, et al.* Inhibition of RET increases the efficacy of antiestrogen and is a novel treatment strategy for luminal breast cancer. *Clin Cancer Res* **20**, 2115-2125 (2014).
78. Schlumberger, M.*, et al.* Overall survival analysis of EXAM, a phase III trial of cabozantinib in patients with radiographically progressive medullary thyroid carcinoma. *Annals of oncology : official journal of the European Society for Medical Oncology* **28**, 2813-2819 (2017).
79. Wells, S.A., Jr.*, et al.* Vandetanib in patients with locally advanced or metastatic medullary thyroid cancer: a randomized, double-blind phase III trial. *Journal of clinical oncology : official journal of the American Society of Clinical Oncology* **30**, 134-141 (2012).
80. Schneider, T.*, et al.* Long term analysis of the efficacy and tolerability of sorafenib in advanced radio-iodine refractory differentiated thyroid carcinoma: final results of a phase II trial. *European Journal of Endocrinology* (2012).
81. Drilon, A.*, et al.* Cabozantinib in patients with advanced RET-rearranged non-small-cell lung cancer: an open-label, single-centre, phase 2, single-arm trial. *The Lancet. Oncology* **17**, 1653-1660 (2016).
82. Lee, S.H.*, et al.* Vandetanib in pretreated patients with advanced non-small cell lung cancer-harboring RET rearrangement: a phase II clinical trial. *Annals of oncology : official journal of the European Society for Medical Oncology* **28**, 292-297 (2017).
83. Gautschi, O.*, et al.* Targeting RET in Patients With RET-Rearranged Lung Cancers: Results From the Global, Multicenter RET Registry. *Journal of clinical oncology : official journal of the American Society of Clinical Oncology* **35**, 1403-1410 (2017).

84. Velcheti, V.*, et al.* Phase 2 study of lenvatinib (LN) in patients (Pts) with RET fusion-positive adenocarcinoma of the lung. *Annals of Oncology* **27**, 1204PD-1204PD (2016).
85. Mayer, E.L.*, et al.* Combination antiangiogenic therapy in advanced breast cancer: a phase 1 trial of vandetanib, a VEGFR inhibitor, and metronomic chemotherapy, with correlative platelet proteomics. *Breast cancer research and treatment* **136**, 169-178 (2012).
86. Tolaney, S.M.*, et al.* Cabozantinib for metastatic breast carcinoma: results of a phase II placebo-controlled randomized discontinuation study. *Breast cancer research and treatment* **160**, 305-312 (2016).
87. McLeer-Florin, A.*, et al.* Dual IHC and FISH testing for ALK gene rearrangement in lung adenocarcinomas in a routine practice: a French study. *Journal of Thoracic Oncology* **7**, 348-354 (2012).
88. Tkachuk, D.*, et al.* Detection of bcr-abl fusion in chronic myelogeneous leukemia by in situ hybridization. *Science* **250**, 559-562 (1990).
89. Frampton, G.M.*, et al.* Development and validation of a clinical cancer genomic profiling test based on massively parallel DNA sequencing. *Nature biotechnology* **31**, 1023-1031 (2013).
90. Hartmaier, R.J.*, et al.* High-Throughput Genomic Profiling of Adult Solid Tumors Reveals Novel Insights into Cancer Pathogenesis. *Cancer Res* **77**, 2464-2475 (2017).
91. Cerami, E.*, et al.* The cBio Cancer Genomics Portal: An Open Platform for Exploring Multidimensional Cancer Genomics Data. *Cancer discovery* **2**, 401 (2012).
92. Gao, J.*, et al.* Integrative analysis of complex cancer genomics and clinical profiles using the cBioPortal. *Science signaling* **6**, pl1 (2013).
93. Curradi, M., Izzo, A., Badaracco, G. & Landsberger, N. Molecular mechanisms of gene silencing mediated by DNA methylation. *Molecular and cellular biology* **22**, 3157-3173 (2002).
94. Pham, K.*, et al.* Isolation of Pancreatic Cancer Cells from a Patient-Derived Xenograft Model Allows for Practical Expansion and Preserved Heterogeneity in Culture. *The American journal of pathology* **186**, 1537-1546 (2016).
95. Monaco, C.*, et al.* The RFG oligomerization domain mediates kinase activation and re-localization of the RET/PTC3 oncoprotein to the plasma membrane. *Oncogene* **20**, 599-608 (2001).
96. Tong, Q., Xing, S. & Jhiang, S.M. Leucine zipper-mediated dimerization is essential for the PTC1 oncogenic activity. *The Journal of biological chemistry* **272**, 9043-9047 (1997).
97. Gainor, J.F. & Shaw, A.T. The new kid on the block: RET in lung cancer. *Cancer discovery* **3**, 604-606 (2013).
98. Muzza, M.*, et al.* Four novel RET germline variants in exons 8 and 11 display an oncogenic potential in vitro. *Eur J Endocrinol* **162**, 771-777 (2010).
99. Mulligan, L.M. RET revisited: expanding the oncogenic portfolio. *Nat Rev Cancer* **14**, 173-186 (2014).

100. Silva, A.L.*, et al.* Identification and characterization of two novel germline RET variants associated with medullary thyroid carcinoma. *Endocrine* **49**, 366-372 (2015).
101. Forbes, S.A.*, et al.* COSMIC: somatic cancer genetics at high-resolution. *Nucleic acids research* **45**, D777-d783 (2017).
102. Sun, J.X.*, et al.* A computational approach to distinguish somatic vs. germline origin of genomic alterations from deep sequencing of cancer specimens without a matched normal. *PLoS computational biology* **14**, e1005965 (2018).
103. Khiabanian, H.*, et al.* Inference of germline mutational status and evaluation of loss of heterozygosity in high-depth tumor-only sequencing data. *Journal of Clinical Oncology Precision Oncology* (2017).
104. Marquard, J. & Eng, C. Multiple Endocrine Neoplasia Type 2. in *GeneReviews((R))* (eds. Adam, M.P.*, et al.*) (University of Washington, Seattle (WA), 1993).
105. Okamoto, K.*, et al.* Antitumor activities of the targeted multi-tyrosine kinase inhibitor lenvatinib (E7080) against RET gene fusion-driven tumor models. *Cancer letters* **340**, 97-103 (2013).
106. Hyndman, B.D., Gujral, T.S., Krieger, J.R., Cockburn, J.G. & Mulligan, L.M. Multiple functional effects of RET kinase domain sequence variants in Hirschsprung disease. *Human mutation* **34**, 132-142 (2013).
107. Mologni, L., Redaelli, S., Morandi, A., Plaza-Menacho, I. & Gambacorti-Passerini, C. Ponatinib is a potent inhibitor of wild-type and drug-resistant gatekeeper mutant RET kinase. *Molecular and cellular endocrinology* **377**, 1-6 (2013).
108. Gu, G., Dustin, D. & Fuqua, S.A. Targeted therapy for breast cancer and molecular mechanisms of resistance to treatment. *Current opinion in pharmacology* **31**, 97-103 (2016).
109. Bray, F., Ren, J.S., Masuyer, E. & Ferlay, J. Global estimates of cancer prevalence for 27 sites in the adult population in 2008. *International journal of cancer* **132**, 1133-1145 (2013).
110. Siegel, R.L., Miller, K.D. & Jemal, A. Cancer statistics, 2017. *CA: A Cancer Journal for Clinicians* **67**, 7-30 (2017).
111. DeSantis, C.E., Ma, J., Goding Sauer, A., Newman, L.A. & Jemal, A. Breast cancer statistics, 2017, racial disparity in mortality by state. *CA Cancer J Clin* **67**, 439-448 (2017).
112. Soda, M.*, et al.* Identification of the transforming EML4-ALK fusion gene in non-small-cell lung cancer. *Nature* **448**, 561-566 (2007).
113. Bilal, E.*, et al.* Amplified Loci on Chromosomes 8 and 17 Predict Early Relapse in ER-Positive Breast Cancers. *PLOS ONE* **7**, e38575 (2012).
114. Loo, L.W.*, et al.* Array comparative genomic hybridization analysis of genomic alterations in breast cancer subtypes. *Cancer Res* **64**, 8541-8549 (2004).
115. Nordgard, S.H.*, et al.* Genome-wide analysis identifies 16q deletion associated with survival, molecular subtypes, mRNA expression, and germline haplotypes in breast cancer patients. *Genes Chromosomes Cancer* **47**, 680-696 (2008).

116. Gattelli, A.*, et al.* Chronic expression of wild-type Ret receptor in the mammary gland induces luminal tumors that are sensitive to Ret inhibition. *Oncogene* (2018).
117. Morandi, A.*, et al.* GDNF-RET signaling in ER-positive breast cancers is a key determinant of response and resistance to aromatase inhibitors. *Cancer Res* **73**, 3783-3795 (2013).
118. Kwei, K.A., Kung, Y., Salari, K., Holcomb, I.N. & Pollack, J.R. Genomic instability in breast cancer: Pathogenesis and clinical implications. *Molecular Oncology* **4**, 255-266 (2010).
119. Baik, C.S., Wu, D., Smith, C., Martins, R.G. & Pritchard, C.C. Durable Response to Tyrosine Kinase Inhibitor Therapy in a Lung Cancer Patient Harboring Epidermal Growth Factor Receptor Tandem Kinase Domain Duplication. *Journal of thoracic oncology : official publication of the International Association for the Study of Lung Cancer* **10**, e97-99 (2015).
120. Klempner, S.J.*, et al.* Identification of BRAF Kinase Domain Duplications Across Multiple Tumor Types and Response to RAF Inhibitor Therapy. *JAMA oncology* **2**, 272-274 (2016).
121. Plenker, D.*, et al.* Structural alterations of MET trigger response to MET kinase inhibition in lung adenocarcinoma patients. *Clinical Cancer Research* (2017).
122. Klugbauer, S., Demidchik, E.P., Lengfelder, E. & Rabes, H.M. Molecular analysis of new subtypes of ELE/RET rearrangements, their reciprocal transcripts and breakpoints in papillary thyroid carcinomas of children after Chernobyl. *Oncogene* **16**, 671-675 (1998).
123. Ali, S.M.*, et al.* A Combination of Targeted Therapy with Chemotherapy Backbone Induces Response in a Treatment-Resistant Triple-Negative MCL1-Amplified Metastatic Breast Cancer Patient. *Case Reports in Oncology* **9**, 112-118 (2016).
124. Kulkarni, A.*, et al.* BRAF Fusion as a Novel Mechanism of Acquired Resistance to Vemurafenib in BRAFV600E Mutant Melanoma. *Clin Cancer Res* **23**, 5631-5638 (2017).
125. Klempner, S.J.*, et al.* Emergence of RET rearrangement co-existing with activated EGFR mutation in EGFR-mutated NSCLC patients who had progressed on first- or second-generation EGFR TKI. *Lung cancer (Amsterdam, Netherlands)* **89**, 357-359 (2015).
126. Kim, M.-S.*, et al.* A draft map of the human proteome. *Nature* **509**, 575-581 (2014).
127. Hubbard, S.R. Juxtamembrane autoinhibition in receptor tyrosine kinases. *Nature reviews. Molecular cell biology* **5**, 464-471 (2004).
128. Lemmon, M.A. & Schlessinger, J. Cell signaling by receptor tyrosine kinases. *Cell* **141**, 1117-1134 (2010).
129. Borrello, M.G.*, et al.* Functional characterization of the MTC-associated germline RET-K666E mutation: evidence of oncogenic potential enhanced by the G691S polymorphism. *Endocr Relat Cancer* **18**, 519-527 (2011).
130. Molina, M.A.*, et al.* NH2-terminal truncated HER-2 protein but not full-length receptor is associated with nodal metastasis in human breast cancer. *Clinical Cancer Research* **8**, 347-353 (2002).

131. Wiesner, T.*, et al.* Alternative transcription initiation leads to expression of a novel ALK isoform in cancer. *Nature* **526**, 453-457 (2015).
132. Paronetto, M.P.*, et al.* Expression of a truncated form of the c-Kit tyrosine kinase receptor and activation of Src kinase in human prostatic cancer. *The American journal of pathology* **164**, 1243-1251 (2004).
133. Huang, P.H., Xu, A.M. & White, F.M. Oncogenic EGFR Signaling Networks in Glioma. *Science signaling* **2**, re6-re6 (2009).
134. Frank-Raue, K., Rondot, S. & Raue, F. Molecular genetics and phenomics of RET mutations: Impact on prognosis of MTC. *Molecular and cellular endocrinology* **322**, 2-7 (2010).
135. Levinson, S. & Cagan, R.L. Drosophila Cancer Models Identify Functional Differences between Ret Fusions. *Cell reports* **16**, 3052-3061 (2016).
136. Miyagi, E.*, et al.* Chronic expression of RET/PTC 3 enhances basal and insulin-stimulated PI3 kinase/AKT signaling and increases IRS-2 expression in FRTL-5 thyroid cells. *Molecular carcinogenesis* **41**, 98-107 (2004).
137. Engelman, J.A.*, et al.* MET amplification leads to gefitinib resistance in lung cancer by activating ERBB3 signaling. *Science* **316**, 1039-1043 (2007).
138. Gardaneh, M., Shojaei, S., Kaviani, A. & Behnam, B. GDNF induces RET-SRC-HER2-dependent growth in trastuzumab-sensitive but SRC-independent growth in resistant breast tumor cells. *Breast cancer research and treatment* **162**, 231-241 (2017).
139. Rahal, R.*, et al.* Abstract 2641: The development of potent, selective RET inhibitors that target both wild-type RET and prospectively identified resistance mutations to multi-kinase inhibitors. *Cancer Research* **76**, 2641-2641 (2016).
140. Brandhuber, B.J.*, et al.* Abstract B192: Identification and characterization of highly potent and selective RET kinase inhibitors for the treatment of RET-driven cancers. *Molecular Cancer Therapeutics* **14**, B192-B192 (2015).

APPENDIX

APPENDIX A. ABBREVIATIONS USED

ALK: anaplastic lymphoma receptor tyrosine kinase

AKT: AKT serine/threonine kinase

ANOVA: analysis of variance

ARTN: artemin

ATCC: American Type Culture Collection

ATG: start codon for methionine

ATP: adenosine triphosphate

AVG: average

AXL: AXL receptor tyrosine kinase

BCS: bovine calf serum

BRAF: b-raf serine/threonine kinase

BRCA1: breast cancer 1, DNA repair associated

BRCA2: breast cancer 2, DNA repair associated

C-terminal: carboxy terminal

CAKUT: congenital anomalies of the kidney and urinary tract

CAB: cabozantinib

CABO: cabozantinib

CAP: College of American Pathologists

CCDC6: coiled-coil domain-containing 6

CCND1: cyclin D1

CDK4/6: cyclin dependent kinase 4/6

CGH: comparative genomic hybridization

CLIA: Clinical Laboratory Improvement Amendments

CLD: cadherin-like domain

CMV: cytomegalovirus

COMBO: combination

CRD: cysteine rich domain

CRISPR: clustered regularly interspaced short palindromic repeats

DMEM: Dulbecco's Modified Eagle Medium

DMSO: dimethyl sulfoxide

DNA: deoxyribonucleic acid

ECL: enhanced chemiluminescence

EDTA: ethylenediaminetetraacetic acid

EF: elongation factor

EGFR: epidermal growth factor receptor

EML4: echinoderm microtubule associated protein like 4

ESR1: estrogen receptor 1 gene

ER: estrogen receptor

ERBB2: erb-B2 receptor tyrosine kinase 2

ERE: estrogen response element

ERK: extracellular signal-regulated kinase

FBS: fetal bovine serum

FFPE: formalin-fixed, paraffin-embedded

FISH: fluorescent in situ hybridization

GFLs: GDNF ligands

GDNF: glial cell line-derived neurotrophic factor

GFRα: GDNF family receptorα

H&E: hematoxylin & eosin

HER1: human epidermal growth factor receptor 1

HER2: human epidermal growth factor receptor 2

HR: hormone receptor

HRP: horseradish peroxidase

HSCR: Hirschsprung's disease

IDC: invasive ductal carcinoma

IgG: immunoglobulin G

IGFR: insulin-like growth factor

IHC: immunohistochemistry

IC-50: half maximal inhibitory concentration

IL6: interleukin 6

JM: juxtamembrane domain

KD: kinase domain

Ki-67: proliferation marker protein Ki-67

KIF5B: kinesin family member 5B

KIT: mast/stem cell growth factor receptor

MAPK: mitogen-activated protein kinase

MCL1: myeloid cell leukemia 1

MEGM: Mammary Epithelial Cell Growth Medium

MEK: mitogen activated protein kinase kinase

MEN2: multiple endocrine neoplasia 2

MET: hepatocyte growth factor receptor

MRI: magnetic resonance imaging

MTC: medullary thyroid cancer

MYC: transcription factor protein

mTOR: mechanistic target of rapamycin

MTS: tetrazolium compound [3-(4,5-dimethylthiazol-2-yl)-5-(3-carboxymethoxyphenyl)-2-(4-sulfophenyl)-2H-tetrazolium, inner salt

N-terminal: amino terminal

NCOA4: nuclear receptor coactivator 4

NCT: National Clinical Trial

NIH: National Institutes of Health

NETN: NaCl EDTA Tris NonidetP40

NRTN: neurturin

NSCLC: non-small cell lung cancer

NSG: NOD, non-obese diabetic /SCID, severe combined immunodeficiency/ GAMMA, interleukin 2 receptor γ null

ORF: open reading frame

ORR: overall response rate

P70 S6: 70kDa ribosomal protein s6 kinase

p: phospho

PARP: poly (ADP-ribose) polymerase

PCR: polymerase chain reaction

PET/CT: positron emission tomography/ computed tomography

PDC: patient-derived cell line

PDX: patient-derived xenograft

PDC-X: patient-derived cell line xenograft

PFS: progression free survival

PI3K: phosphoinositide 3-kinase

PIK3CA: phosphatidylinositol 4,5-bisphosphate 3-kinase catalytic subunit alpha isoform

PKC: protein kinase C

PR: progesterone receptor

PSPN: persephin

PT: patient

PTC: papillary thyroid cancer

PTEN: phosphatase and tensin homolog

RAS: RAS proto-oncogene, GTPase

RASGEF1A: RasGEF domain family member 1A

RET: RET proto-oncogene, receptor tyrosine kinase

RET^{amp}: RET amplification

RNA: ribonucleic acid

RTK: receptor tyrosine kinase

RT-PCR: reverse transcriptase polymerase chain reaction

siRNA: small interfering ribonucleic acid

SRC: SRC proto-oncogene, non-receptor tyrosine kinase

STAT3: signal transducer and activator of transcription 3

t: total

TBS: tris buffered saline

TDM1: antibody-drug conjugate containing trastuzumab and DM1

TKI: tyrosine kinase inhibitor

TM: transmembrane domain

TNBC: triple negative breast cancer

TP53: tumor protein P53

TRAS: trastuzumab

TX: treatment

UTR: untranslated region

V5–tag: small epitope (Pk) found on the P and V proteins of the paramyxovirus of simian virus 5

VEGFR: vascular endothelial growth factor receptor

ZNF: zinc finger

APPENDIX B.

pDONR221 vector map

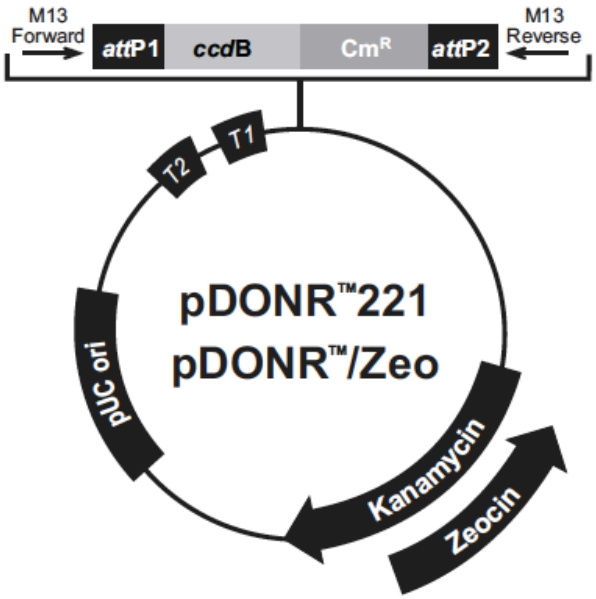

Comments for:	pDONR™221 4761 nucleotides	pDONR™/Zeo 4291 nucleotides
*rrn*B T2 transcription termination sequence (c):	268-295	268-295
rmB T1 transcription termination sequence (c):	427-470	427-470
M13 Forward (-20) priming site:	537-552	537-552
*att*P1:	570-801	570-801
*ccd*B gene (c):	1197-1502	1197-1502
Chloramphenicol resistance gene (c):	1825-2505	1847-2506
*att*P2 (c):	2753-2984	2754-2985
M13 Reverse priming site:	3026-3042	3027-3043
Kanamycin resistance gene:	3155-3964	---
EM7 promoter (c):	---	3486-3552
Zeocin resistance gene (c):	---	3111-3485
pUC origin:	4085-4758	3615-4288

(c) = complementary strand

pLenti6.3/V5-DEST vector map:

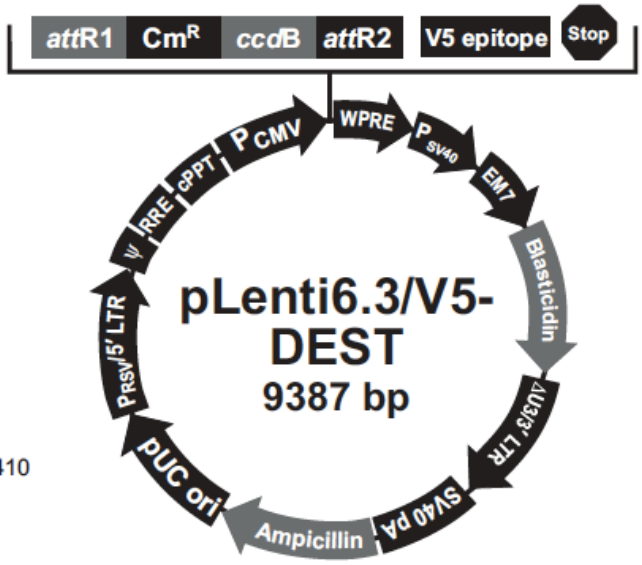

Comments for pLenti6.3/V5-DEST
9387 nucleotides

RSV/5′ LTR hybrid promoter: bases 1-410
RSV promoter: bases 1-229
HIV-1 5′ LTR: bases 230-410
5′ splice donor: base 520
HIV-1 psi (ψ) packaging signal: bases 521-565
HIV-1 Rev response element (RRE): bases 1075-1308
3′ splice acceptor: base 1656
3′ splice acceptor: base 1684
cPPT: bases 1801-1923
CMV promoter: bases 1935-2519
attR1 site: bases 2568-2692
Chloramphenicol resistance gene (Cm^R): bases 2801-3460
ccdB gene: bases 3802-4107
attR2 site: bases 4148-4272
V5 epitope: bases 4325-4366
WPRE: bases 4385-4982
SV40 promoter: bases 4993-5301
EM7 promoter: bases 5356-5422
Blasticidin resistance gene: bases 5423-5821
ΔU3/3′ LTR: bases 5907-6141
ΔU3: bases 5907-5960
3′ LTR: bases 5961-6141
SV40 polyadenylation signal: bases 6213-6344
bla promoter: bases 7203-7301
Ampicillin (*bla*) resistance gene: bases 7302-8162
pUC origin: bases 8307-8980

pEF-DEST51 vector map:

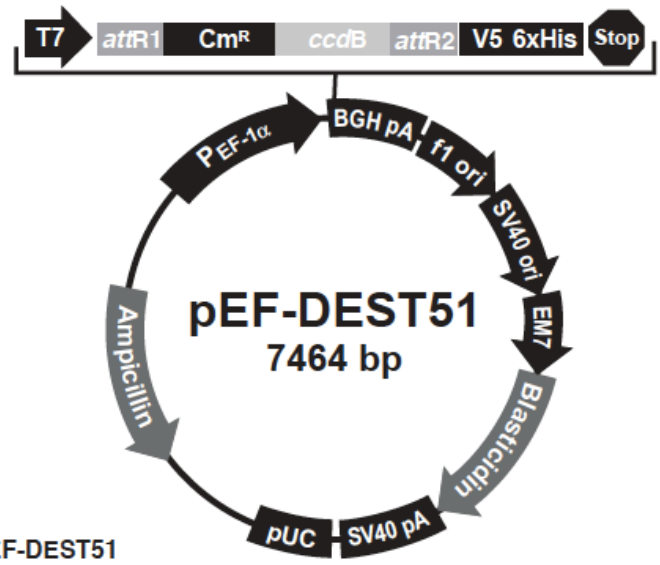

Features of pEF-DEST51
7464 nucleotides

EF-1α promoter: bases 470-1653
T7 promoter: bases 1670-1689
attR1 recombination site: bases 1720-1844
Chloramphenicol resistance gene: bases 1953-2612
ccdB gene: bases 2954-3259
attR2 recombination site: bases 3300-3424
V5 epitope: bases 3450-3491
6xHis tag: bases 3501-3518
BGH polyadenylation region: 3544-3771
f1 origin: bases 3817-4245
SV40 early promoter and origin: bases 4250-4594
EM7 promoter: bases 4629-4684
Blasticidin resistance gene: bases 4703-5101
SV40 early polyadenylation region: bases 5259-5389
pUC origin: bases 5772-6445
Ampicillin resistance gene (*bla*): bases 6590-7450 (c)
bla promoter: bases 7451-85 (c)
(c) = complementary strand

APPENDIX C: Full length sequences for gene and gene fusions

RET full length- wildtype sequence

ATGGCGAAGGCGACGTCCGGTGCCGCGGGGCTGCGTCTGCTGTTGCTGCTGC
TGCTGCCGCTGCTAGGCAAAGTGGCATTGGGCCTCTACTTCTCGAGGGATGCT
TACTGGGAGAAGCTGTATGTGGACCAGGCAGCCGGCACGCCCTTGCTGTACG
TCCATGCCCTGCGGGACGCCCCTGAGGAGGTGCCCAGCTTCCGCCTGGGCCA
GCATCTCTACGGCACGTACCGCACACGGCTGCATGAGAACAACTGGATCTGC
ATCCAGGAGGACACCGGCCTCCTCTACCTTAACCGGAGCCTGGACCATAGCT
CCTGGGAGAAGCTCAGTGTCCGCAACCGCGGCTTTCCCCTGCTCACCGTCTAC
CTCAAGGTCTTCCTGTCACCCACATCCCTTCGTGAGGGCGAGTGCCAGTGGCC
AGGCTGTGCCCGCGTATACTTCTCCTTCTTCAACACCTCCTTTCCAGCCTGCA
GCTCCCTCAAGCCCCGGGAGCTCTGCTTCCCAGAGACAAGGCCCTCCTTCCGC
ATTCGGGAGAACCGACCCCCAGGCACCTTCCACCAGTTCCGCCTGCTGCCTGT
GCAGTTCTTGTGCCCCAACATCAGCGTGGCCTACAGGCTCCTGGAGGGTGAG
GGTCTGCCCTTCCGCTGCGCCCCGGACAGCCTGGAGGTGAGCACGCGCTGGG
CCCTGGACCGCGAGCAGCGGGAGAAGTACGAGCTGGTGGCCGTGTGCACCGT
GCACGCCGGCGCGCGCGAGGAGGTGGTGATGGTGCCCTTCCCGGTGACCGTG
TACGACGAGGACGACTCGGCGCCCACCTTCCCCGCGGGCGTCGACACCGCCA
GCGCCGTGGTGGAGTTCAAGCGGAAGGAGGACACCGTGGTGGCCACGCTGC
GTGTCTTCGATGCAGACGTGGTACCTGCATCAGGGGAGCTGGTGAGGCGGTA
CACAAGCACGCTGCTCCCCGGGGACACCTGGGCCCAGCAGACCTTCCGGGTG
GAACACTGGCCCAACGAGACCTCGGTCCAGGCCAACGGCAGCTTCGTGCGGG
CGACCGTACATGACTATAGGCTGGTTCTCAACCGGAACCTCTCCATCTCGGA
GAACCGCACCATGCAGCTGGCGGTGCTGGTCAATGACTCAGACTTCCAGGGC
CCAGGAGCGGGCGTCCTCTTGCTCCACTTCAACGTGTCGGTGCTGCCGGTCAG
CCTGCACCTGCCCAGTACCTACTCCCTCTCCGTGAGCAGGAGGGCTCGCCGAT
TTGCCCAGATCGGGAAAGTCTGTGTGGAAAACTGCCAGGCATTCAGTGGCAT
CAACGTCCAGTACAAGCTGCATTCCTCTGGTGCCAACTGCAGCACGCTAGGG
GTGGTCACCTCAGCCGAGGACACCTCGGGGATCCTGTTTGTGAATGACACCA
AGGCCCTGCGGCGGCCCAAGTGTGCCGAACTTCACTACATGGTGGTGGCCAC
CGACCAGCAGACCTCTAGGCAGGCCCAGGCCCAGCTGCTTGTAACAGTGGAG
GGGTCATATGTGGCCGAGGAGGCGGGCTGCCCCCTGTCCTGTGCAGTCAGCA
AGAGACGGCTGGAGTGTGAGGAGTGTGGCGGCCTGGGCTCCCCAACAGGCA
GGTGTGAGTGGAGGCAAGGAGATGGCAAAGGGATCACCAGGAACTTCTCCA
CCTGCTCTCCCAGCACCAAGACCTGCCCCGACGGCCACTGCGATGTTGTGGA
GACCCAAGACATCAACATTTGCCCTCAGGACTGCCTCCGGGGCAGCATTGTT
GGGGGACACGAGCCTGGGGAGCCCCGGGGGATTAAAGCTGGCTATGGCACC
TGCAACTGCTTCCCTGAGGAGGAGAAGTGCTTCTGCGAGCCCGAAGACATCC
AGGATCCACTGTGCGACGAGCTGTGCCGCACGGTGATCGCAGCCGCTGTCCT
CTTCTCCTTCATCGTCTCGGTGCTGCTGTCTGCCTTCTGCATCCACTGCTACCA
CAAGTTTGCCCACAAGCCACCCATCTCCTCAGCTGAGATGACCTTCCGGAGG
CCCGCCCAGGCCTTCCCGGTCAGCTACTCCTCTTCCGGTGCCCGCCGGCCCTC
GCTGGACTCCATGGAGAACCAGGTCTCCGTGGATGCCTTCAAGATCCTGGAG
GATCCAAAGTGGGAATTCCCTCGGAAGAACTTGGTTCTTGGAAAAACTCTAG

GAGAAGGCGAATTTGGAAAAGTGGTCAAGGCAACGGCCTTCCATCTGAAAG
GCAGAGCAGGGTACACCACGGTGGCCGTGAAGATGCTGAAAGAGAACGCCT
CCCCGAGTGAGCTGCGAGACCTGCTGTCAGAGTTCAACGTCCTGAAGCAGGT
CAACCACCCACATGTCATCAAATTGTATGGGGCCTGCAGCCAGGATGGCCCG
CTCCTCCTCATCGTGGAGTACGCCAAATACGGCTCCCTGCGGGGCTTCCTCCG
CGAGAGCCGCAAAGTGGGGCCTGGCTACCTGGGCAGTGGAGGCAGCCGCAA
CTCCAGCTCCCTGGACCACCCGGATGAGCGGGCCCTCACCATGGGCGACCTC
ATCTCATTTGCCTGGCAGATCTCACAGGGGATGCAGTATCTGGCCGAGATGA
AGCTCGTTCATCGGGACTTGGCAGCCAGAAACATCCTGGTAGCTGAGGGGCG
GAAGATGAAGATTTCGGATTTCGGCTTGTCCCGAGATGTTTATGAAGAGGAT
TCCTACGTGAAGAGGAGCCAGGGTCGGATTCCAGTTAAATGGATGGCAATTG
AATCCCTTTTTGATCATATCTACACCACGCAAAGTGATGTATGGTCTTTTGGT
GTCCTGCTGTGGGAGATCGTGACCCTAGGGGGAAACCCCTATCCTGGGATTC
CTCCTGAGCGGCTCTTCAACCTTCTGAAGACCGGCCACCGGATGGAGAGGCC
AGACAACTGCAGCGAGGAGATGTACCGCCTGATGCTGCAATGCTGGAAGCAG
GAGCCGGACAAAAGGCCGGTGTTTGCGGACATCAGCAAAGACCTGGAGAAG
ATGATGGTTAAGAGGAGAGACTACTTGGACCTTGCGGCGTCCACTCCATCTG
ACTCCCTGATTTATGACGACGGCCTCTCAGAGGAGGAGACACCGCTGGTGGA
CTGTAATAATGCCCCCCTCCCTCGAGCCCTCCCTTCCACATGGATTGAAAACA
AACTCTATGGTAGAATTTCCCATGCATTTACTAGATTCTAG

NCOA4-RET (NCOA4, exon 2-exon 7 and RET, exon 12-exon 19)

ATGAATACCTTCCAAGACCAGAGTGGCAGCTCCAGTAATAGAGAACCCCTTT
TGAGGTGTAGTGATGCACGGAGGGACTTGGAGCTTGCTATTGGTGGAGTTCT
CCGGGCTGAACAGCAAATTAAAGATAACTTGCGAGAGGTCAAAGCTCAGATT
CACAGTTGCATAAGCCGTCACCTGGAATGTCTTAGAAGCCGTGAGGTATGGC
TGTATGAACAGGTGGACCTTATTTATCAGCTTAAAGAGGAGACACTTCAACA
GCAGGCTCAGCAGCTCTACTCGTTATTGGGCCAGTTCAATTGTCTTACTCATC
AACTGGAGTGTACCCAAAACAAAGATCTAGCCAATCAAGTCTCTGTGTGCCT
GGAGAGACTGGGCAGTTTGACCCTTAAGCCTGAAGATTCAACTGTCCTGCTCT
TTGAAGCTGACACAATTACTCTGCGCCAGACCATCACCACATTTGGGTCTCTC
AAAACCATTCAAATTCCTGAGCACTTGATGGCTCATGCTAGTTCAGCAAATAT
TGGGCCCTTCCTGGAGAAGAGAGGCTGTATCTCCATGCCAGAGCAGAAGTCA
GCATCCGGTATTGTAGCTGTCCCTTTCAGCGAATGGCTCCTTGGAAGCAAACC
TGCCAGTGGTTATCAAGCTCCTTACATACCCAGCACCGACCCCCAGGACTGG
CTTACCCAAAAGCAGACCTTGGAGAACAGTCAGGAGGATCCAAAGTGGGAA
TTCCCTCGGAAGAACTTGGTTCTTGGAAAAACTCTAGGAGAAGGCGAATTTG
GAAAAGTGGTCAAGGCAACGGCCTTCCATCTGAAAGGCAGAGCAGGGTACA
CCACGGTGGCCGTGAAGATGCTGAAAGAGAACGCCTCCCCGAGTGAGCTGCG
AGACCTGCTGTCAGAGTTCAACGTCCTGAAGCAGGTCAACCACCCACATGTC
ATCAAATTGTATGGGGCCTGCAGCCAGGATGGCCCGCTCCTCCTCATCGTGG
AGTACGCCAAATACGGCTCCCTGCGGGGCTTCCTCCGCGAGAGCCGCAAAGT
GGGGCCTGGCTACCTGGGCAGTGGAGGCAGCCGCAACTCCAGCTCCCTGGAC
CACCCGGATGAGCGGGCCCTCACCATGGGCGACCTCATCTCATTTGCCTGGC
AGATCTCACAGGGGATGCAGTATCTGGCCGAGATGAAGCTCGTTCATCGGGA

CTTGGCAGCCAGAAACATCCTGGTAGCTGAGGGGCGGAAGATGAAGATTTCG
GATTTCGGCTTGTCCCGAGATGTTTATGAAGAGGATTCCTACGTGAAGAGGA
GCCAGGGTCGGATTCCAGTTAAATGGATGGCAATTGAATCCCTTTTTGATCAT
ATCTACACCACGCAAAGTGATGTATGGTCTTTTGGTGTCCTGCTGTGGGAGAT
CGTGACCCTAGGGGGAAACCCCTATCCTGGGATTCCTCCTGAGCGGCTCTTCA
ACCTTCTGAAGACCGGCCACCGGATGGAGAGGCCAGACAACTGCAGCGAGG
AGATGTACCGCCTGATGCTGCAATGCTGGAAGCAGGAGCCGGACAAAAGGC
CGGTGTTTGCGGACATCAGCAAAGACCTGGAGAAGATGATGGTTAAGAGGA
GAGACTACTTGGACCTTGCGGCGTCCACTCCATCTGACTCCCTGATTTATGAC
GACGGCCTCTCAGAGGAGGAGACACCGCTGGTGGACTGTAATAATGCCCCCC
TCCCTCGAGCCCTCCCTTCCACATGGATTGAAAACAAACTCTATGGTAGAATT
TCCCATGCATTTACTAGATTCTAG

ΔRET (exon 11 ATG- exon 19)

ATGACCTTCCGGAGGCCCGCCCAGGCCTTCCCGGTCAGCTACTCCTCTTCCGG
TGCCCGCCGGCCCTCGCTGGACTCCATGGAGAACCAGGTCTCCGTGGATGCC
TTCAAGATCCTGGAGGATCCAAAGTGGGAATTCCCTCGGAAGAACTTGGTTC
TTGGAAAAACTCTAGGAGAAGGCGAATTTGGAAAAGTGGTCAAGGCAACGG
CCTTCCATCTGAAAGGCAGAGCAGGGTACACCACGGTGGCCGTGAAGATGCT
GAAAGAGAACGCCTCCCCGAGTGAGCTGCGAGACCTGCTGTCAGAGTTCAAC
GTCCTGAAGCAGGTCAACCACCCACATGTCATCAAATTGTATGGGGCCTGCA
GCCAGGATGGCCCGCTCCTCCTCATCGTGGAGTACGCCAAATACGGCTCCCT
GCGGGGCTTCCTCCGCGAGAGCCGCAAAGTGGGGCCTGGCTACCTGGGCAGT
GGAGGCAGCCGCAACTCCAGCTCCCTGGACCACCCGGATGAGCGGGCCCTCA
CCATGGGCGACCTCATCTCATTTGCCTGGCAGATCTCACAGGGGATGCAGTAT
CTGGCCGAGATGAAGCTCGTTCATCGGGACTTGGCAGCCAGAAACATCCTGG
TAGCTGAGGGGCGGAAGATGAAGATTTCGGATTTCGGCTTGTCCCGAGATGT
TTATGAAGAGGATTCCTACGTGAAGAGGAGCCAGGGTCGGATTCCAGTTAAA
TGGATGGCAATTGAATCCCTTTTTGATCATATCTACACCACGCAAAGTGATG
TATGGTCTTTTGGTGTCCTGCTGTGGGAGATCGTGACCCTAGGGGGAAACCCC
TATCCTGGGATTCCTCCTGAGCGGCTCTTCAACCTTCTGAAGACCGGCCACCG
GATGGAGAGGCCAGACAACTGCAGCGAGGAGATGTACCGCCTGATGCTGCA
ATGCTGGAAGCAGGAGCCGGACAAAAGGCCGGTGTTTGCGGACATCAGCAA
AGACCTGGAGAAGATGATGGTTAAGAGGAGAGACTACTTGGACCTTGCGGCG
TCCACTCCATCTGACTCCCTGATTTATGACGACGGCCTCTCAGAGGAGGAGA
CACCGCTGGTGGACTGTAATAATGCCCCCCTCCCTCGAGCCCTCCCTTCCACA
TGGATTGAAAACAAACTCTATGGTAGAATTTCCCATGCATTTACTAGATTCTA
G

APPENDIX D: SUPPLEMENTARY RESULTS

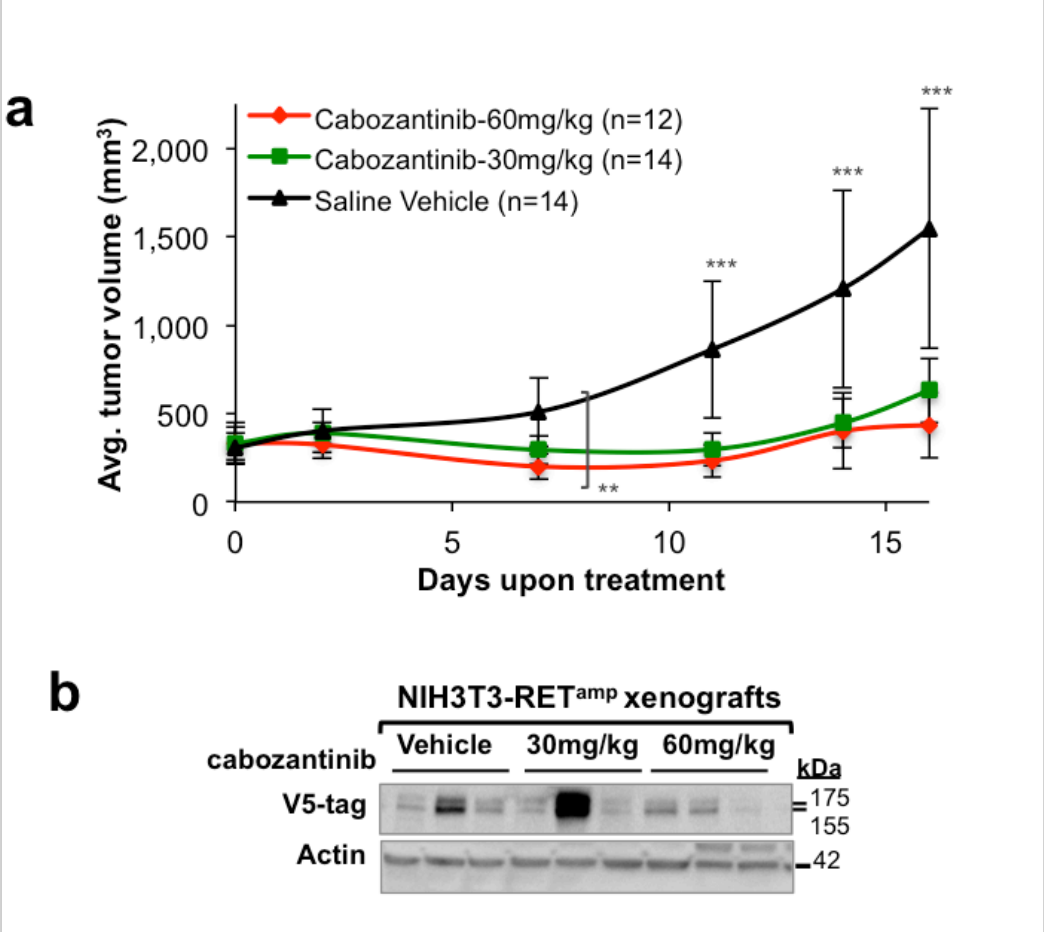

Supplementary Figure 1. Growth inhibition and RET protein expression in RET^{amp} xenografts.

(a) Mean tumor volume was measured in NIH/3T3 xenografts driven by RET^{amp}. Mice were treated with either cabozantinib at 30mg/kg (n=14), 60mg/kg (n=12) or saline vehicle (n=14) control for 16 days. Error bars represent mean ± s.d. p-values are after two-way ANOVA with Tukey's multiple comparisons test. ***p<0.001 between vehicle and treatment groups at days 11, 14, and 16. **p<0.01 between vehicle and 60mg/kg. (b) Immunoblot for V5-tag measured in tumor lysates at the end of 16-day treatment in mice harboring NIH/3T3- RET^{amp} tumors. Mice were treated on the day of collection for 4 hours with saline vehicle or cabozantinib (30mg/kg or 60mg/kg). Actin used as loading controls.

Supplementary Table 1. Clinicopathologic and *RET* variant details for 121 breast cancers

Patient #	RET alteration	ER status	PR status	*ERBB2* amplification status	Specimen site of collection	Tumor nuclei %	Copy number (for amplifications)
1	CCDC6-RET fusion	UNK	UNK	NEG	Mediastinum	50	N.A
2	CCDC6-RET fusion	NEG	NEG	NEG	Lymph Node	40	N.A.
3	NCOA4-RET fusion	POS	NEG	NEG	Soft Tissue	35	N.A.
4	CCDC6-RET fusion	NEG	NEG	NEG	Breast	80	N.A.
5	CCDC6-RET fusion	NEG	NEG	NEG	Breast	80	N.A.
6	CCDC6-RET fusion	POS	NEG	NEG	Liver	40	N.A.
7	CCDC6-RET fusion	NEG	NEG	NEG	Breast	25	N.A.
8	RASGEF1A-RET fusion	NEG	NEG	NEG	Breast	87	N.A.
9	rearrangement (Fig.7)	NEG	NEG	NEG	Breast	60	N.A.
10	rearrangement (Fig.7)	POS	POS	NEG	Liver	30	N.A.
11	rearrangement (Fig.7)	NEG	NEG	NEG	Breast	20	N.A.
12	rearrangement (Fig.7)	NEG	NEG	NEG	Breast	70	N.A.
13	rearrangement (Fig.7)	POS	NEG	NEG	Skin	50	N.A.
14	rearrangement (Fig.7)	NEG	NEG	NEG	Skin	20	N.A.
15	rearrangement (Fig.7)	NEG	NEG	POS	Breast	50	N.A.
16	rearrangement (Fig.7)	UNK	UNK	NEG	Skin	60	N.A.
17	C634R	POS	POS	NEG	Bone	30	N.A.
18	R114H	POS	POS	NEG	Breast	20	N.A.
19	E632K	POS	NEG	NEG	Liver	30	N.A
20	C634F	POS	POS	NEG	Pleura	70	N.A.
21	V804M	UNK	UNK	NEG	Soft Tissue	40	N.A.
22	D925H	POS	POS	NEG	Small Intestine	40	N.A.

23	V706M	UNK	UNK	NEG	Breast	30	N.A.
24	R600Q	NEG	NEG	NEG	Lymph Node	80	N.A.
25	V591I	UNK	UNK	NEG	Lymph Node	30	N.A.
26	L633V	POS	POS	NEG	Brain	40	N.A.
27	S462L	NEG	POS	NEG	Chest Wall	20	N.A.
28	M918T	UNK	UNK	NEG	Liver	25	N.A.
29	E511K	POS	UNK	POS	Liver	30	N.A.
30	E511K	POS	UNK	NEG	Liver	70	N.A.
31	E511K	POS	POS	NEG	Breast	70	N.A.
32	E511K	POS	POS	NEG	Mediastinum	20	N.A.
33	C620F	NEG	NEG	POS	Breast	40	N.A.
34	S462L	NEG	NEG	POS	Breast	80	N.A.
35	V804M	POS	POS	NEG	Liver	70	N.A.
36	E511K	NEG	NEG	NEG	Breast	70	N.A.
37	E232K	POS	NEG	NEG	Liver	60	N.A.
38	C611R	POS	NEG	NEG	Liver	60	N.A.
39	V804M	POS	POS	POS	Bone	25	N.A.
40	T636M	NEG	NEG	NEG	Lung	20	N.A.
41	V804M	POS	POS	POS	Breast	20	N.A.
42	amplification	UNK	UNK	NEG	chest wall	60	13
43	amplification	NEG	NEG	NEG	Breast	40	8
44	amplification	NEG	NEG	NEG	Breast	50	6
45	amplification	UNK	UNK	NEG	Lung	40	11
46	amplification	UNK	UNK	POS	Lymph Node	60	10
47	amplification	NEG	NEG	NEG	Bone	50	8
48	amplification	UNK	UNK	NEG	Rectum	70	7
49	amplification	NEG	POS	NEG	Breast	20	9

50	amplification	NEG	NEG	NEG	Breast	50	7
51	amplification	NEG	NEG	POS	Breast	20	8
52	amplification	NEG	NEG	NEG	Skin	20	6
53	amplification	NEG	NEG	NEG	Chest Wall	60	14
54	amplification	NEG	NEG	NEG	Lymph Node	80	9
55	amplification	UNK	UNK	NEG	Liver	20	7
56	amplification	NEG	NEG	NEG	Breast	30	13
57	amplification	NEG	NEG	NEG	Skin	40	21
58	amplification	POS	POS	NEG	Liver	60	6
59	amplification	NEG	NEG	NEG	Liver	60	7
60	amplification	NEG	NEG	NEG	Breast	60	12
61	amplification	NEG	POS	NEG	Breast	20	8
62	amplification	NEG	NEG	NEG	Breast	40	7
63	amplification	POS	NEG	NEG	Breast	20	8
64	amplification	NEG	NEG	NEG	Breast	80	16
65	amplification	NEG	NEG	NEG	Breast	40	9
66	amplification	NEG	NEG	NEG	Breast	50	13
67	amplification	NEG	NEG	POS	Breast	60	7
68	amplification	NEG	NEG	NEG	Lung	30	9
69	amplification	NEG	NEG	NEG	Breast	30	13
70	amplification	POS	UNK	NEG	Liver	30	11
71	amplification	NEG	NEG	NEG	Breast	30	12
72	amplification	UNK	UNK	NEG	Breast	30	7
73	amplification	UNK	UNK	POS	Soft Tissue	30	9
74	amplification	POS	NEG	NEG	Breast	50	6
75	amplification	POS	NEG	NEG	Breast	50	10
76	amplification	NEG	NEG	NEG	Breast	30	8

77	amplification	NEG	NEG	NEG	Breast	60	9
78	amplification	NEG	NEG	NEG	Breast	70	9
79	amplification	POS	POS	POS	Liver	70	9
80	amplification	NEG	NEG	NEG	Breast	30	11
81	amplification	POS	POS	NEG	Liver	40	6
82	amplification	UNK	UNK	NEG	Chest Wall	90	6
83	amplification	NEG	NEG	NEG	Breast	40	8
84	amplification	UNK	UNK	POS	Brain	60	9
85	amplification	POS	NEG	POS	Liver	70	10
86	amplification	POS	POS	NEG	Breast	70	7
87	amplification	POS	NEG	NEG	Breast	30	8
88	amplification	NEG	NEG	NEG	Breast	30	7
89	amplification	NEG	NEG	NEG	Breast	70	6
90	amplification	POS	POS	NEG	Liver	20	11
91	amplification	UNK	UNK	NEG	Lung	50	15
92	amplification	NEG	NEG	NEG	Head/neck	50	9
93	amplification	NEG	NEG	NEG	Liver	50	8
94	amplification	UNK	UNK	NEG	Skin	25	9
95	amplification	UNK	UNK	POS	Breast	70	9
96	amplification	NEG	NEG	NEG	Chest Wall	25	9
97	amplification	UNK	UNK	NEG	Skin	30	8
98	amplification	UNK	UNK	POS	Skin	20	8
99	amplification	NEG	NEG	NEG	Lung	25	9
100	amplification	NEG	NEG	NEG	Breast	30	8
101	amplification	NEG	NEG	NEG	Breast	40	15
102	amplification	NEG	NEG	NEG	Breast	20	7
103	amplification	NEG	NEG	NEG	Chest Wall	60	11

104	amplification	POS	POS	NEG	Liver	30	8
105	amplification	NEG	NEG	NEG	Lymph Node	20	11
106	amplification	UNK	UNK	NEG	Chest Wall	40	7
107	amplification	NEG	NEG	NEG	Lymph Node	20	7
108	amplification	NEG	NEG	NEG	Lymph Node	60	6
109	amplification	NEG	NEG	NEG	Liver	30	9
110	amplification	POS	UNK	NEG	Pleura	60	7
13	amplification	POS	NEG	NEG	Skin	50	12
111	amplification	UNK	UNK	NEG	Brain	20	8
112	amplification	NEG	NEG	POS	Lymph Node	30	7
113	amplification	NEG	NEG	POS	Breast	50	6
114	amplification	POS	NEG	POS	Chest Wall	20	7
115	amplification	POS	NEG	NEG	Skin	70	8
116	amplification	NEG	NEG	POS	Head/neck	20	6
117	amplification	NEG	NEG	NEG	Breast	70	6
118	amplification	UNK	UNK	NEG	Adrenal Gland	70	7
119	amplification	NEG	NEG	POS	Liver	70	11
120	amplification	NEG	NEG	NEG	Lymph Node	20	8
121	amplification	NEG	POS	NEG	Liver	20	8

ER, Estrogen Receptor; PR, Progesterone Receptor; ER, PR status measured by routine clinical immunohistochemistry; ERBB2 amplification status as measured by comprehensive genomic profiling, N.A., Not applicable; UNK, unknown; POS, positive; NEG, negative